Puʻukoholā Heiau National Historic Site and Kaloko-Honokōhau Historical Park, Big Island of Hawaiʻi

Coastal Hazard Analysis Report

Prepared By Vitousek, S., Barbee, M.M., Fletcher, C.H., Richmond, B.M., Genz, A.S.

May 20, 2009

Table of Contents

List of Figures iv
List of Tables vi
Executive Summary 1
Scope of work 1
Results and Recommendations 1
Introduction 3
Background 3
Geologic setting 3
Coastal historic sites 3
Wave Climate 5
Hawaiian swell regimes 5
North Pacific swell 5
Trade winds and trade-wind swell 6
Southern swell 6
Kona storms 6
Maximum annual recurring wave heights in Hawaiʻi 6
Tides 6
Coincidence of waves and tides 7
Runup and inundation 7
Sea-level rise 7
Coastal Inundation, Overtopping of Swells and Sea-level Rise 11
Modeling the wave cycle of the Big Island of Hawaiʻi 11
Overtopping and Inundation Hazard 13
Joint Probability Model of Tide and Runup 14
Tsunami Hazards 40
Paleotsunami 40
Tsunami Inundation Model 41
Shoreline Morphology 50
Integrated Coastal Digital Elevation Model (C-DEM) 50
Data Sources 50
Methods – vertical datum migration 50
Results 50
Coastal Erosion Hazard 53
Compilation of historical shorelines 53
Delineation of aerial photo based shoreline 53
Uncertainties and errors 53
Analysis methods 54
Single-Transect (ST) method 54
Eigenbeaches (EX and EXT): Alternatives to ST method 54
Reporting ST, EX and EXT results 55
Rectification of vertical aerial photography 55
ST, EX and EXT results at Kaloko-Honokōhau NHP and Puʻukoholā Heiau NHS 56
Kaloko-Honokōhau NHP 56
Puʻukoholā Heiau NHS 56
Impacts and Recommendations 62
Kaloko-Honokōhau NHP 62
Puʻukoholā Heiau NHS 62
Conclusion 63
Acknowledgements 64
References 65
Appendix A: Model Settings 68
Appendix B: Model Results 69
Appendix C: Historical Imagery 77
Appendix D: Shoreline Change Results 83

List of Figures

Figure 1. Locations of Pu'ukoholā Heiau NHS and Kaloko-Honokōhau NHP on the Big Island of Hawai'i. 4
Figure 2. Hawai'i dominant swell regimes after Moberly & Chamberlain (1964), and wave monitoring buoy locations. From Vitousek & Fletcher (2008). 8
Figure 3. Satellite (JASON-1) derived average wave heights [m] over the North Pacific in the summer and winter. 9
Figure 4. The number of days per season that the trade winds occur with a certain speed (data from Buoy 51001). The days per season are shown in red for winter months and blue for summer months. Notice the persistence of typical trade winds (~ 16 mph) during summer months. 9
Figure 5. Sea-level history [mm] in Hawai'i as observed from several tide gauges. 10
Figure 6. Four of 85 SWAN model simulations each with representative annual maximum significant wave height from a particular direction. Ho is the deep water wave height (m) and Tp is the wave period (s). Case A: South swell, Ho=2.3 m Tp=16 s Dir=200°. Case B: Northwest swell, Ho=4.1 m Tp=14 s Dir=290°. Case C: North swell, Ho=5.8 m Tp=16 s Dir=340°. Case D: Northeast swell, Ho=6 m Tp=16 s Dir=45°. 18
Figure 7. The maximum annual significant wave height for the Big Island national park sites as a function of wave direction (Pu'ukoholā Heiau NHS = red, Kaloko-Honokōhau NHP = blue). The blue and red 'x's on the map of the wave field around the Big Island indicate the virtual buoy (model) locations. The maximum wave height case occurs during west northwest swell where the wave direction is about 290°. There is a small secondary peak associated with north wrap when the wave direction approach can fit in the gap between Maui and the Big Island. Also indicated on the figure is the degree of island blockage, which is the difference between the dashed line and the solid blue and red lines. 19
Figure 8. The relationship between the open-swell significant wave height and the return period determined from Generalized Extreme Value Analysis (GEV) for the 282°-305° window. 20
Figure 9. The relationship between the significant wave height and the return period at Pu'ukoholā Heiau NHS and Kaloko-Honokōhau NHP (green) determined from Generalized Extreme Value Analysis (GEV) for the 282°-305° window used as a boundary condition for a wave transformation model from deep water to the national park sites. The x's are the individual cases modeled. The GEV model is compared with the recurrence relationship for open ocean swell given in Figure 8 (blue). The difference between the blue line and the green line is the effect of island blockage. 21
Figure 10. The relationship between the runup elevation and the return period at Pu'ukoholā Heiau NHS and Kaloko-Honokōhau NHP (red) determined from the Stockdon equation. The runup relationship is compared with the recurrence relationship for open ocean swell (blue) given in Figure 8 and for local swell (green) given in Figure 9. As is typical, the runup elevations are much smaller than the wave heights as there is significant energy dissipation due to breaking. 22
Figure 11. Inundation maps of Pu'ukoholā Heiau NHS and a portion of the Ala Kahakai National Historic Trail under sea-level rise scenarios. 23
Figure 12. Inundation maps of the northern beach at Pelekane Bay, Pu'ukoholā Heiau NHS under sea-level rise scenarios. 24
Figure 13. Inundation maps of Spencer Beach Park under sea-level rise scenarios. 25
Figure 14. Inundation maps of portions of Kaloko-Honokōhau NHP under sea-level rise scenarios. 26
Figure 15. Inundation maps of the Honokōhau Beach fronting the 'Aimakapā Fishpond under sea-level rise scenarios. 27
Figure 16. Inundation maps of Maliu Point at 'Ai'ōpio, in the southern portion of Kaloko-Honokōhau NHP, under sea-level rise scenarios. 28
Figure 17. The shoreline trail, the Ala Kahakai NHT, at Pelekane Bay experiences erosion and root exposure of the sand seaward of the trail. 29
Figure 18. The debris lines on Pelekane Beach are evidence of high wave wash. 30
Figure 19. The debris lines on Spencer Beach are evidence of high wave wash. 31
Figure 20. 'Aimakapā Fishpond wetland on the shoreline at Kaloko-Honokōhau NHP that partially flooded during a spring high tide. 32
Figure 21. Flooding of low-lying lands vegetated with saltwater tolerant species at Kaloko-Honokōhau NHP. 33
Figure 22. The debris lines on Honokōhau Beach fronting the 'Aimakapā Fishpond are evidence of high-wave wash and partial overtopping of the dune/sand berm. 34
Figure 23. The base of Pu'uoina Heiau at sea level during spring tides. 35
Figure 24. Joint probability model of tide and runup: smooth PDFs of tide (part A) and wave height (part B) are constructed from empirical PDFs. The wave height PDF is translated into a runup PDF (part C). The total water level PDF is then constructed as the convolution of the tide and runup PDFs (part D). 36
Figure 25. Exceedance curves for runup only, a combination of tide and runup, and for a combination of tide, runup and sea-level rise (SLR). Vertical differences (lines of constant elevation) between curves represent the increase in frequency of one curve vs. the other. Horizontal changes (lines of constant frequency) represent the increase in severity. If a curve is translated on the x-axis, the amount that it is translated represents the scenario of future sea-level rise. 37
Figure 26. The increase in frequency of overtopping vs. elevation for the sea-level rise (SLR) scenarios of +0.25, +0.5, +0.75, and +1.0 m. Elevation 1 is at 1.5 m, elevation 2 is at 2 m, and elevation 3 is at 2.25 m. 38

Figure 27. Kaloko Seawall overwash on a moderate south swell at high tide. 39
Figure 28. Coastal hazards for Kawaihae Bay, Hawai'i (from Fletcher et al. 2002).. Pu'ukoholā Heiau NHS is part of Kawaihae. The map shows 7 natural hazards, including tsunami hazards (http://pubs.usgs.gov/imap/i2761/). 42
Figure 29. Coastal hazards for Keahole (A) and Kailua-Kona (B), Hawai'i (from Fletcher et al. 2002).. Kaloko-Honokōhau NHP is part of Keahole and Kailua-Kona. The map shows 7 natural hazards, including tsunami hazards (http://pubs.usgs.gov/imap/i2761/). 43
Figure 30. 1946 Alaska Aleutian tsunami scenario modeled water-levels for the Hawaiian Island regional grid at Pu'ukoholā Heiau NHS and Kaloko-Honokōhau NHP using Delft3D. 44
Figure 31. The maximum water levels of the 1946 tsunami model. 45
Figure 32. Maximum 1946 tsunami scenario water levels at Pu'ukoholā Heiau NHS modeled by Delft3D. 46
Figure 33. Maximum 1946 tsunami scenario water levels at Kaloko-Honokōhau NHP modeled by Delft3D. 47
Figure 34. 1946 tsunami scenario maximum inundation contours at Pu'ukoholā Heiau NHS. 48
Figure 35. 1946 tsunami scenario maximum inundation contours at Kaloko-Honokōhau NHP. 49
Figure 36. Elevation source data extents for Pu'ukoholā Heiau NHS (left) and Kaloko-Honokōhau NHP (right). White space indicates No Data while the dark blue features were added into the final DEM from the extracted features product of the FEMA LiDAR datasets. 52
Figure 37. 0. 5 m horizontal resolution hillshade characterizations of the final C-DEMs for Pu'ukoholā Heiau NHS (left) and Kaloko-Honokōhau NHP (right). These DEMS are composites of SHOALS LiDAR (bathymetric), FEMA terrain LiDAR, and USGS 10 m DEM data. 52
Figure 38. EX fit at each transect. The rates are modeled spatially along the transect location, but are constant through time. 57
Figure 39. EXT fit at each transect. The rates are modeled spatially along the transect location, and are modeled with a quadratic fit though time. 57
Figure 40. Maliu Point to north of 'Aimakapā Fishpond shoreline positions, transects and results. Shoreline change rates are displayed in graph form offshore. Each bar corresponds to a transect location (yellow shore-normal lines) on the shoreline. Negative rates (erosion) are indicated in red. Positive rates (accretion) are indicated in blue. 58
Figure 41. North of Kaloko Fishpond shoreline positions, transects and results. Shoreline change rates are displayed in graph form offshore. Each bar corresponds to a transect location (yellow shore-normal lines) on the shoreline. Negative rates (erosion) are indicated in red. Positive rates (accretion) are indicated in blue. 59
Figure 42. Pelekane Beach shoreline positions, transects and results. Shoreline change rates are displayed in graphs offshore. Each bar corresponds to a transect location (yellow shore-normal lines) on the shoreline. Negative rates (erosion) are indicated in red. Positive rates (accretion) are indicated in blue. 60
Figure 43. Ohaiula Beach shoreline positions, transects and results. Shoreline change rates are displayed in graphs offshore. Each bar corresponds to a transect location (yellow shore-normal lines) on the shoreline. Negative rates (erosion) are indicated in red. Positive rates (accretion) are indicated in blue. 61

List of Tables

TABLE 1. The observed maximum annually recurring significant wave heights(Hs) in meters and the largest 10% ($H_{1/10}$) and 1% ($H_{1/100}$)wave heights for various directions around Hawai'i. GEV is the Generalized Extreme Value Analysis.....6
TABLE 2. Hierarchy of sea-level rise scenarios. 7
TABLE 3. Wave and runup summary of Pu'ukoholā Heiau NHS and Kaloko-Honokōhau NHP.....12
TABLE 4. Boundary conditions of nearshore wave simulations using SWAN. Tr is the return period, Hs is the significant wave height, Tp is the wave period and Dir is direction.....12
TABLE 5. Nearshore wave and runup modeling summaries for Pu'ukoholā HeiauNHS. Tr is the return period and Hs is the significant wave height. 16
TABLE 6. Nearshore wave and runup modeling summaries for Kaloko-Honokōhau NHP.....16
TABLE 7. Overtopping frequencies and the influence of sea-level rise (SLR) for historic structures and beach profiles at Kaloko-Honokōhau NHP. 17
TABLE 8. Range of errors for Kaloko-Honokōhau NHP and Pu'ukoholā Heiau NHS.....54
TABLE 9. Imagery acquired for Pu'ukoholā Heiau NHS and Kaloko-Honokōhau NHP areas. Delineated into two groups: Reference Imagery and Processed Imagery. 55

Executive Summary

This report accompanies the digital hazard posters for Pu‘ukoholā Heiau National Historic Site (Pu‘ukoholā Heiau NHS or PUHE) and Kaloko-Honokōhau National Historical Park (Kaloko-Honokōhau NHP or KAHO) on the island of Hawai‘i. It contains information relevant to resource management and scientific research.

The Hawaiian Islands are seldom directly hit by hurricanes. However, high waves from low-pressure systems and other storms affect the coastline on a regular basis. As sea level rises, these high wave events will have further impacts on the coast, which will threaten the ecology and cultural resources found in this region. For planning and emergency response purposes, the National Park Service (NPS) requested that the University of Hawaii Coastal Geology Group and USGS complete an assessment of coastal vulnerability to wave overtopping, sea-level rise, and flooding for two national park units in the Pacific Islands Network (PACN). By identifying vulnerable sections within these parks, NPS managers can identify and document cultural structures that might be threatened and plan safety protocols when storms approach. Storm vulnerability assessments are completed for Pu‘ukoholā Heiau National Historic Site (Pu‘ukoholā Heiau NHS or PUHE) and Kaloko-Honokōhau National Historical Park (Kaloko-Honokōhau NHP or KAHO) on the Island of Hawai‘i.

This report includes assessment of the current shoreline morphology and several coastal hazards at the National Parks. The addressed hazards are coastal inundation and overtopping from large swells, sea-level rise, tsunamis, and coastal erosion. This report includes an interpretation of the results and provides explanations regarding coastal hazards. Products also include maps of historical shoreline change showing coastal erosion areas for each park and a paleotsunami evaluation.

Scope of work

One goal of this project is to generate maps revealing areas vulnerable to storms, extreme wave events, and sea-level rise. Other objectives include viewing the shoreline morphology through digital elevation models and producing posters that depict rates of shoreline change for each park. The approach taken for each hazard assessment in this report is listed below:

- *Coastal Inundation Maps (wave over-topping, sea-level rise and tsunami)*
  A time series of overtopping frequencies are provided using various published sea level scenarios (e.g., IPCC, 2007; Rahmstorf, 2007, and others). Inundation by tsunami is numerically modeled using the 1946 Gulf of Alaska source event as a base scenario. Overtopping and tsunami inundation hazard areas are defined on maps for each park.
- *Shoreline Morphology*
  Digital elevation models of shoreline morphology including photogrammetry and interpretive layers will be provided for the parks.
- *Historical Shoreline Change and Coastal Erosion*
  A 50-year projection of shoreline change is produced in the form of a poster. Deliverables consist of maps for each park showing modern change rates spaced 20 m along the shore and a 2050 erosion hazard zone at 95% probability.
- *Paleotsunami assessment*
  Evaluation of paleotsunami history is included within the tsunami hazard section.

Results and Recommendations

Regions of the parks vulnerable to many or specific coastal hazards are detailed in this report. A description of specific areas that are vulnerable to coastal hazards is provided along with recommended mitigation steps. For both parks, potential tsunami hazards appear to be minimal. However, impacts to Pelekane Beach at Pu‘ukoholā Heiau NHS have the greatest threat of damage to historical and cultural sections of the park. Both parks will also see an increase in the frequency of wave overtopping due to sea-level rise.

Sea-level rise is a subtle process and there may not be a clear trigger for adaptive management. Most likely, seasonal wave damage will increase and this will be the clearest indication. In order to prevent a state of disrepair and preserve key coastal features and points of interest, park personnel should monitor regions vulnerable to coastal impacts detailed in this report. Ideally, monitoring should last 25-50 years. For areas that will be flooded or submerged in the future due to sea-level rise, continuous monitoring of the wave action should start now. Begin monitoring the vulnerable areas during maximum annual high tide events (monitoring should start a few days before the high tide event) and large swell events. Use photography to record the wave wash and any damage associated with it, beach profiles to record the beach shape (if a beach exists), and differential GPS on archeological sites. As sea level rises with time, increase the frequency of monitoring. If enough erosion or inundation and overtopping events threaten the archeological sites, coordinate with local agencies to determine if the historic sites should be preserved in the short- (or long-) term. If preservation of the sites is the goal, consider enacting active measures (e.g. sandbagging).

The Ala Kahakai National Historic Trail (NHT) along the Pu‘ukoholā Heiau NHS coast will see a higher frequency in flooding due to sea-level rise. The trail at Pelekane currently experiences wave spray and overwash on a yearly basis, with visible erosion and root exposure seaward of the trail. The southern end of the trail may experience wave spray and overwash at sea-level conditions of 0.5 – 1 m and greater.

At Pu‘ukoholā Heiau NHS, Pelekane Bay and the remaining archeological sites are threatened by coastal hazards. Wave runup at sea-level scenarios of 0.25 – 0.5 m will extend inland under the trees at Pelekane beach. This will cause extensive erosion and tree loss.

Erosion and sea-level rise above 0.5 m will cause the beach to be mostly submerged at high tide. As sea level rises to 1m, the beach at its present state will be constantly submerged. The archeological sites at Pelekane will be exposed to wave overwash and spray at sea-level scenarios of 0.5 – 1 m. At sea-level rise greater than 1 m, the sites may be submerged at high tide.

The kuapā (seawall) at Kaloko Fishpond, the beach seaward of ‘Aimakapā Fishpond, and the archeological sites at the southern portion of Kaloko-Honokōhau NHP including the ‘Ai‘ōpio Fishtrap and Pu`uoina Heiau are the historic sites and features that are at greatest risk to deterioration from coastal hazards. Kaloko seawall and the northern section of Honokōhau beach incur the largest risk of overtopping and deterioration from wave impacts because they are at the park’s lowest elevation. Currently, Kaloko seawall experiences overwash and wave spray during small to moderate swell and high tides. Continual maintenance of Kaloko Seawall is recommended to prevent loss.

The beach fronting ‘Aimakapā Fishpond is eroding at average rates of 0.08 -0.15 m (0.25-0.5 ft) per year. If these rates continue and if sea level continues to rise, the fishpond will be breached by 2050, affecting the coastal trail and the ecology of the wetland habitat. The beach separates the fishpond from the ocean. Presently, areas of this beach are partially overtopped more than once a year. As sea level rises, the frequency of overwash will increase. At sea-level scenarios of 0.5 – 1 m, the entire beach will be fully overtopped several times a year, which may cause significant erosion and breaching of the sand barrier. Breaching will result in mixing seawater with groundwater, causing the salinity and nutrient levels of the estuary to be similar to seawater. The change in salinity and nutrient levels may pose a serious hazard to the park by impacting the flora and fauna of the estuary, including two federally endangered waterbirds. Monitoring salinity because of increased overtopping is recommended.

For ‘Ai‘ōpio Fishtrap, significant impacts such as flooding will occur during projected sea-level conditions. Since 1950, sand has been migrating north along Honokōhau Beach and out to ‘Aimakapā Fishpond, exposing several cultural sites to minor wave action. ‘Ai‘ōpio Fishtrap will be entirely submerged by 2100. The Heiau at ‘Ai‘ōpio Fishtrap will feel the effects of higher sea levels, but should not experience failure based on 2050 sea-level conditions.

Introduction

The following section briefly describes the regional geologic setting and coastal historic sites of Puʻukoholā Heiau NHS and Kaloko-Honokōhau NHP.

The mandate of the National Park Service is to: *"…conserve the scenery and the natural and historic objects and the wild life therein and to provide for the enjoyment of the same in such manner and by such means as will leave them unimpaired for the enjoyment of future generations." (The NPS Organic Act of 1916, 16 USC §1)*
In addition, the mission of Kaloko-Honokōhau NHP park enabling legislation is to perpetuate Hawaiian Culture and maintain/sustain fishponds and other cultural/recreational resources (beaches for canoe launching, ceremony, etc.). Coastal hazards including erosion, waves from large swell, hurricanes, tsunamis and sea-level rise threaten several National Parks and National Seashores on the United States coastline. To conserve such regions and allow for their enjoyment by future generations, it is important to assess the extent of coastal hazard vulnerability and manage such risks accordingly. This project details a coastal hazard analysis and assessment of Puʻukoholā Heiau NHS and Kaloko-Honokōhau NHP located on the Big Island of Hawaiʻi.

Background

Puʻukoholā Heiau NHS (PUHE) and Kaloko-Honokōhau NHP (KAHO) contain several natural and cultural landmarks including ancient Hawaiian Heiau, loko iʻa and loko kuapā (fishponds), and coastal wetlands of intrinsic value (Figure 1). Coastal hazards threaten the preservation of these landmarks. Thus, the goal of this project is to assess the risk of coastal hazards to the parks. The coastal hazards under evaluation include coastal erosion, waves from large swell, sea-level rise, and tsunamis.

Geologic setting

Puʻukoholā Heiau NHS and Kaloko-Honokōhau NHP, located at the base of the Kohala and Hualalai volcanoes (respectively), were created by basaltic lava flows with ages dating approximately 400,000 years and less than 3,000 years (respectively). Both regions receive little rainfall 250-760 mm (10- 30 in) per year (Giambelluca, et al. 1986).

Puʻukoholā Heiau NHS, being the older of the two regions, has fewer basaltic lava outcrops and a better developed topsoil. The northern beach of Puʻukoholā Heiau NHS near the historic site of Pelekane has a significant patch of trees and vegetation due to a small intermittent stream extending up the Kohala mountains, which is also likely to have continuous groundwater input. The shorelines of Puʻukoholā Heiau NHS consist of embayed beaches of carbonate sand located on the northern and southern portions of the park. The beaches of the park are backed by dry grass and trees.

Unlike Puʻukoholā Heiau NHS, Kaloko-Honokōhau NHP has numerous basaltic lava outcrops, and little topsoil cover. Kaloko-Honokōhau NHP also contains more green vegetation and trees fed by significant groundwater input. The shorelines of Kaloko-Honokōhau NHP are mostly perched beaches of basaltic lava flows, which are heavily encroached by salt tolerant vegetation. The beach fronting the ʻAimakapā Fishpond is the largest sandy beach of the park, with a width of about 32 m (105 ft) and a maximum height of 3 m (10 ft) above Mean Lower Low Water (MLLW). This beach is a natural barrier between the ʻAimakapā Fishpond and the ocean.

Coastal historic sites

Our hazard assessment for the parks has found coastal historic sites to be at risk. At Puʻukoholā Heiau NHS, the beach at Pelekane Bay, as well as the remaining archeological sites, are threatened by coastal hazards.

The kuapā (seawall) at Kaloko Fishpond, the beach fronting the ʻAimakapā Fishpond, and the archeological sites at the southern portion of the Kaloko-Honokōhau NHP including the ʻAiʻōpio Fishtrap and Puʻuoina Heiau are the historic sites and features that are at greatest risk to deterioration from coastal hazards. The Kaloko Fishpond is fronted by a seawall or kuapā that is approximately 9 m (30 ft) wide and a maximum height of 2 m (6.5 ft) above Mean Lower Low Water (MLLW). There are also a number of significant historic and cultural sites in the southern end (near the harbor entrance) of Kaloko-Honokōhau NHP, including ʻAiʻōpio Fishtrap, Puʻuoina Heiau, and other significant archeological structures.

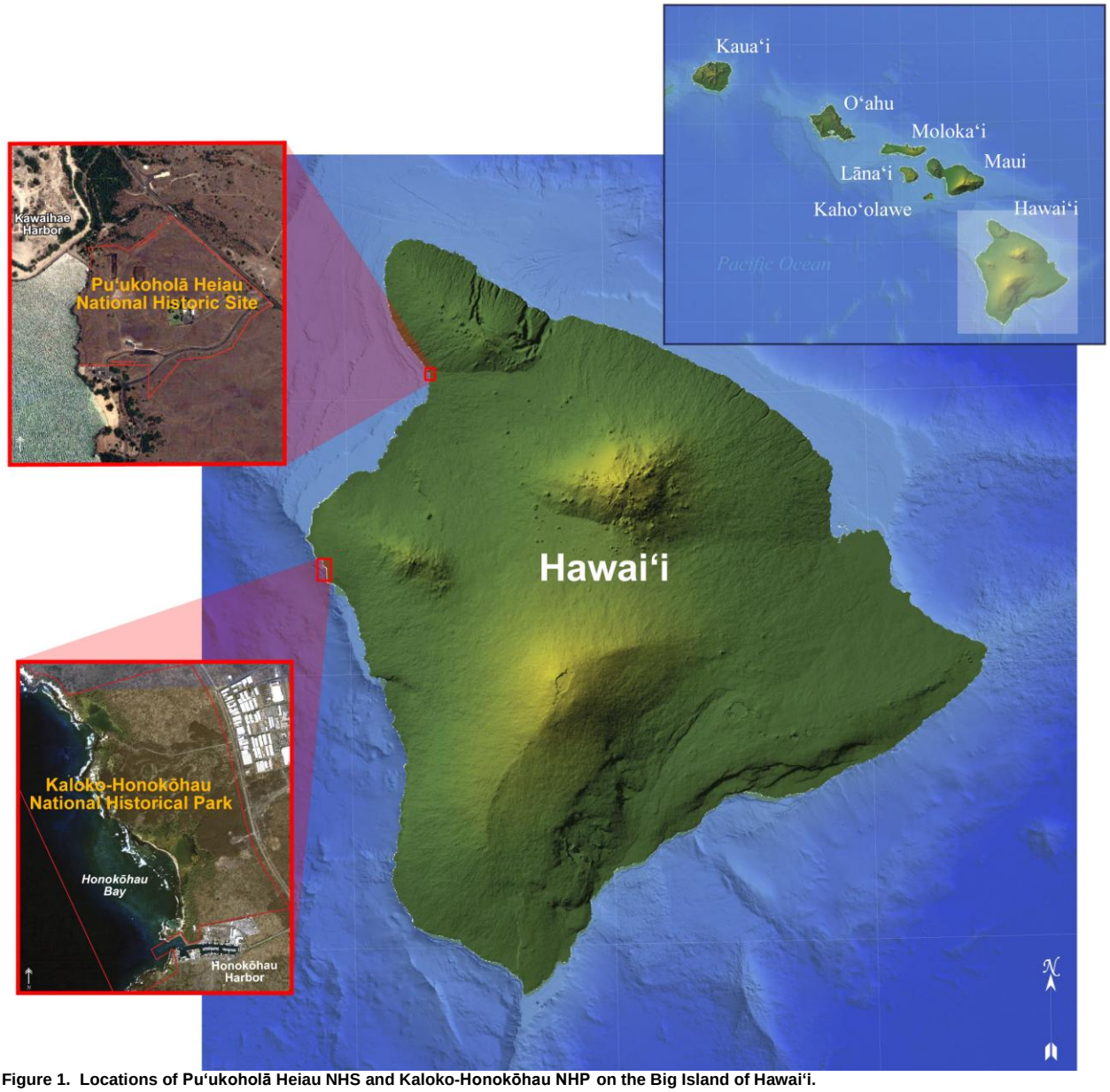

Figure 1. Locations of Pu‘ukoholā Heiau NHS and Kaloko-Honokōhau NHP on the Big Island of Hawai‘i.

Wave Climate

The following section briefly describes the wave regime of Pu‘ukoholā Heiau NHS and Kaloko-Honokōhau NHP.

Pu‘ukoholā Heiau NHS and Kaloko-Honokōhau NHP are located on the Kohala and Kona coasts (respectively) of the Big Island of Hawai‘i. These coasts are primarily west facing coastlines, and receive large north and south Pacific swell during winter and summer months respectively. These large swells produce coastal impacts in the form of coastal erosion, overtopping and inundation. However the nature of these impacts is seasonal: they occur during high swell season, and are followed by calm conditions which favor recovery. Thus to understand the seasonal nature of the waves and coastal impacts, we must investigate the seasonal nature of the occurrence of large swell in Hawai‘i. The following is a description of the Hawaiian wave cycle and how it affects the coastal hazards at Pu‘ukoholā Heiau NHS and Kaloko-Honokōhau NHP.

Hawaiian swell regimes

The four dominant regimes responsible for large swells in Hawai‘i are: north Pacific swell, trade wind swell, south swell, and Kona storms. The regions of influence of these regimes, outlined by Moberly & Chamberlain (1964), are shown in Figure 2. A wave rose depicting annual swell heights and directions (Vitousek & Fletcher 2008) has been added to their original graphic. The average directional wave spectrum in Hawaiian waters is bimodal and dominated by the north Pacific and trade wind swell regimes (Aucan 2006). Although quite important to the complete Hawaiian wave climate, south swell and Kona storm regimes do not occur with comparative magnitude and frequency as north Pacific and trade wind swell regimes. The Hawai‘i buoy network from the National Oceanic and Atmospheric Administration (NOAA) National Data Buoy Center (NDBC), shown in Figure 2, provides data for understanding the local wave climate. Buoy reports are available via the World Wide Web at: http://www.ndbc.noaa.gov/maps/Hawaii.shtml.

Inter-annual and decadal cycles including El Niño Southern Oscillation (ENSO) occurring approximately every three to four years (Goddard & Graham 1997), and Pacific Decadal Oscillation (PDO) occurring around 20-30 years (Mantua et al. 1997; Zhang et al. 1997), influence the variability of the Hawaiian wave climate. These large-scale oceanic and atmospheric phenomena are thought to control the magnitude and frequency of extreme swell events. For example, strong ENSO events are thought to result in larger and more frequent swell events (Seymour et al. 1984, Caldwell 1992, Inman and Jenkins 1997, Seymore 1998, Allan & Komar 2000, Wang & Swail 2001, Graham & Diaz 2001, Aucan 2006). Understanding the magnitude and frequency of extreme wave events is important as they may control processes such as coral development (Dollar & Tribble 1993, Rooney et al. 2004), sediment supply (Harney et al. 2000, Harney & Fletcher 2003) and beach morphology in Hawai‘i and abroad (Moberly & Chamberlain 1964, Ruggiero et al. 1997, Kaminsky et al. 1998, Storlazzi and Griggs 2000, Rooney & Fletcher 2005, Ruggiero et al. 2005).

North Pacific swell

Hawai‘i, located in the middle of a large swell-generating basin, the north Pacific, receives large ocean swell from extra-tropical storms that track predominantly eastward from origins in the northwest Pacific. The north Pacific storminess reaches a peak in the boreal winter, as the Aleutian low intensifies and the north Pacific high moves southward. The strong winds associated with these storms produce large swell events, which can travel for thousands of miles until reaching the shores of Hawai‘i. In summer months, the north Pacific high moves northward and storms in the north Pacific become infrequent (Flament et al. 1996). Figure 3 shows the satellite-derived wave average heights over the north Pacific in the winter and summer. The average winter wave heights in the north Pacific are approximately ≥3 m while the summer wave heights are approximately ≤2 m. Figure 3 gives the average wave heights of the north Pacific, however the dynamic system typically involves individual storm events tracking eastward with wave heights of 5-10 m. These swell-producing storms occur during winter months with typical periods of 1-1.5 weeks (for 5-7 m swells), 2-3 weeks for (for 7-9 m swells) and one month (for swells 9 m or greater). Many north Pacific storms produce swells that do not reach Hawai‘i. Storms that originate in high latitudes and those that track to the northeast send swells to the Aleutians and the Pacific Northwest. Swells that originate from storms in lower latitudes, and those that track slightly to the southeast, reach Hawai‘i with the largest wave heights.

Hawai‘i receives north Pacific swell with an annually recurring maximum deep-water significant wave height of 7.7 m (Vitousek & Fletcher 2008) with peak periods of 14-18 sec. However, the size and number of swell events in Hawai‘i each year is highly variable – varying by a factor of 2 (Caldwell 2005). The annual maximum wave height recorded from buoy 51001 ranges from about 6.8 m (in 1994, 1997, 2001) to 12.3 m (1988).

The seasonal cycle of north Pacific swell reaches a peak in winter and a trough in summer, with a daily average significant wave height around 4 m. Aucan (2006) depicted the monthly average directional spectra from buoy data at Waimea (buoy 51201) and Mokapu (buoy 51202) that showed the dominance of north Pacific swell out of the northwest in winter months, and relatively persistent energy out of the northeast associated with trade wind swell. Buoy locations can be seen via the World Wide Web at: http://www.ndbc.noaa.gov/maps/Hawaii.shtml.

Trade winds and trade-wind swell

Occurring about 75% of the year, the trade winds are northeasterly winds with an average speed of 15.7 mph and direction 73° with standard deviations (1s) of 5 mph and 23°. In winter months, the north Pacific high flattens and moves closer to the islands decreasing trade wind persistence. Although the number of windy days in summer months increases, the mean trade-wind speed in summer and winter months remains relatively similar (**Figure 4**).

The persistent trades generate limited fetch trade wind swell on northeast facing coasts. Choppy seas with average wave heights of 2 m (1s = 0.5 m) and peak periods of 9 sec. (1s = 2.5 sec.) from the northeast characterize trade wind swell in Hawai‘i. Although these represent nominal conditions, trade-wind swell can exceed 5 m in height and have periods of 15-20 sec.

Southern swell

Southern swell arriving in Hawai‘i is typically generated farther away than north Pacific swell. These swells are usually generated from storms south of the equator near Australia, New Zealand and as far as the Southern Ocean and propagate to Hawai‘i with little attenuation outside the storm-generated region (Snodgrass et al. 1966). South swell occur in summer months (Southern hemisphere winter months) and reach Hawai‘i with an annual significant wave height of 2.5-3 m and peak periods of 14-22 sec, which are slightly longer than north Pacific swell (Armstrong 1983, Vitousek & Fletcher 2008).

Kona storms

Giambelluca & Schroeder (1998) describe Kona storms as:

"low-pressure areas (cyclones) of subtropical origin that usually develop northwest of Hawai‘i in winter and move slowly eastward, accompanied by southerly winds from whose direction the storm derives its name, and by the clouds and rain that have made these storms synonymous with bad weather in Hawai‘i".

Strong Kona storms generate wave heights of 3-4 m and periods of 8-11 sec., along with wind and rain, and can cause extensive damage to south and west facing shores (Rooney & Fletcher 2005). While minor Kona storms occur practically every year in Hawai‘i, major Kona storms producing strong winds, large wave heights and resulting shoreline change tend to occur every 5-10 years, during the 20-30 year negative PDO cycle (Rooney & Fletcher 2005). Consequently, Positive (warm) PDO, and El Niño phases tend to suppress Kona storm activity (Rooney & Fletcher 2005).

Maximum annual recurring wave heights in Hawai‘i

Although each wave regime (trade wind swell, north Pacific swell, south swell, and Kona storms) has its own underlying processes and mechanics, the sum of all of these regimes contribute to the wave heights and shoreline change in Hawai‘i. Thus evaluating extreme wave heights on a continuous scale around these islands is informative. Breaking waves at the shoreline are often composed of many swell sources from different storms and swell regimes. North Pacific (south) swell and trade wind swell are the most common sources of swell for north (south) facing shores. Thus the spectral approach to understanding swell and surf patterns, following Aucan (2006), is quite informative.

The maximum annually recurring significant wave heights and the largest 10% and 1% wave heights for various directions in 30° windows around Hawai‘i are given in Table 1 (Vitousek & Fletcher 2008). These annual wave heights are also depicted in Figure 2**.**

TABLE 1. The observed maximum annually recurring significant wave heights(Hs) in meters and the largest 10% ($H_{1/10}$) and 1% ($H_{1/100}$)wave heights for various directions around Hawai‘i. GEV is the Generalized Extreme Value Analysis.

Wave Direction		***Annual Hs (m) – GEV Model***		
Lower	Upper	Observed - H_s	$H_{1/10}$	$H_{1/100}$
0	30	5.9	7.4	9.8
30	60	6.0	7.6	10.0
60	90	5.1	6.5	8.5
90	120	4.3	5.5	7.2
120	150	2.8	3.5	4.6
150	180	3.0	3.8	5.0
180	210	2.4	3.0	3.9
210	240	1.6	2.0	2.7
240	270	1.5	1.9	2.5
270	300	3.7	4.7	6.2
300	330	5.9	7.5	9.9
330	360	5.8	7.4	9.7

Tides

The tides result from the varying gravitational attraction of the Earth to the Moon and Sun during orbit. Tides are composed as a sum of sinusoidal components that typically have their largest variability in diurnal (one cycle per day) and semi-diurnal (two cycles per day) frequencies. Large gravitational forces and maximum tides are also produced when the Earth, Moon, Sun system are aligned (referred to as syzygy). Conversely, minimal gravitational forces and tides result when the Earth, Moon, Sun systems are at right angles (referred to as quadrature). This alignment occurs on a monthly cycle as related to the moon phases in Hawai‘i, and periods when the tides are the largest (smallest) are referred to as spring (neap) cycles. The tide range in Hawai‘i is quite small compared with the rest the world, having a typical tide range [Mean Higher High Water (MHHW)– Mean Lower Low Water (MLLW)] of 0.58 m and a spring tide range around 1.0 m.

The astronomic tide typically represents the largest water level variability at a particular location. However other factors such as atmospheric pressure, wind setup, ENSO cycles, and oceanic disturbances can produce water level variability on the order of tens of centimeters. One important process influencing extreme sea level events in Hawai‘i is the occurrence of mesoscale eddies, which are large oceanic disturbances (a few hundred km in diameter), having elevated sea levels of around 15 cm (Firing & Merrifield 2004).

Coincidence of waves and tides

Coincidence of large swell and high tide events can cause severe coastal flooding and overtopping in Hawai‘i, whereas swell events occurring on low tides or neap cycles can be less severe (Caldwell et al. 2008). Using joint probabilities of wave and tide distributions, Caldwell et al. (2008) found the number of hours a particular combination of surf height and tide level are expected to be exceeded. We will employ a similar approach to estimating the overtopping frequency and severity for the parks.

Runup and inundation

We are most interested in the recurrence of high surf events because these events control many natural beach processes like rip current formation, erosion, and reef growth. Additionally the high surf events pose significant risk to coastal communities and ocean users in the form of overtopping and coastal flooding due to large runup events, property damage and drowning and ocean safety concerns. Wave runup is the maximum vertical height of the wave on a beach, and is influenced by the wave swash and setup. Coastal events such as tsunamis and hurricanes pose the greatest potential hazards in terms of the magnitude of flooding, property damage and loss of life; however they are rare (occurring with return periods of several decades) compared with high surf events, which occur several times per year. Many sources contribute to the maximum water level on a beach, including tide, wave setup, wave runup and other sources of water level variability (mesoscale eddies, sea-level rise). Coincidence of large swell and tide events can cause severe coastal flooding and overtopping in Hawai‘i (Caldwell et al. 2008).

Sea-level rise

Sea-level rise is a significant coastal hazard. If we consider sea-level rise as a coastal hazard alone, then low-lying coastal lands will be at greatest risk to sea-level impacts in the form of passive flooding. The time horizons for such impacts are often distant, relative to the rate of sea-level rise and the elevation of structures at risk. However considering sea-level rise as a coastal hazard interacting with large wave and tide events, we see that potential impacts due to sea-level rise (in the form of increased overtopping frequency associated erosion and shoreline change) appear on a much shorter time horizon.

There is much debate over quantifying potential sea-level rise scenarios. The IPCC has estimated six sea-level rise scenarios, which predict a range of sea levels from 0.1 - 0.88 m by 2100 (based on data and various climate models). Rahmstorf (2007) estimates sea-level scenarios of 0.5 - 1.4 m by 2100 (based on a fit of global temperature to sea-level and the projection of IPCC temperature predictions). Church & White (2006) found global sea-level to rise almost 20 cm between 1870 and 2004 based on data from tide gauges, and estimated 0.28 – 0.34 m of sea-level rise by 2100 based on a constant acceleration rate of 0.013 mm/yr^2 from the historical data. Beckley et al. (2007), using satellite altimetry, found global sea-level rise rates increased from ~2.75 mm/yr (during 1993-2000) to ~3.75 mm/yr (during 2000-2007).

If we consider Hawai‘i as an isolated region in terms of global sea level and examine its unique sea-level history we see that sea-level rise ranges from ~1.4 mm/yr to ~3.8 mm/yr (Figure 5**)**. The sea-level rise rates for the Big Island (and islands close to it) are larger than the rest of the islands due to island subsidence. The tide gauge at Kawaihae Harbor, near Pu‘ukoholā Heiau NHS, on the Big Island has reported the largest sea-level rise rate of 3.8 mm/yr. It is also the gauge with the shortest observation record. If we consider the Big Island to experience a sea-level rise rate that is the average of the Hilo and Kawaihae we find a rate of ~ 3.5 mm/yr. We have determined a hierarchy of sea-level rise scenarios based on rates found from Big Island tide gauges and global acceleration terms reported in the literature. The future sea-level predictions based on these scenarios are reported in Table 2.

TABLE 2. Hierarchy of sea-level rise scenarios.

Mean Sea Level (MSL) increase [in m] relative to present (2008)					
Scenario	*Rate (mm/yr)*	*Acceleration (mm/yr^2)*	***2025** (m)*	***2050** (m)*	***2100** (m)*
Modest	3.5	0	0.06	0.15	0.32
Probable	4	0.013	0.07	0.19	0.48
Extreme	4	0.14	0.11	0.41	1.55

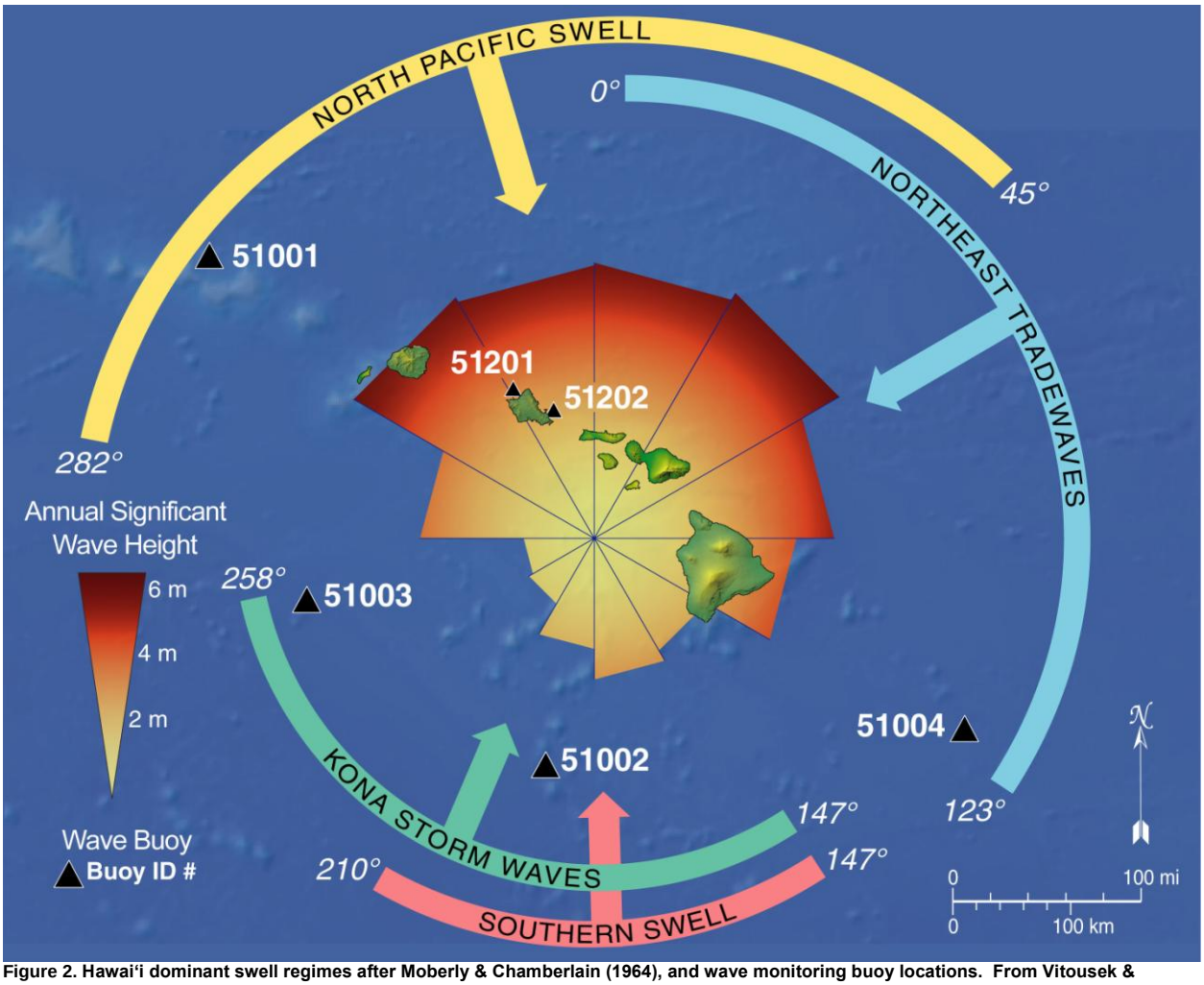

Figure 2. Hawai'i dominant swell regimes after Moberly & Chamberlain (1964), and wave monitoring buoy locations. From Vitousek & Fletcher (2008).

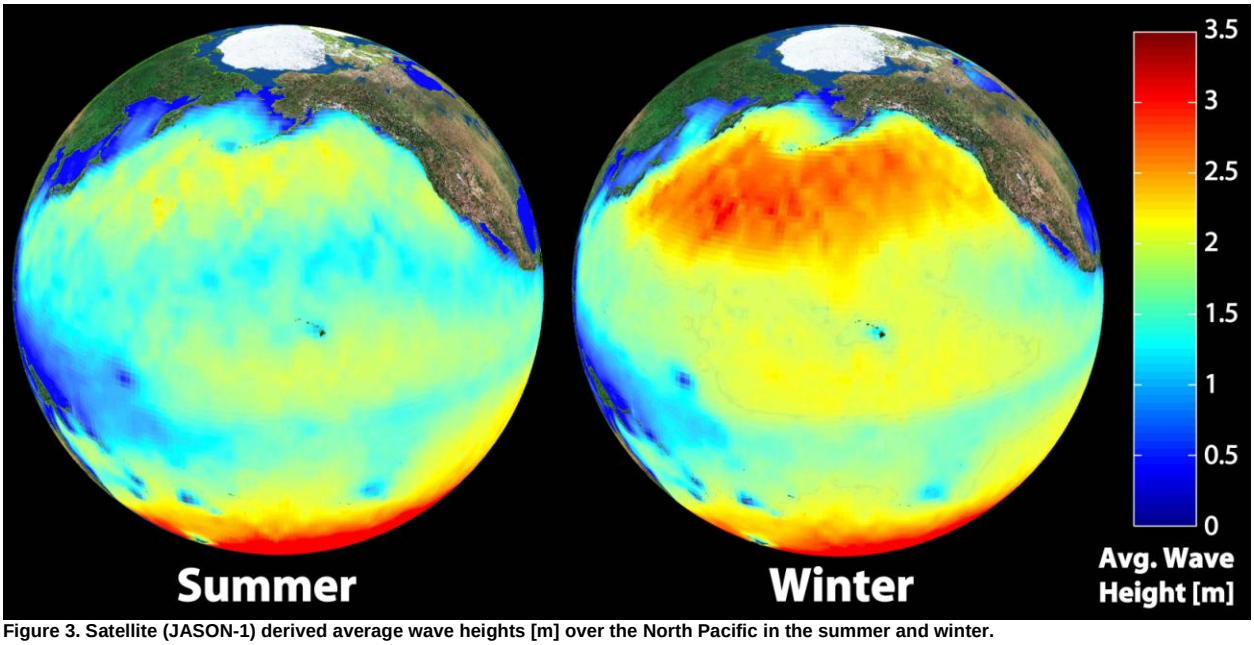

Figure 3. Satellite (JASON-1) derived average wave heights [m] over the North Pacific in the summer and winter.

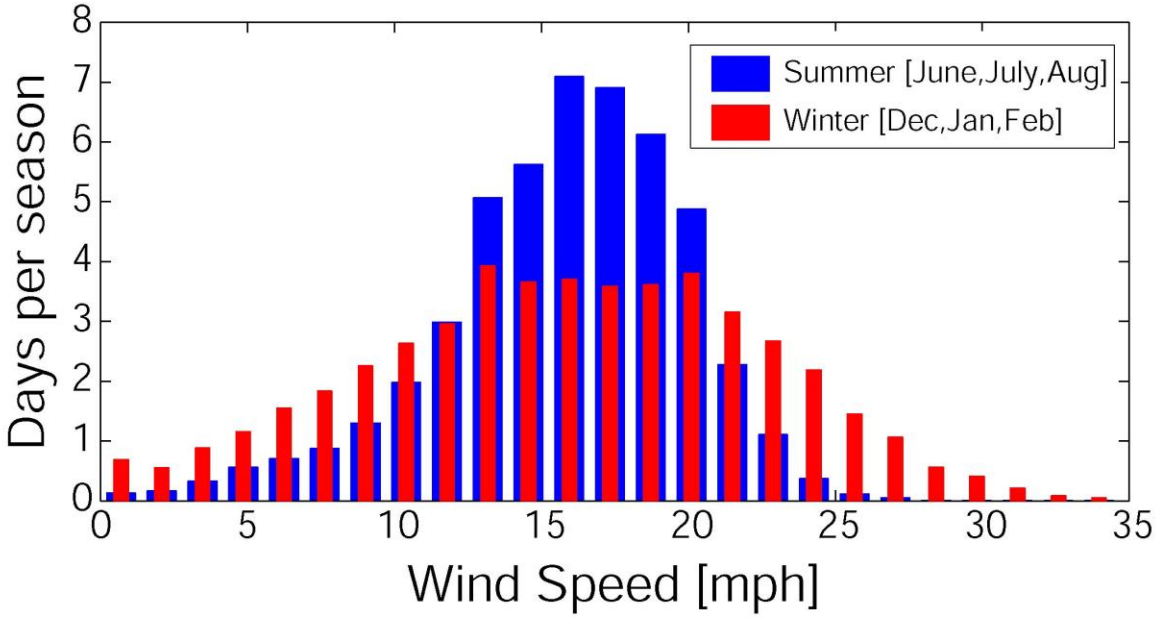

Figure 4. The number of days per season that the trade winds occur with a certain speed (data from Buoy 51001). The days per season are shown in red for winter months and blue for summer months. Notice the persistence of typical trade winds (~ 16 mph) during summer months.

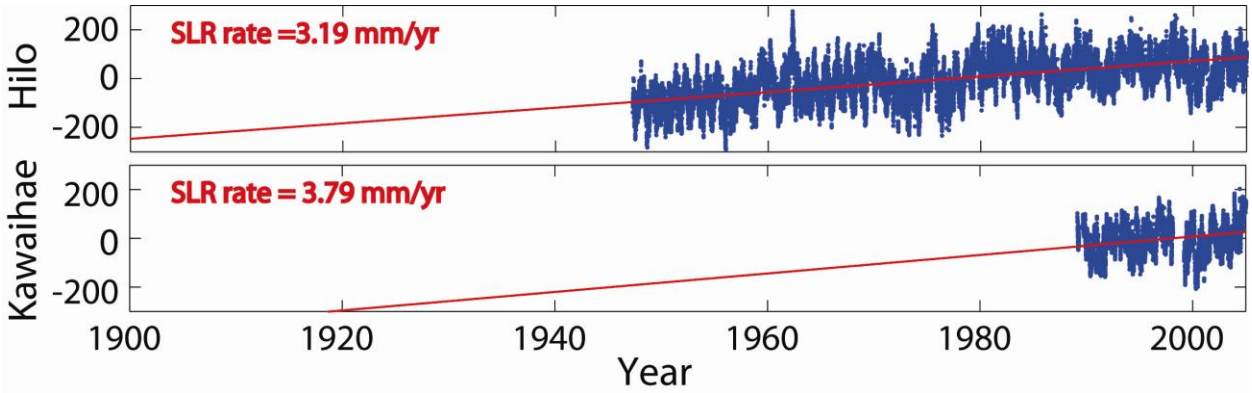

Figure 5. Sea-level history [mm] in Hawai‘i as observed from several tide gauges.

Coastal Inundation, Overtopping of Swells and Sea-level Rise

This section describes the methods and results for inundation, overtopping of swells and sea-level rise at Pu‘ukoholā Heiau NHS and Kaloko-Honokōhau NHP.

Modeling the wave cycle of the Big Island of Hawai‘i

It is important to keep in mind that the annually recurring maximum wave (swell) heights (Figure 2 or Table 1) represent open ocean, deep-water wave heights that are unaffected by the presence of the other islands. Because seven of the main eight Hawaiian Islands lie to the northwest of the Big Island, significant blockage (i.e., shadowing) and reduction in nearshore wave heights occurs. Therefore adequate modeling of the wave transformation from deep-water to the nearshore, particularly to capture the reduction in wave height due to island blockage, is important. The ultimate goal of the wave transformation model is to find the maximum annually recurring wave heights in the nearshore at the study sites. These wave heights will provide the boundary conditions (initial assumptions of wave heights) for runup modeling. Without island blockage, the maximum annual wave height would occur from the northwest and the north, somewhere between 300° and 60° as found simply from the annual wave heights (Figure 2, Table 1). However, using this information directly would overestimate the annual wave heights near the national park sites. Instead, we use the information of the open annually recurring maximum wave heights found in Figure 2 or Table 1, as the required boundary conditions (starting point) for nearshore wave transformation modeling.

To model the wave transformation from deep-water to nearshore we use the SWAN (Simulating WAves Nearshore) model, which is widely used within the oceanographic and wave forecasting community. Details on the development and validation of the SWAN model are reported in Booij et al. (1999) and Ris et al. (1999).

To find the maximum annually recurring wave height and direction near the study sites we ran 85 model simulations of the wave field for the Big Island (spatial resolution of 1 km), each of which is nested in the model for the main eight Hawaiian Islands (spatial resolution of 3.5 km). Nesting brings open ocean wave height data to the nearshore environment. The 85 simulations were run in 2.5^o directional increments for the south to northeast window (clockwise) from 195° to 45° with maximum annual significant wave heights interpolated from values of the wave heights found in Table 1. Four of the 85 simulations representing different annual wave heights from particular directions are shown in Figure 6.

The goal of these 85 different simulations is to find the maximum annually recurring wave height as a function of wave direction at the national park sites. Plotting the annual significant wave height as a function of wave angle for virtual buoys near the national park sites, we find a maximum annual significant height of 3.3 m from about 290° (Figure 7), for both Pu‘ukoholā Heiau NHS and Kaloko-Honokōhau NHP. The similarity between the wave heights for both Pu‘ukoholā Heiau NHS and Kaloko-Honokōhau NHP allow us to treat the recurrence relationships in a uniform manner rather than individually.

Coastal locations may receive large swell, or lie in the shadow of nearby islands and thus have reduced exposure to seasonal waves. The most important result from the directional annual wave height modeling is to characterize the island blockage and find the direction of maximum swell impact for the study sites. This occurs for the very westerly segment, 282°-305° of the North Pacific swell window shown in Figure 2. Knowing the swell window that results in the largest wave heights close to the national park sites, we can return to an extreme value analysis on the open-ocean buoy data (similar to the approach outlined in Vitousek & Fletcher 2008) to determine the relationship between the open swell deep-water wave height and the return period for the 282°-305° window (Figure 8).

Again, this analysis is relevant to deep-water open-ocean wave heights and thus it is necessary to transform these wave heights into nearshore wave heights near the national park sites using the SWAN model (model settings in Appendix A). The output from this model will give the relationship between significant wave height and return period; however this model will also include the effects of island blockage. The effective island blockage, or reduction in wave height, from this particular window (282°-305°) is about 20%. For more northerly directions, the reduction can increase to around 75% (Figure 7). The relevant relationship for the maximum recurring wave heights at the national park sites is given in Figure 9.

The maximum recurring wave heights are then translated to maximum recurring runup elevations at the national park sites using empirical equations following the approach of Vitousek et al. (2008). These empirical equations are best-fit relationships determined from field observations of wave height and runup, and are widely used in engineering computation for lack of a more robust physical or process-based approach. Our approach uses a recently developed equation for the 2% exceedance runup derived from 10 datasets primarily from the continental US, which we refer to as the Stockdon equation (Stockdon et al. 2006):

$$R_{2\%} = \langle \eta \rangle + S$$

$$R_{2\%} = 1.1\left(0.35\beta_f\left(H_o L_o\right)^{1/2} + \frac{\left[H_o L_o\left(0.563\beta_f^2 + 0.004\right)\right]^{1/2}}{2}\right),$$

which similarly gives runup as a function of beach slope (foreshore slope β_f), deep-water wave height (H_o), and deep-water wavelength (L_o). We use the Stockdon formula because it is complete: it formulates runup as

the sum of setup $<\eta>$, and swash S, due to both incident and infragravity energy. Wave setup is the increase in nearshore sea level due to the presence of waves, and it can be as large as 10-20% of the significant wave height. Swash is the wave action on the dry beach itself; it is composed of an incident part (at frequencies very close to that of the offshore waves) and an infragravity part (at frequencies much lower than the offshore waves).

The infragravity component can be as large as 10-20% of the significant wave height, while depending on the beach slope and breaking conditions the incident swash component can range from nothing (on fringing reefs or beaches with intense breaking) to larger than the offshore wave heights (on steep beaches with little or no breaking). Using the Stockdon equation, we find the following relationship between the maximum runup elevations and return period at the national park sites (Figure 10). The results for the wave and runup characteristics that exert the greatest influence on Pu‘ukoholā Heiau NHS and Kaloko-Honokōhau NHP are summarized in Table 3.

TABLE 3. Wave and runup summary of Pu‘ukoholā Heiau NHS and Kaloko-Honokōhau NHP.

Return period [years]	*Open Wave heights [m]*	*Local Wave heights [m]*	*Stockdon Runup [m]*
1	4.1	3.3	1.7
5	5.6	4.5	2.1
10	6.1	4.9	2.2
25	6.9	5.4	2.4
50	7.4	5.8	2.5

The Stockdon runup values (Table 3) may help explain the formation of perched beaches at Kaloko-Honokōhau NHP. Approximately 60% of the beaches at Kaloko-Honokōhau NHP are perched beaches (Hapke et al. 2005). The origins of perched beaches are not well understood, but are thought to be controlled by wave runup during large wave events and the elevation of the slope of the underlying rock platform (Hapke et al. 2005, Richmond et al. 2008). The perched beach behind Kaloko Point is at an elevation ranging from 1 to 3 m and is well within the Stockdon runup values.

The runup predicted by the Stockdon equation may not be the best way of predicting the runup at these particular locations. The equation was developed from datasets of mildly sloping barred beaches without fringing reefs, which are significantly different from many beaches in Hawai‘i. Both Pu‘ukoholā Heiau NHS and Kaloko-Honokōhau NHP have reefs (**see Appendix B**) that cause waves to break offshore, which will significantly reduce the incident swell energy, incident swash magnitude and overall runup compared to the predictions from the Stockdon equation.

To make better predictions of the runup we make simulations of nearshore wave fields using SWAN. The important features of the nearshore simulations we are looking for are the nearshore wave height, wavelength and wave setup. SWAN can accurately predict these features, although it cannot predict runup. To improve our predictions of runup we use the setup predicted from SWAN and add it to the incident swash component of the Stockdon equation with the nearshore wave heights in place of the deep-water wave heights, and include an infragravity term that comes from the offshore wave height rather than the nearshore wave height. Our modified equation for the 2% runup looks like the following:

$$R_{2\%} = <\eta> + S$$

$$R_{2\%} = <\eta>_{\text{SWAN}} + 1.1\left(\frac{.75\beta_f\left(H_n L_n\right)^{1/2}}{2} + .15H_o\right)$$

,

where β_f is the foreshore slope, which is given by LIDAR topography and bathymetry data, H_n is the nearshore significant wave height, H_o is the offshore (deep-water) significant wave height, and L_n is the nearshore wave length.

The nearshore significant wave height and wavelength for different return periods are modeled using SWAN and forced with deep-water boundary conditions determined from the analysis in Figure 9 and are summarized in Table 4.

TABLE 4. Boundary conditions of nearshore wave simulations using SWAN. Tr is the return period, Hs is the significant wave height, Tp is the wave period and Dir is direction.

Case	*Tr [yrs]*	*Hs [m]*	*Tp [s]*	*Dir [o]*
A	1	3.3	14	285
B	5	4.5	14.5	285
C	10	4.9	15	285
D	25	5.4	15.5	285
E	50	5.8	16	285

The modeling results from the five different cases are shown in the following figures. The wave (height, length, and setup) fields for Pu‘ukoholā Heiau NHS and Kaloko-Honokōhau NHP are shown in **Appendix B**.

Based on the results of the nearshore wave height, wavelength, and wave setup fields we can determine the regions that are protected from exposure to large offshore wave heights. These protected regions naturally happen to be the reef fronted areas. At Pu‘ukoholā Heiau NHS there is a significant offshore reef providing a barrier to the entire park. Kaloko-Honokōhau NHP has reef fronting the majority of the park, but it is not significant. Only the beach fronting the ‘Aimakapā Fishpond has a significant offshore reef (Gibbs et al. 2006). It is clear from the nearshore wave field that the

reef structure and bathymetry (shown in **Appendix B**) offshore of Puʻukoholā Heiau NHS is very efficient at dissipating wave energy. The offshore reef structure at Puʻukoholā Heiau NHS, classified as "spur and groove", is clearly identified from the characteristic fingers or "spurs" of corals extending offshore separated by pockets or "grooves" of sand (Cochran et al. 2006). The spur and groove structure at Puʻukoholā Heiau NHS is a function of the underlying lava flow with very little accreted reef. In addition to being a very rough hydraulic structure the spurs and grooves cause localized divergence and convergence, which directly or due to the breaking (respectively) lead to energy dissipation. The reef at Kaloko-Honokōhau NHP is much flatter and has less structure than Puʻukoholā Heiau NHS, which results in a much smoother wave field, less dissipation and larger wave heights nearshore. Because there is so much dissipation, and thus wave height and setup variability at Puʻukoholā Heiau NHS, we must consider the regions of the park separately in our runup and overtopping hazard analysis. At Kaloko-Honokōhau NHP we must consider the beach fronting the ʻAimakapā Fishpond separately, in contrast to the rest of the shoreline, which we expect to be exposed to runup levels consistent with those computed from the deep-water wave heights (Table 3, Figure 10). Summaries of the wave fields and total runup at Puʻukoholā Heiau NHS and Kaloko-Honokōhau NHP are given in Table 5 and Table 6.

Storlazzi & Presto (2005) and Presto et al. (2007) collected oceanographic data (e.g., directional wave data, water depth, current speed, current direction, etc.) at Kaloko-Honokōhau NHP. The largest significant wave height that they measured during their winter deployments was 2.26 m. Our one-year modeled significant wave height calculations range between 1 m and 2 m, which is in agreement with the collected wave data.

The values computed for the beach fronting ʻAimakapā Fishpond (Table 6) are very similar to the nominal runup values given in Table 3. This similarity is likely the result of the steep slopes on this portion of the beach, which lead to larger runup values.

Overtopping and Inundation Hazard

Based on the runup values for the different portions of both parks we can now create inundation maps showing the landward extent of the runup or the wash of the waves for a given return period. For particular areas of interest including the kuapā (seawall) at Kaloko Fishpond and the beach the ʻAimakapā Fishpond we will use a different method with estimates of the number hours per year that a structure is overtopped by waves. This method is more informative when the structure is overtopped much more frequently than once per year. The inundation maps based on the total runup levels computed in Table 5 and Table 6 are given in Figure 11, Figure 12, **Figure 13**, **Figure 14**, **Figure 15**, and **Figure 16**.

The inundation contours of the Puʻukoholā Heiau NHS shoreline from the beach at Pelekane Bay to the northern portion by Spencer Park are shown in Figure 11. This shoreline should be fairly resilient to large wave attack. It is rocky and steeply sloping and thus reaches a fairly high elevation very quickly. The contours of inundation do not extend very far inland at present sea level or under future sea-level scenarios. The slight impacts in the inundation map for the region in Figure 11 shows inundation of the Ala Kahakai National Historic Trail (NHT). The extent of the flooding of the trail does increase with sea-level rise. Particularly, the southern portions of Ala Kahakai NHT may begin to experience wave spray and overwash under future sea-level conditions of 0.5-1 m and greater. Ala Kahakai NHT at Pelekane appears to experience wave spray and overwash on a yearly basis; there is also clearly erosion and root exposure of the sand seaward of the coastal trail as shown in **Figure 17**. The erosion of the bank fronting the trail should be isolated to the trail near Pelekane beach. Rocky outcrops with vegetation and small amounts of topsoil above the seasonal wave wash are located in front of majority of the shoreline trail at Puʻukoholā Heiau NHS . This section of shoreline should be resistant to erosion and to future effects of sea-level rise.

The inundation contours of the beach at Pelekane Bay are shown in Figure 12. The annual inundation contour at present sea level extends to the base of the tree line of the beach. Several inundation lines at Pelekane Beach can be seen as evidenced by the multiple debris lines on the beach (Figure 18). Under future sea-level scenarios of 0.25-0.5 m, these runup contours will extend further inland under the trees. This runup will lead to significant erosion and tree loss. Eventually, through erosion and sea-level rise above 0.5 m, the beach will be mostly submerged at high tide. Under sea-level rise conditions above 1 m the beach in its present state will be constantly submerged. Additionally, under sea-level conditions of 0.5-1 m the archeological sites at Pelekane will be exposed to wave overwash and spray. Under sea-level conditions exceeding 1 m, the sites may be submerged under high tide.

The inundation contours of Spencer Beach Park are shown in **Figure 13**. The 5-year return period inundation contour at present sea level extends to the vegetation line and small rock wall backing the beach. Several inundation lines at Spencer Beach can be seen as evidenced by the multiple debris lines on the beach (Figure 19). Under future sea-level scenarios of 0.25-0.5 m, the overwash of the small rock wall will occur for greater than 5-10 yr. return period events. Under sea-level rise conditions above 1 m, the majority of the beach in its present state will be submerged or eroded close to the small rock wall barrier. The barrier itself will be overtopped several times per year during large swell events under this scenario.

The inundation contours of the Kaloko-Honokōhau NHP shoreline are shown in **Figure 14**. Kaloko-Honokōhau NHP is flat, low-lying, and exposed to significantly larger open swell than Puʻukoholā Heiau NHS, due to the lack of shallow reef fronting a majority of the park. As a result of such characteristics the park will likely be exposed to significant impact from sea-level rise scenarios in the form of increased erosion, deterioration of coastal historic sites and estuary and marsh ecosystem change. Under future sea-level scenarios of 0.25-0.5 m, the

overwash of the shoreline trail (a portion of the Ala Kahakai NHT) will increase in frequency. However, the impacts of this increase in overwash frequency should be fairly minimal for the rocky stretch of shoreline between the two fishponds due to the strong dissipation of wave and runup bore energy by basaltic lava outcrops along this portion of shoreline. Only under sea-level scenarios of 0.5 – 1+ m, which submerge many of the once exposed rocky outcrops, do significant impacts occur. **Figure 14** shows that the northern portion of the ‘Aimakapā Fishpond wetland will be constantly submerged under 0.5 – 1 m of sea-level rise. Currently there are low-lying areas in the park supporting thick cover of saltwater tolerant species, the alien pickleweed, *Batis maritima,* and the native *Sesuvium portulacastrum,* that regularly become partially submerged during spring tides (**Figure 20**).

When such low areas become permanently flooded through island subsidence, ecosystem and habitat changes occur. In **Figure 21**, a large rocky outcrop extends seaward from the shoreline. This rocky outcrop is now submerged and the vegetated areas that may have once existed are now submerged in shallow water. Several ecosystem and habitat changes such as this will occur with regular island subsidence and under scenarios of 0.5-1 m. For instance, water depth will increase over shallow reef areas, intertidal zones, and coastal wetlands.

The inundation contours of the Honokōhau Beach fronting the ‘Aimakapā Fishpond shoreline are shown in **Figure 15**. This beach is the barrier between ocean and the fishpond/wetland, and the protection provided by this barrier is responsible for the existence of the low salinity (~12 PSU) fishpond habitat. Sections of this beach are partially overtopped more than once per year as evidenced by the debris lines shown in Figure 22. Under future sea-level scenarios of 0.25-0.5 m, the overwash of the dune will increase slightly in frequency. The impacts of this increase in overwash frequency should be fairly minimal initially and lead to slightly increased erosion. Under considerable sea-level scenarios (0.5 – 1+ m), the entire beach (barrier) will be fully overtopped several times per year. This could potentially lead to significant erosion and breaching of the sand barrier where the berm is permanently broken and water flows between the pond and ocean. A breaching event may increase salinity levels and lower nutrient levels. Significant increases in salinity of the fishpond may impact breeding habitat for the endangered Hawaiian stilt (*Himantopus mexicanus knudseni*) and Hawaiian coot (*Fulica alai*) .

The inundation contours of Maliu Point of Kaloko-Honokōhau NHP at the northern side of the Honokōhau Small Boat Harbor entrance are shown in **Figure 16**. Inundation contours for inside ‘Ai‘ōpio were not done because a data gap in the elevation model resulted in poorly resolved nearshore bathymetry at this location. The Maliu Point region contains many important cultural sites. The base of Pu‘uoina Heiau facing ‘Ai‘ōpio Fishtrap is at sea-level during spring high tide (**Figure 23**). These portions of Pu‘uoina Heiau however are only exposed to extremely small swell, as it is sheltered by Maliu Point, and northern side of ‘Ai‘ōpio Fishtrap.

Regardless of swell exposure, the Heiau, standing approximately 2-3 m in elevation, will be partially submerged under future sea levels. However, lack of swell exposure suggests slight potential deterioration to the structure. Monitoring the Heiau during maximum annual high tide will help determine the rate of deterioration. Monitoring should increase in frequency as sea level rises.

The potential for direct swell exposure comes from the west, although the exposure and impacts also seem to be minimal. Under future sea-level scenarios of 0.25-0.5 m the overwash of the point will increase in extent inland but the overwash will most likely not reach the Heiau as anything but residual spray. Under sea-level scenarios of 0.5 – 1+ m inland extent of the overwash may begin to impact the westward side of the Heiau, although the impacts do not seem severe or frequent enough to undermine the Heiau. Nonetheless, undermining of the Heiau may be possible and should be carefully monitored.

Joint Probability Model of Tide and Runup

A few of the historic sites at Kaloko-Honokōhau NHP are already overtopped several times per year, which makes it unfeasible to assess their overtopping hazard using the analysis performed with inundation maps. Instead we consider and evaluate runup risk in terms of overtopping events with frequencies of several hours per year as opposed to a single event per year. With frequent swell events, tidal fluctuation has a much greater influence on the occurrence of overtopping, and extreme water levels. For Pu‘ukoholā Heiau NHS, the inundation map analysis is sufficient as most of the important coastal features of the park lie outside the 1-year inundation zone.

The idea behind joint probability models is that both tides and runup contribute to the total water level on a beach. Thus combining the individual frequency (or rather probability) distributions for both tides and runup into a joint probability model, will provide a better estimate than either alone. A typical joint probability distribution, $p(R,T)$, gives the probability that the runup, R, is a particular level, R_0, and the tide, T, is a particular level, T_0:

$$p(R,T) = \Pr(R = R_o \ \ \& \ \ T = T_o)$$

A more useful form of the joint probability distribution gives the probability of the sum of runup and tide, $p(R+T)$. This distribution is achieved through a convolution of the individual probability distribution functions (PDF) of runup and tides.

$$p(R+T) = \Pr(R = R_o) * \Pr(T = T_o)$$

where the $*$ is the operator that represents convolution. Figure 24 shows how the total water level

distribution, $p(R + T)$, is constructed from individual PDFs of tides, waves and runup.

Empirical PDFs of the tidal and wave height datasets are constructed individually from the observed data. Smooth probability distributions are fit to the empirical PDFs and used as marginals of joint distributions, Figure 24 (A, B). The wave height dataset is then translated into runup using empirical equations Figure 24(C). Then a numerical convolution is performed on the tide and runup PDFs to give a total water level PDF Figure 24(D). The PDFs shown in Figure 24 can be written in terms of exceedance probability or hours per year an expected overtopping elevation is reached or exceeded. Figure 25 shows the comparison of the exceedance probability models for runup alone and for tide and runup.

Figure 25 also shows the exceedance distribution for a combination of tide, runup, and sea-level rise. The key to interpreting this figure, and the influence of tide and sea-level rise on overtopping levels and frequency, is noticing the horizontal and vertical distances between the exceedance curves. For example, in comparing the exceedance curves from the runup only and the combined tide and runup curve, we see that including the tides in the exceedance probability models decreases the frequency of the low overtopping elevations and increases the frequency of the large overtopping elevations. The influence of sea-level rise, which is the equivalent of translating the exceedance distribution horizontally on Figure 25 (vertically in real life), increases the frequency of overtopping at all levels. Figure 26 shows the increase in frequency of overtopping (relative to present sea level) vs. elevation for the sea-level rise scenarios under consideration.

It is clear from Figure 25 and Figure 26 that sea-level rise increases the frequency of overtopping at all levels, however this increase is small for long return-period events. The elevations where the most significant increase in frequency occurs are the peaks of Figure 26. The location, corresponding to elevation, of the peak increases with sea-level rise. An effect of this feature, shown in Figure 26, is that impacts to fixed structures do not increase linearly; they accelerate. If we consider fixed elevations (the dashed lines shown in Figure 26), which correspond to elevations of historic sites at Kaloko-Honokōhau NHP, we can determine the increase in frequency of overtopping at these particular locations (Table 7)**.**

In summary, Kaloko Seawall and the sandy beach north of ‘Aimakapā Fishpond incur the largest risk of overtopping and deterioration from wave impacts. These impacts occur because they are at the lowest elevation and will be inundated each year with increasing duration because of the combined increase of sea-level rise, high tide, and large waves. Presently, Kaloko Seawall is impacted by overwash and wave spray during small to moderate swell and high tides (**Figure 27**). During large swell and under scenarios of sea-level rise, the wave overwash will become full-wave overtopping where the wave bore will run across the entire length of the seawall and create much greater damage to the seawall. Catastrophic failure and undermining of the seawall may be possible and should be carefully monitored. The sandy beach at Honokōhau Beach (‘Aimakapā Fishpond to ‘Ai‘ōpio Fishtrap) at higher elevation (greater that 2 m elevation) should be relatively resilient against overtopping impacts until sea-level rise scenarios greater than +0.5 m become reality.

TABLE 5. Nearshore wave and runup modeling summaries for Puʻukoholā Heiau NHS. Tr is the return period and Hs is the significant wave height.

Puʻukoholā Park beach slope ~ 1/14

Case	*Tr [years]*	*Hs [m]*	*wave length [m]*	*Setup [m]*	*Total runup [m]*
A	1	2	100	0.24	1.20
B	5	2	100	0.27	**1.43**
C	10	2	100	0.32	**1.55**
D	25	2	100	0.35	**1.66**
E	50	2	100	0.4	**1.77**

Pelekane Beach beach slope ~ 1/150

Case	*Tr [years]*	*Hs [m]*	*wave length [m]*	*Setup [m]*	*Total runup [m]*
A	1	1	100	0.28	0.85
B	5	1	100	0.32	**1.09**
C	10	1	100	0.35	**1.19**
D	25	1	100	0.4	**1.32**
E	50	1	100	0.45	**1.43**

Spencer Beach beach slope ~ 1/50

Case	*Tr [years]*	*Hs [m]*	*wave length [m]*	*Setup [m]*	*Total runup [m]*
A	1	2	100	0.25	0.91
B	5	2	100	0.3	**1.16**
C	10	2	100	0.32	**1.25**
D	25	2	100	0.35	**1.36**
E	50	2	100	0.4	**1.47**

***Note*:** The uncertainties of the values reported in these tables come from many sources including buoy error, model error, and empirical equation error. By far the largest source of error is the estimation of runup based on empirical equations, which can be as large as 50%. The best uncertainty estimate for the final runup value would be ± 0.3 - 0.5 m.

TABLE 6. Nearshore wave and runup modeling summaries for Kaloko-Honokōhau NHP.

Beach fronting ʻAimakapā Fishpond beach slope ~ 1/7

Case	*Tr [years]*	*Hs [m]*	*wave length [m]*	*Setup [m]*	*Total runup [m]*
A	1	1.6	80	0.4	**1.61**
B	5	1.8	85	0.5	**1.97**
C	10	2	90	0.55	**2.15**
D	25	2.2	95	0.6	**2.34**
E	50	2.5	100	0.65	**2.54**

***Note*:** The uncertainties of the values reported in these tables come from many sources including buoy error, model error, and empirical equation error. By far the largest source of error is the estimation of runup based on empirical equations, which can be as large as 50%. The best uncertainty estimate for the final runup value would be ± 0.3 - 0.5 m.

TABLE 7. Overtopping frequencies and the influence of sea-level rise (SLR) for historic structures and beach profiles at Kaloko-Honokōhau NHP.

Elevation 1 = 1.5 m : Kaloko Seawall and sandy beach north of ‘Aimakapā Fishpond				
SLR	*Overtop freq. [hrs/yr] - Present*	*Overtop freq. [hrs/yr] - w/ SLR*	*Increase [hrs/yr]*	*Relative Increase [factor]*
0.25	44	155	111	3.5
0.5	44	540	496	12.3
0.75	44	1660	1616	37.7
1	44	3950	3906	89.8

Elevation 2 = 2 m : Sandy beach between ‘Aimakapā Fishpond and ‘Ai‘ōpio Fishtrap				
SLR	*Overtop freq. [hrs/yr] - Present*	*Overtop freq. [hrs/yr] - w/ SLR*	*Increase [hrs/yr]*	*Relative Increase [factor]*
0.25	3.5	12	8.5	3.4
0.5	3.5	43	39.5	12.3
0.75	3.5	156	152.5	44.6
1	3.5	542	538.5	154.9

Elevation 3 = 2.25 m : Honokōhau Beach fronting ‘Aimakapā Fishpond				
SLR	*Overtop freq. [hrs/yr] - Present*	*Overtop freq. [hrs/yr] - w/ SLR*	*Increase [hrs/yr]*	*Relative Increase [factor]*
0.25	1	3.5	2.5	3.5
0.5	1	12.126	11.126	12.1
0.75	1	43	42	43.0
1	1	156	155	156.0

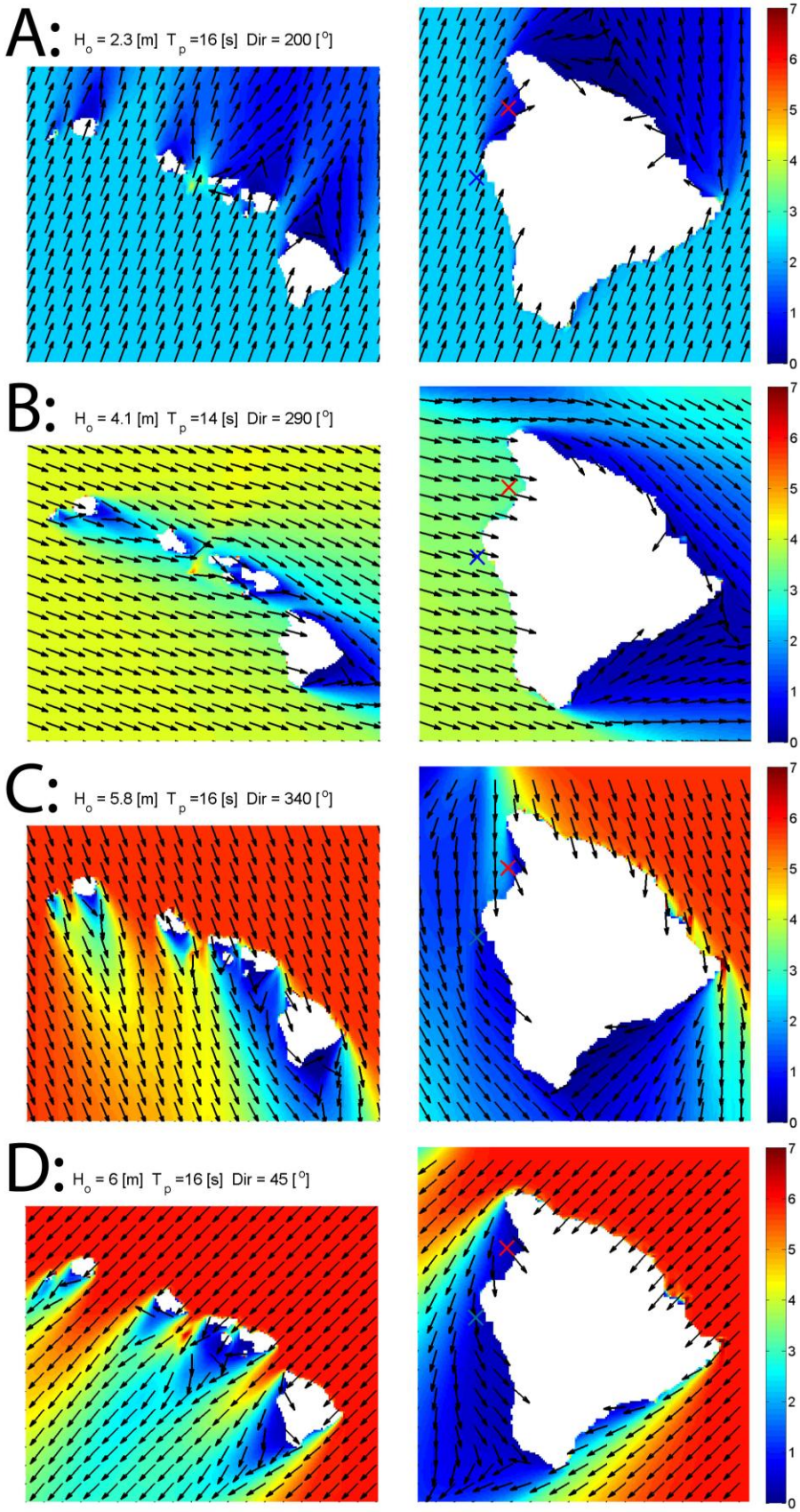

Figure 6. Four of 85 SWAN model simulations each with representative annual maximum significant wave height from a particular direction. Ho is the deep water wave height (m) and Tp is the wave period (s). Case A: South swell, Ho=2.3 m Tp=16 s Dir=200°. Case B: Northwest swell, Ho=4.1 m Tp=14 s Dir=290°. Case C: North swell, Ho=5.8 m Tp=16 s Dir=340°. Case D: Northeast swell, Ho=6 m Tp=16 s Dir=45°.

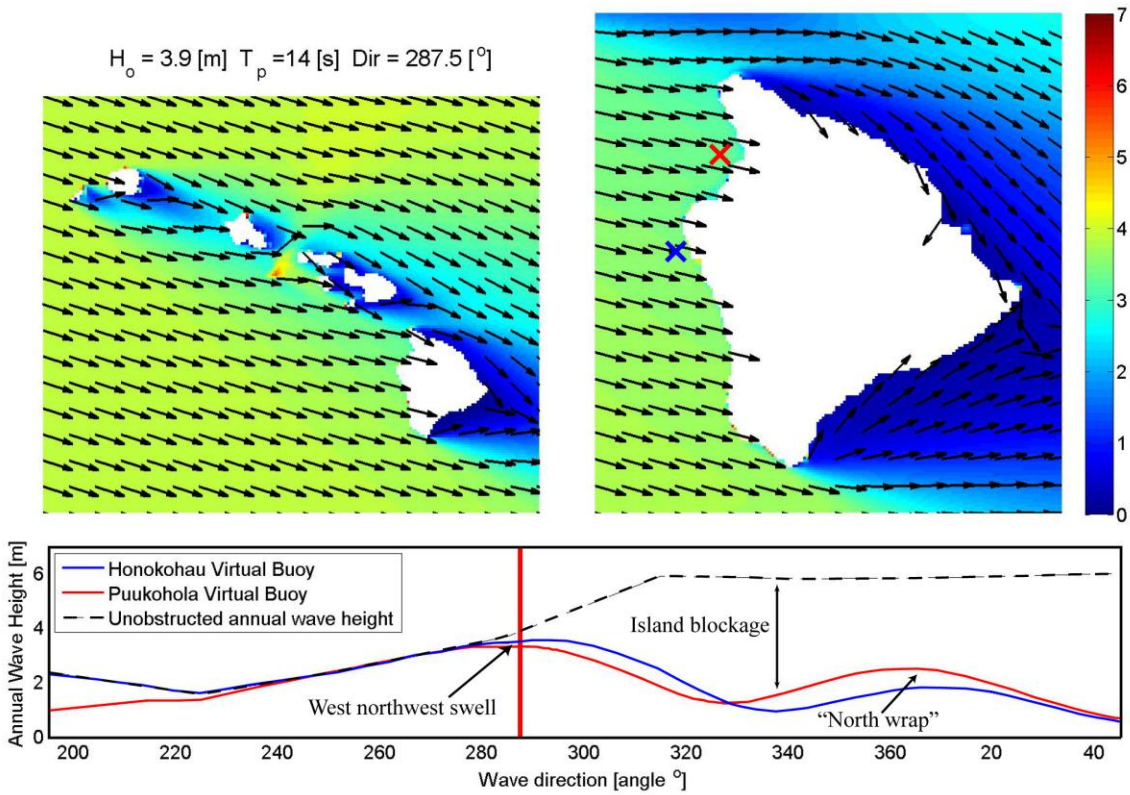

Figure 7. The maximum annual significant wave height for the Big Island national park sites as a function of wave direction (Pu'ukoholā Heiau NHS = red, Kaloko-Honokōhau NHP = blue). The blue and red 'x's on the map of the wave field around the Big Island indicate the virtual buoy (model) locations. The maximum wave height case occurs during west northwest swell where the wave direction is about 290°. There is a small secondary peak associated with north wrap when the wave direction approach can fit in the gap between Maui and the Big Island. Also indicated on the figure is the degree of island blockage, which is the difference between the dashed line and the solid blue and red lines.

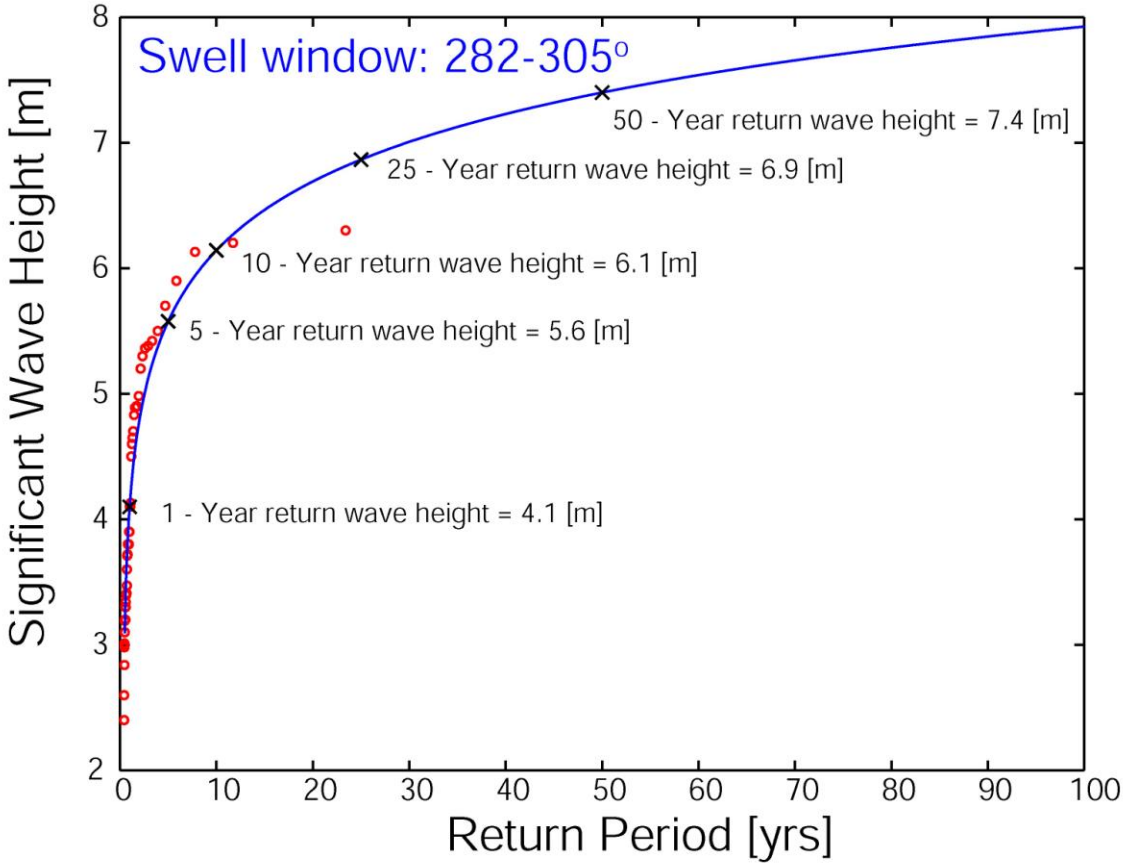

Figure 8. The relationship between the open-swell significant wave height and the return period determined from Generalized Extreme Value Analysis (GEV) for the 282°-305° window.

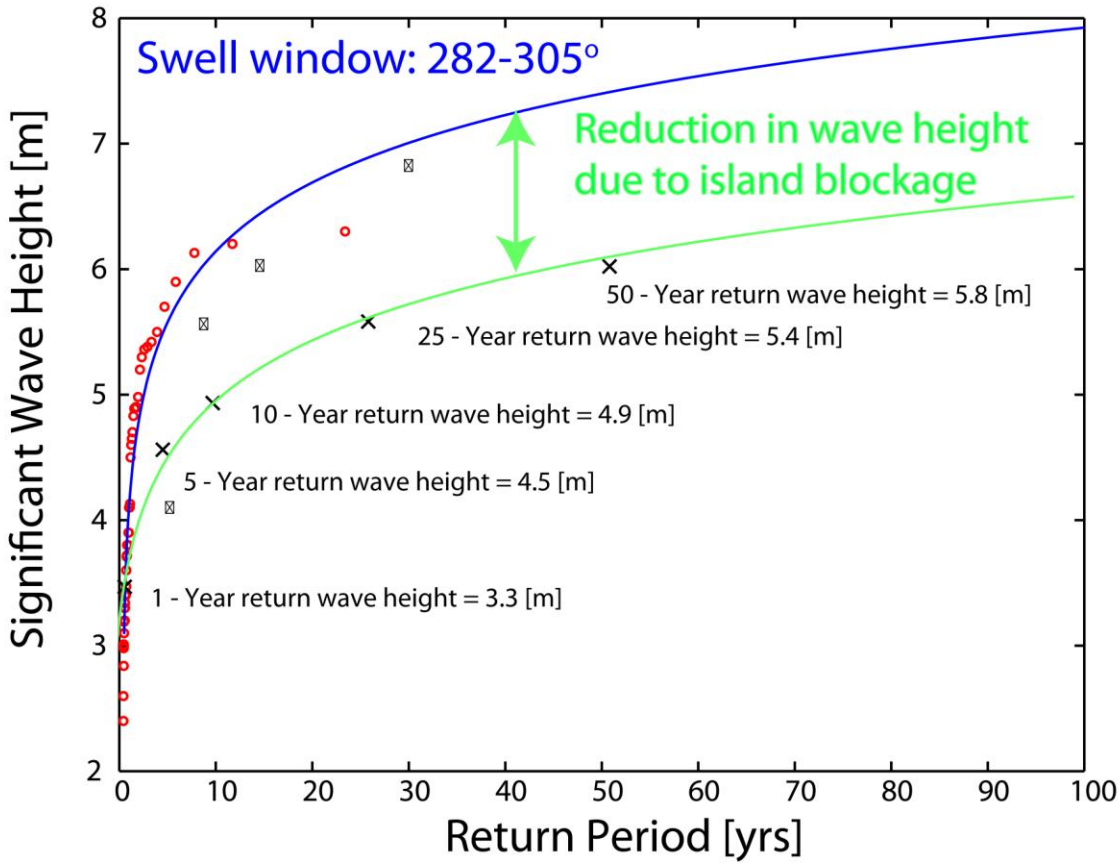

Figure 9. The relationship between the significant wave height and the return period at Pu'ukoholā Heiau NHS and Kaloko-Honokōhau NHP (green) determined from Generalized Extreme Value Analysis (GEV) for the 282°-305° window used as a boundary condition for a wave transformation model from deep water to the national park sites. The *x*'s are the individual cases modeled. The GEV model is compared with the recurrence relationship for open ocean swell given in Figure 8 (blue). The difference between the blue line and the green line is the effect of island blockage.

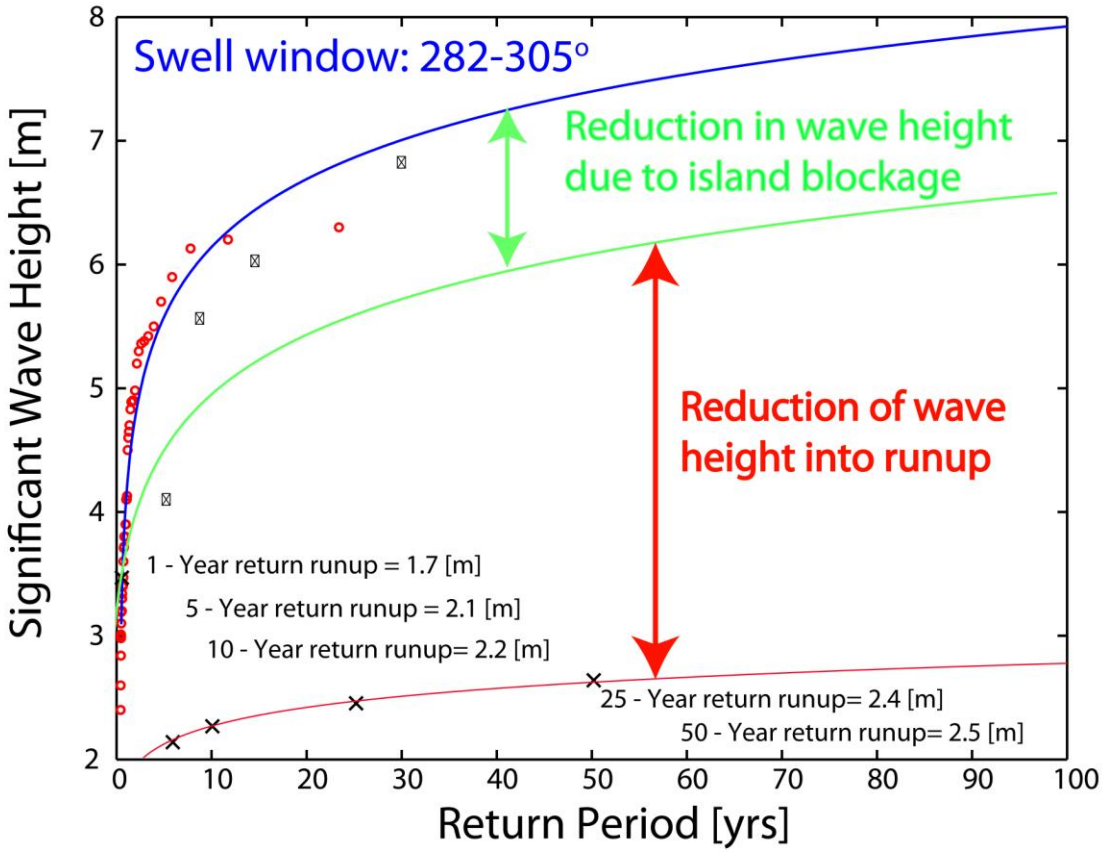

Figure 10. The relationship between the runup elevation and the return period at Pu'ukoholā Heiau NHS and Kaloko-Honokōhau NHP (red) determined from the Stockdon equation. The runup relationship is compared with the recurrence relationship for open ocean swell (blue) given in Figure 8 and for local swell (green) given in Figure 9. As is typical, the runup elevations are much smaller than the wave heights as there is significant energy dissipation due to breaking.

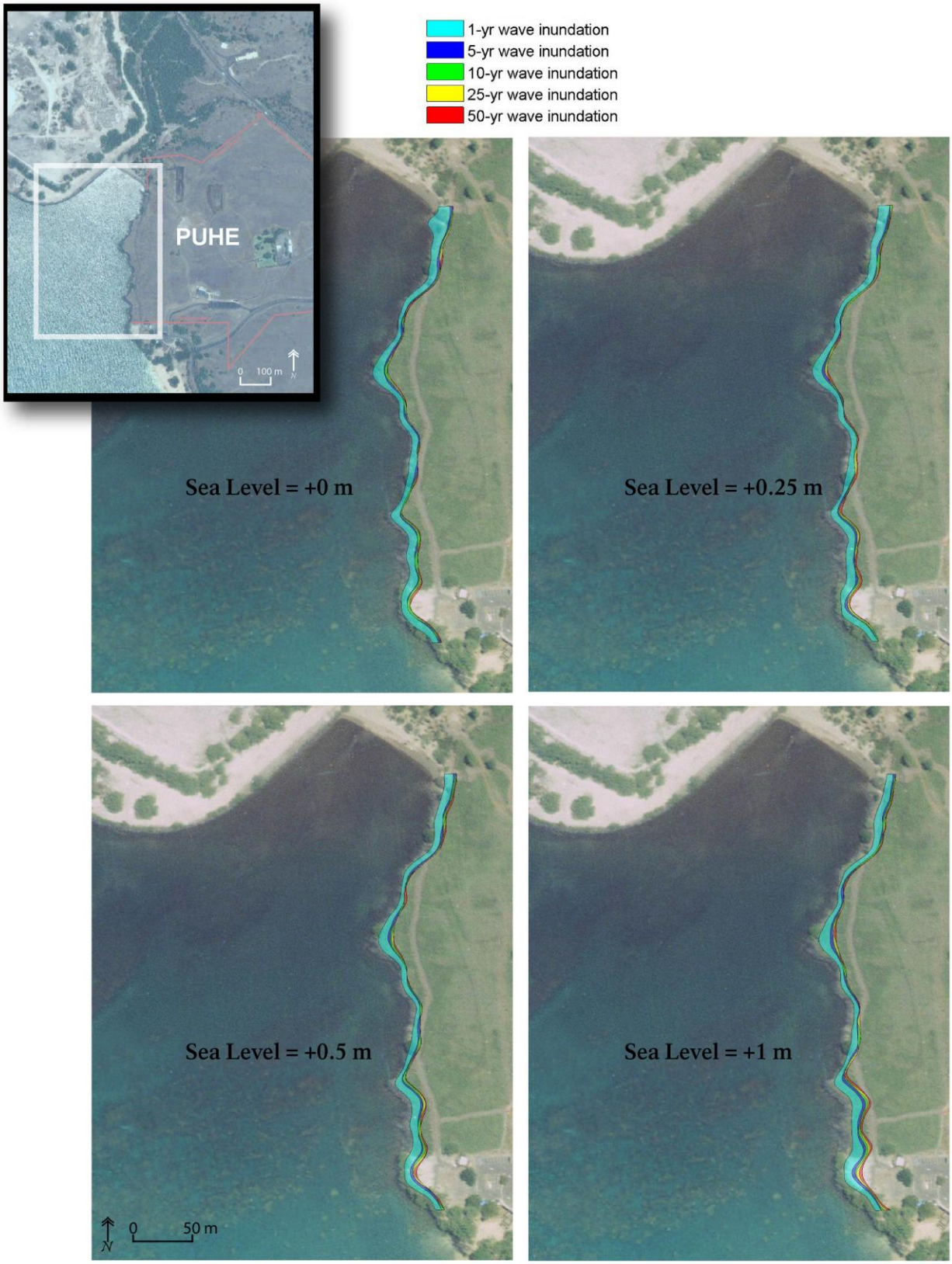

Figure 11. Inundation maps of Puʻukoholā Heiau NHS and a portion of the Ala Kahakai National Historic Trail under sea-level rise scenarios.

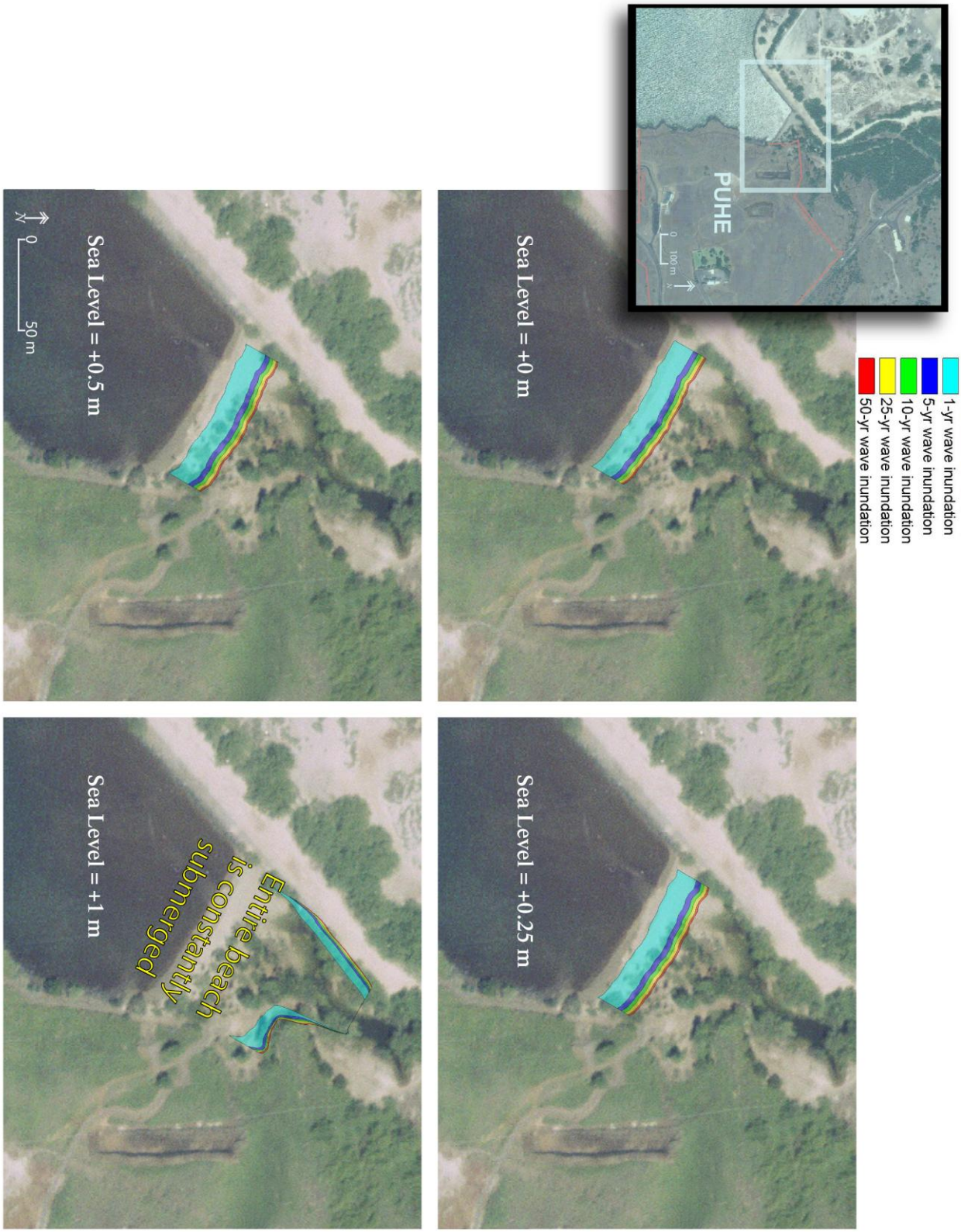

Figure 12. Inundation maps of the northern beach at Pelekane Bay, Pu'ukoholā Heiau NHS under sea-level rise scenarios.

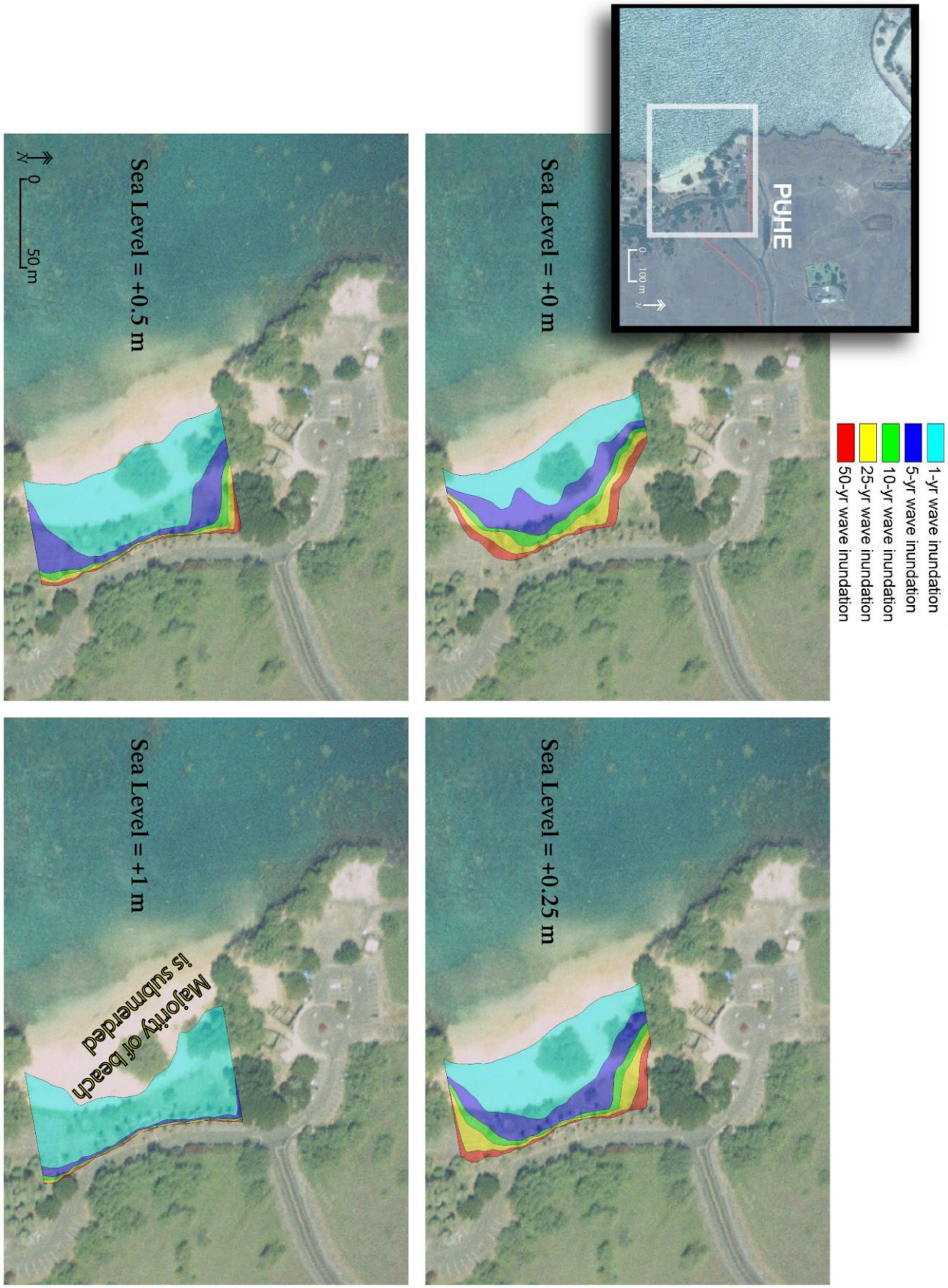

Figure 13. Inundation maps of Spencer Beach Park under sea-level rise scenarios.

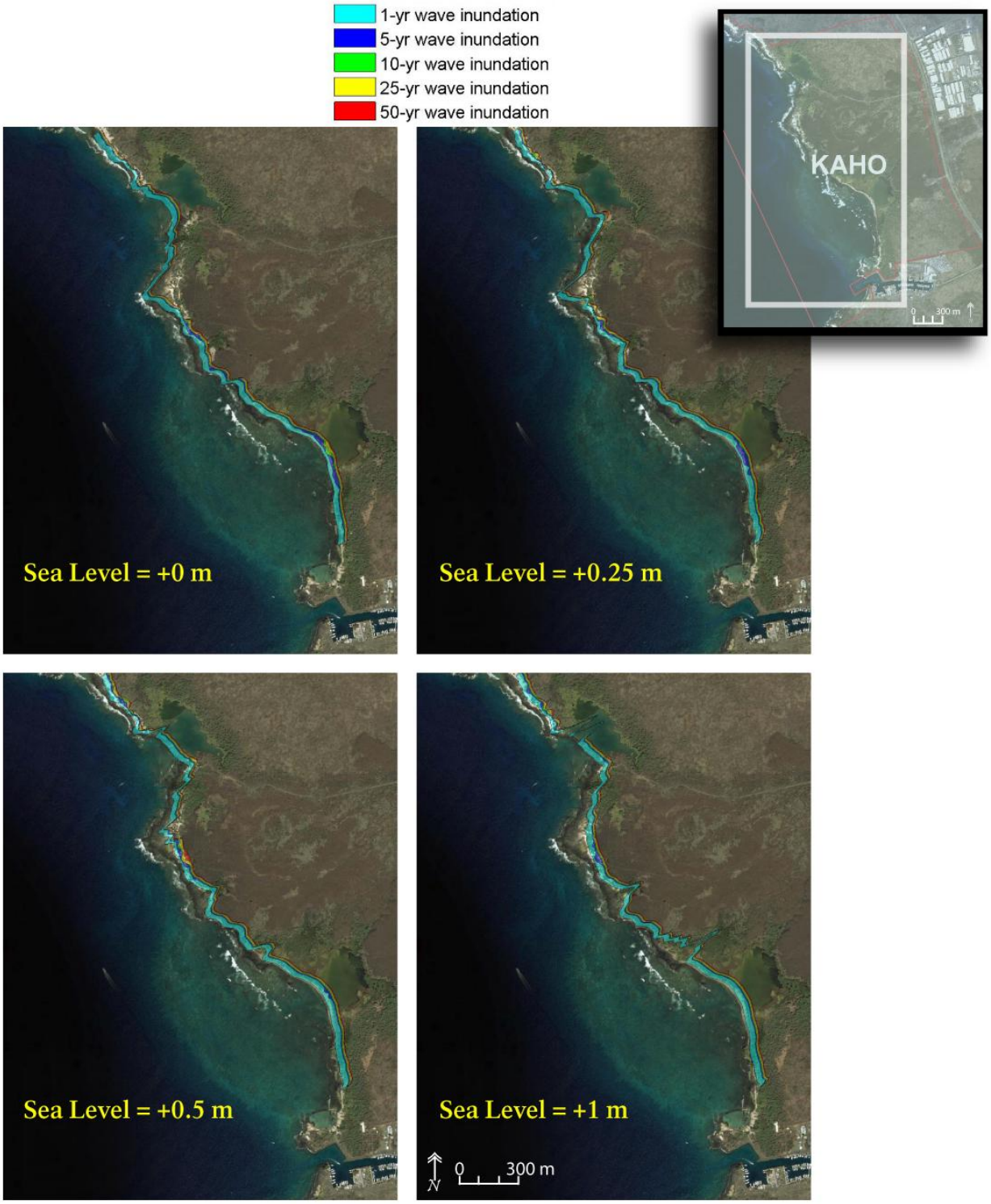

Figure 14. Inundation maps of portions of Kaloko-Honokōhau NHP under sea-level rise scenarios.

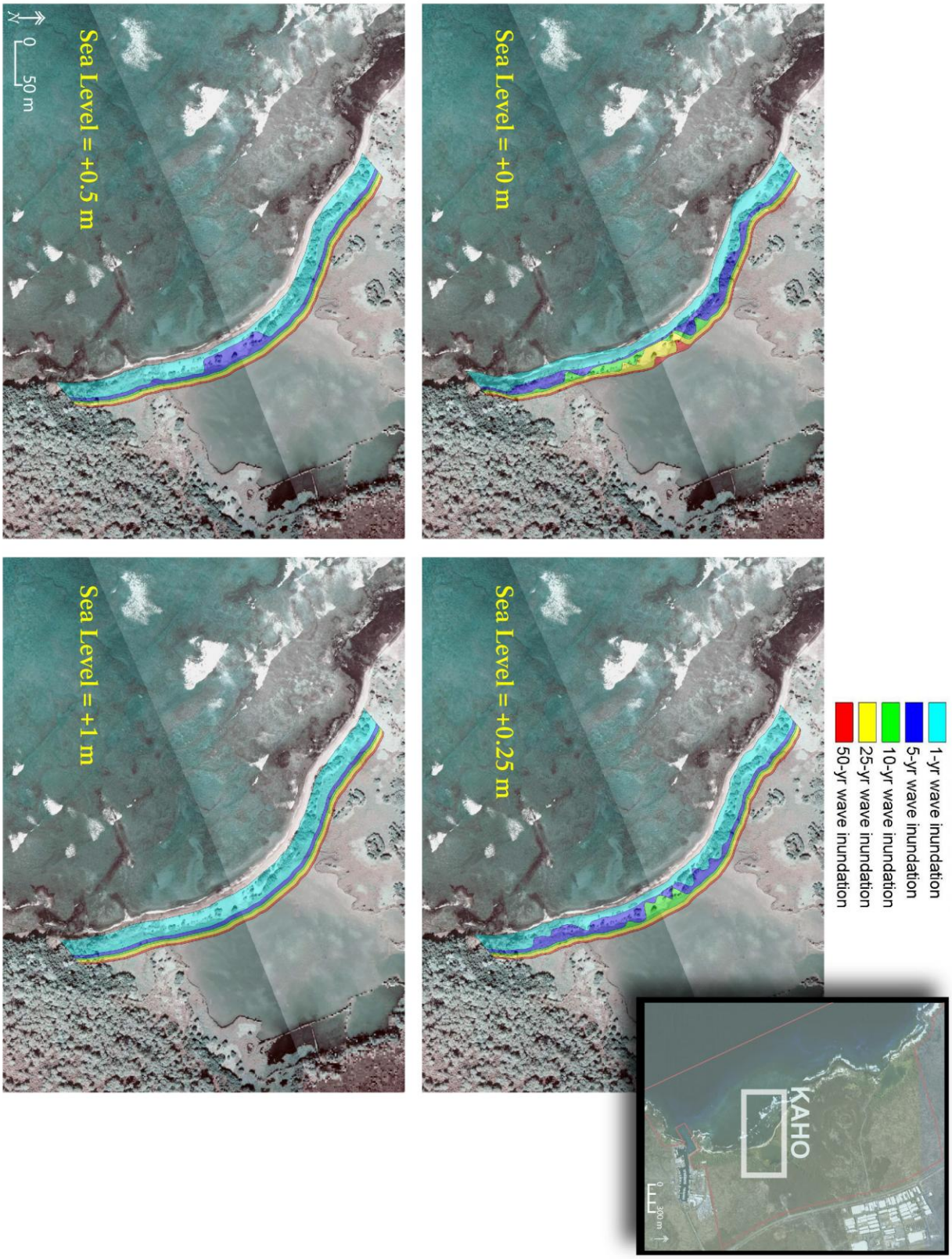

Figure 15. Inundation maps of the Honokōhau Beach fronting the ʻAimakapā Fishpond under sea-level rise scenarios.

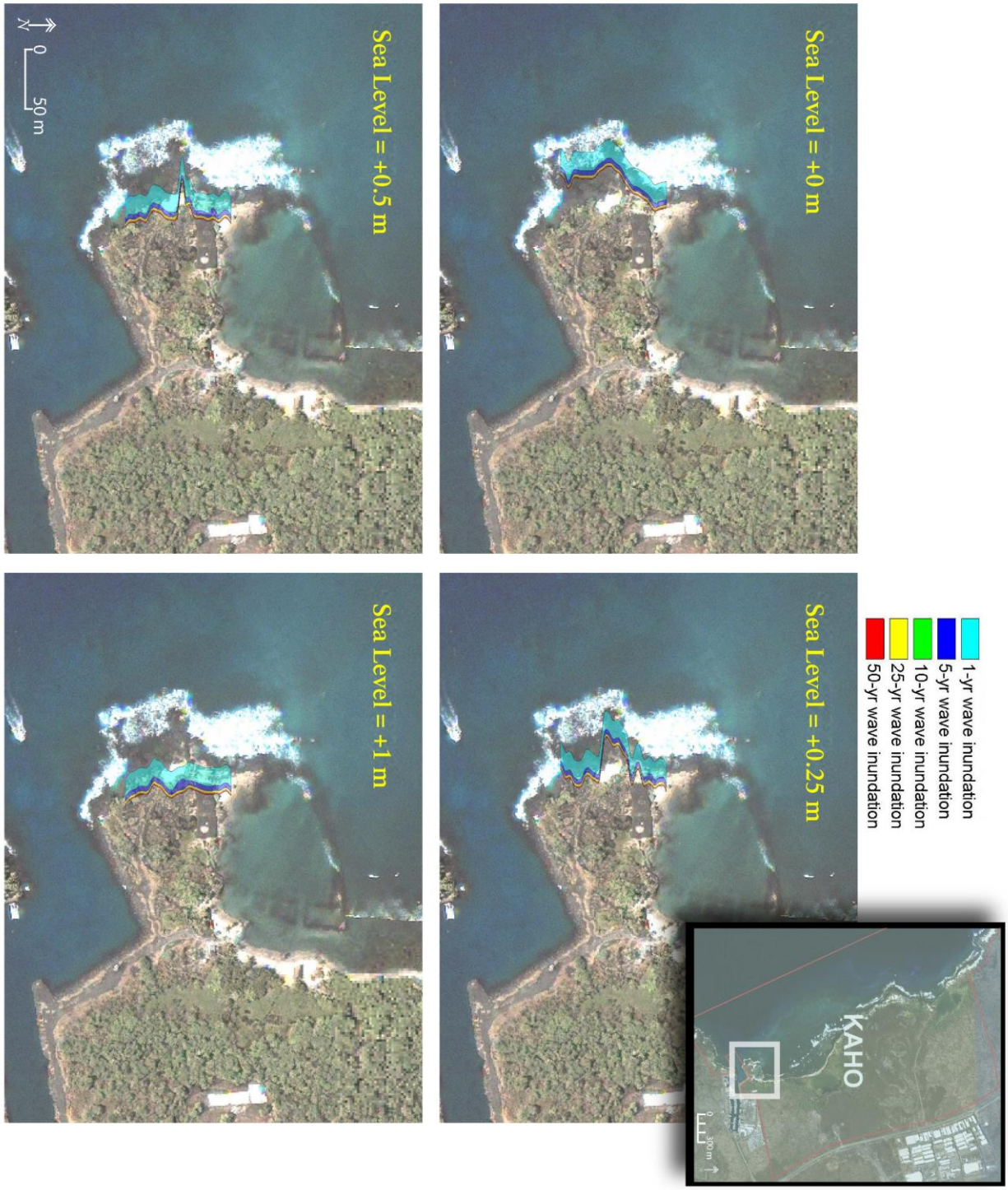

Figure 16. Inundation maps of Maliu Point at ʻAiʻōpio, in the southern portion of Kaloko-Honokōhau NHP, under sea-level rise scenarios.

Figure 17. The shoreline trail, the Ala Kahakai NHT, at Pelekane Bay experiences erosion and root exposure of the sand seaward of the trail.

Figure 18. The debris lines on Pelekane Beach are evidence of high wave wash.

Figure 19. The debris lines on Spencer Beach are evidence of high wave wash.

Figure 20. ‘Aimakapā Fishpond wetland on the shoreline at Kaloko-Honokōhau NHP that partially flooded during a spring high tide.

Figure 21. Flooding of low-lying lands vegetated with saltwater tolerant species at Kaloko-Honokōhau NHP.

Figure 22. The debris lines on Honokōhau Beach fronting the ʻAimakapā Fishpond are evidence of high-wave wash and partial overtopping of the dune/sand berm.

Figure 23. The base of Pu‘uoina Heiau at sea level during spring tides.

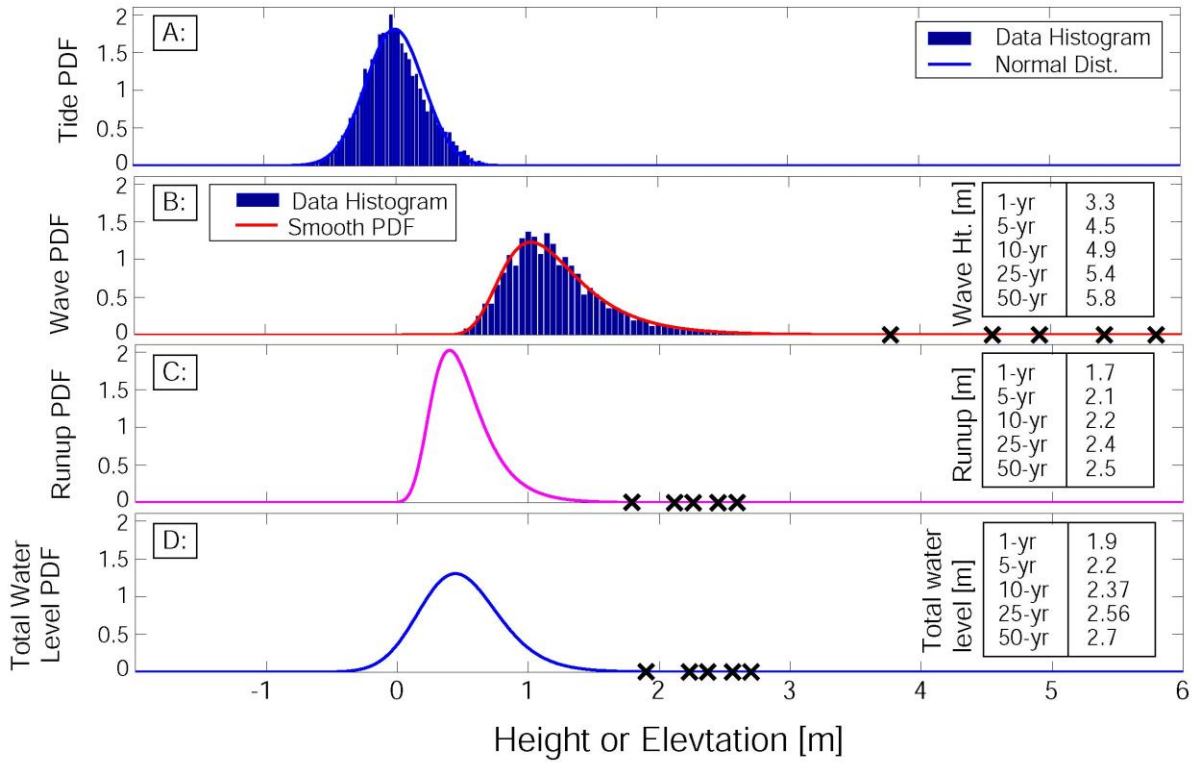

Figure 24. Joint probability model of tide and runup: smooth PDFs of tide (part A) and wave height (part B) are constructed from empirical PDFs. The wave height PDF is translated into a runup PDF (part C). The total water level PDF is then constructed as the convolution of the tide and runup PDFs (part D).

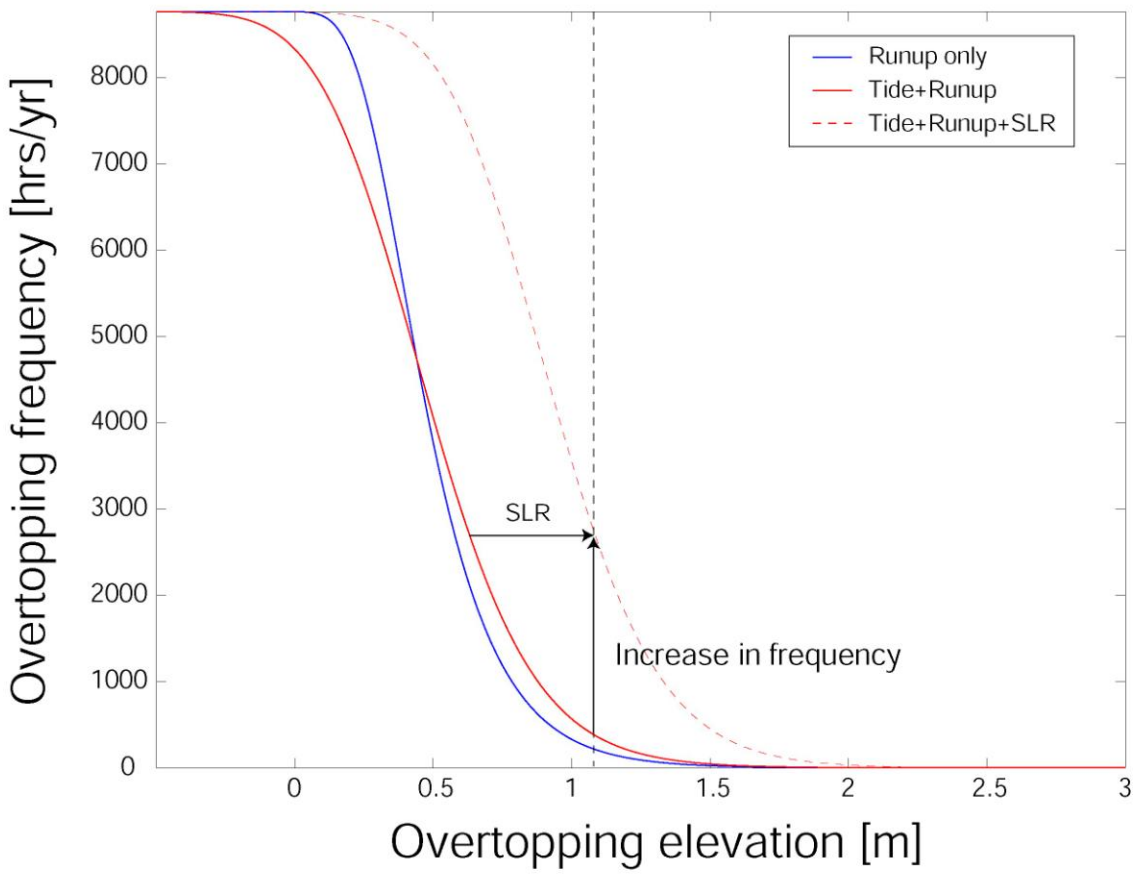

Figure 25. Exceedance curves for runup only, a combination of tide and runup, and for a combination of tide, runup and sea-level rise (SLR). Vertical differences (lines of constant elevation) between curves represent the increase in frequency of one curve vs. the other. Horizontal changes (lines of constant frequency) represent the increase in severity. If a curve is translated on the x-axis, the amount that it is translated represents the scenario of future sea-level rise.

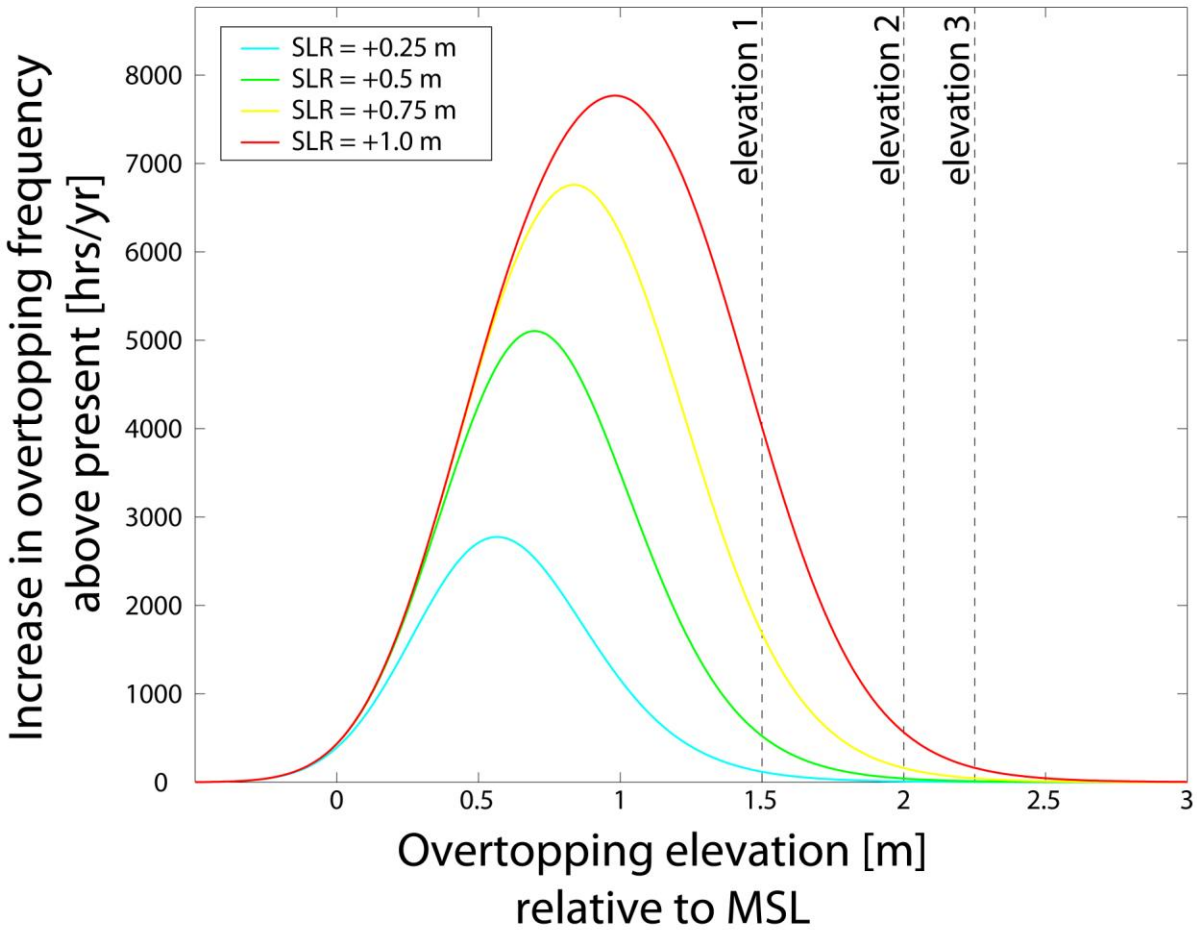

Figure 26. The increase in frequency of overtopping vs. elevation for the sea-level rise (SLR) scenarios of +0.25, +0.5, +0.75, and +1.0 m. Elevation 1 is at 1.5 m, Elevation 2 is at 2 m, and Elevation 3 is at 2.25 m.

Figure 27. Kaloko Seawall overwash on a moderate south swell at high tide.

Tsunami Hazards

This section describes the paleotsunami evaluation and the modeling of inundation by tsunami at Pu'ukoholā Heiau NHS and Kaloko-Honokōhau NHP.

Tsunamis are a series of waves of very long wavelength (100's km) and period (10's minutes – 1 hour or more) that can travel up to 1,000 km/hr in the open ocean. They are caused by disturbances that displace large volumes of water and are usually generated by seafloor displacement during earthquakes, but they can also be caused by volcanic eruptions, submarine landslides, and oceanic bolide impacts. Tsunamis can impact coasts on either ocean-wide, regional (~ 1,000 km) or local (~100 km) scales. In the open ocean the tsunami wave height may be only a meter or two, but as the wave approaches shallow water it slows down and begins shoaling resulting in dramatic increases in wave height. Damage from a tsunami is caused by inundation (flooding of the land surface), wave impact, and sediment erosion and deposition. In general the larger the tsunami the greater the impact. However, tsunami runup height (elevation at the limit of inundation) and inundation from an individual tsunami typically vary greatly over short distances due to complex interactions between the wave and land surface.

Historic tsunamis are events that have either been observed or measured and are documented in some type of written or oral record. Historic tsunamis in Hawai'i have either been caused by ocean-wide events derived from distant earthquakes, or locally-derived phenomena. Located in the middle of the Pacific Ocean, Hawai'i may receive tsunamis from a number of seismic sources including the Aleutian Islands, Japan, Chile, Kamchatka, and South Pacific islands. Walker (1994) noted 22 Pacific basin tsunamis with runup greater than 1 m have been observed in Hawai'i since 1812. The highest Hawai'i tsunami runup elevation reported by Lander & Lockridge (1989) was 16.4 m at Waikolu Valley, Molokai as a result of the 1946 Aleutian Islands earthquake event. Tsunami runup on the island of Hawai'i from the 1946 tsunami ranged from 2 m at Honaunau to 12 m at Waipio Valley (Lander & Lockridge, 1989). The last large tsunami of distant origin to affect the Hawaiian Islands was generated by a great (magnitude 9.5) earthquake in Chile in 1960 that caused extensive damage in the Hilo area (Dudley & Lee, 1998). Since that last occurrence there has been widespread and intensive human development along the Hawaiian shoreline. Recently installed monitoring systems in the Pacific Ocean are designed to give early warning of impending ocean-wide tsunamis.

In addition to ocean-wide events, the Hawaiian Islands are subject to locally generated tsunamis. Twenty-three tsunamis with measurable runup and a local source have been recorded for Hawaii since 1840 as documented in the NOAA World Data Center (WDC) Historical Tsunami Database at the National Geophysical Data Center (NGDC; available on-line at: http://www.ngdc.noaa.gov/hazard/tsu_db.shtml , last accessed on 11/21/08). Maximum runup height from the NGDC data base is 14.3 m at Keauhou Landing (SE Hawaii) as a result of the locally generated tsunami created by the 1975 Kalapana earthquake (M 7.2) characterized by rapid coastal subsidence and associated submarine slump (Day et al. 2005). This was the largest locally generated tsunami to impact Hawai'i in the 20th century and it produced deposits as much as 320 m inland and up to 10 m above sea level (Goff et al. 2006). A similar locally generated tsunami was caused by magnitude 7.9 shock of 1868 located on the south flank of Mauna Loa. Locally generated tsunamis arrive very soon after the generating event, therefore the generating event, such as an earthquake or volcanic eruption, should serve as a warning to evacuate from the coast.

Because of its coastal setting, Pu'ukoholā Heiau NHS is vulnerable to increased ocean-inundation potential from tsunamis (Figure 28). An event similar to the tsunami generated by the 1946 Aleutian Islands would most likely severely damage the beach and park infrastructure at Pelekane Beach, while causing less damage to the rocky shoreline of the park.

Kaloko-Honokōhau NHP is also vulnerable to hazards that increase ocean inundation potential such as tsunamis, storms, and sea-level rise (Figure 29). Lander & Lockridge (1989) identified historical tsunamis that have struck the coast near Kailua-Kona since 1896. The tsunami runup ranged in height from 0.6 m to 3.4 m with the largest runup originating from a 1946 earthquake in the Aleutian Islands. A tsunami of similar magnitude occurring today would most-likely cause damage to the beaches and park infrastructure and historical sites near the coast. The basalt rock areas are relatively stable and would likely undergo little change.

Paleotsunami

Tsunamis in which there is no historical record are termed paleotsunamis, and their occurrence and distribution is based primarily on the identification, dating, and mapping of sedimentary deposits formed by a tsunami. Identification of tsunami deposits can be used to delineate areas impacted by tsunamis and provide clues to the magnitude of the event. Multiple deposits can provide information on the recurrence interval and extend the record of tsunami impacts back through time. Tsunami deposits are created during the erosion and deposition of sediment that occurs during the passage of the tsunami waves. They have similar characteristics to other wave formed deposits such as those formed by storm waves, but there are a number of criteria that aid in their identification, such as:

- marine debris, such as skeletal material from marine organisms deposited well inland (100's m) and at high elevations (up to 10+ m)
- sheet-like deposits that gradually thin inland

- deposits that infill topographic lows and thin on topographic highs
- large blocks (> 2m) transported 100's m inland
- sharp erosional basal contact with underlying material
- normally graded (fining upward) sand layer(s)

In general, the morphology of tsunami deposits tend to be sheet-like and extend farther inland than storm deposits that tend to form shore-parallel ridges of limited inland extent. Perched beach ridges are prominent features at Kaloko-Honokōhau NHP and are most-likely the products of seasonal storms that strike the coast. No paleotsunami deposits have been described from either Kaloko-Honokōhau NHP or Pu'ukoholā Heiau NHS, although these areas lack detailed geologic studies using recent advancements in paleotsunami identification.

Elsewhere on the Island of Hawai'i there is paleotsunami evidence in the geologic record indicating there have been extremely rare, but locally severe, mega-tsunamis (McMurtry et al. 2004). Fossiliferous marine conglomerates along the northwest coast of Kohala Volcano have been interpreted as mega-tsunami deposits generated by a flank-failure submarine landslide on western Mauna Loa. According to McMurtry et al. (2004), that landslide and tsunami occurred about 110,000 years ago; the tsunami had an estimated runup more than 400 m high and an inundation greater than 6 km inland on the flanks of Kohala Volcano. Catastrophic flank failures are extremely rare geologic events but are an important process in volcanic island evolution. These flank failures influence the island shape and the morphology of the coastal zone.

Tsunami Inundation Model

We have constructed a tsunami model of the national parks based on the April 1, 1946 tsunami that originated from a magnitude 7.5 earthquake in the Aleutian Islands. This event is regarded as one of the most devastating tsunamis in Hawai'i and is thus a candidate to evaluate tsunami risk assessment. The tsunami was recorded in the Honolulu tide gauge, and reported to have a period of 15 minutes (Green 1946). Mader (2004) conducted extensive tsunami modeling studies of Hawai'i including the 1946 tsunami, which used tsunami water-level boundary conditions of 1 m wave heights with 1000 sec period as boundary conditions for a model of the Hawaiian Island. We employed this approach in our assessment of the national parks. High-resolution models of the national parks were nested in the regional model of the Hawaiian Islands to estimate the extent of inundation. The modeling was performed with the Delft3D modeling system, which is a non-linear shallow water equations model capable of simulating tsunami propagation and inundation (see Appendix A for model settings). The model output of the 1946 tsunami scenario is shown in Figure 30. While the tsunami wave heights were only slightly larger than 1 m in the open waters north of the Hawaiian Islands, the nearshore water levels on north facing shores of the islands were significantly larger than 1 m due to shoaling(Figure 31).

As seen in both Figure 30 and Figure 31, the maximum water levels at the national parks sites were very small. The tsunami loses energy as it refracts around the islands, and the national parks sites are in such a location that energy loss is significant. Kaloko-Honokōhau NHP is particularly in a tsunami shadow zone, while Pu'ukoholā Heiau NHS does receive tsunami energy that refracts between the Alenuihaha Channel between Maui and the Big Island.

The maximum water levels modeled in high-resolution grids near at the national parks sites are reported in Figure 32 and Figure 33. Predicted water levels, or runup, is greater at Pu'ukoholā Heiau NHS than Kaloko-Honokōhau NHP due to the larger offshore tsunami wave heights seen in Figure 30, and resonance inside the partially enclosed basin of the southern portion of the Kawaihae breakwater, Pelekane Beach, and the coastline of the park. Maximum water levels inside this region reach 1.8 m. Such elevated water levels would extend far inland into the marsh area backing Pelekane Beach. Additionally, the archeological sites at Pelekane would be threatened by flooding and wave impacts.

The majority of Kaloko-Honokōhau NHP experiences slightly elevated tsunami water levels of 0.2 m, which should not cause any major impacts. The beach fronting 'Aimakapā Fishpond experiences the largest tsunami water levels (0.4 m) at the park, due to shoaling over the reef. However, these water levels are still much smaller than the high swell runup levels reported in Table 6. Historical records of the 1946 tsunami show that Kawaihae had a runup value of 4.3 m and Kailua-Kona had a runup value of 3.4 m (Lander & Lockridge 1989). These values exceed our model predictions.

The flooding model of the parks shown in Figure 32 and Figure 33 was performed on grids that are not as high resolution as the digital elevation model grids, thus we use GIS software to map the tsunami inundation extent. The final inundation contours for the 1946 tsunami scenario are given in Figure 34 and Figure 35. Based on these maps, impacts to Pelekane Beach at Pu'ukoholā Heiau NHS seem to be the greatest threat of damage to culturally and historically significant regions of the parks posed by tsunami hazards. The risk posed by Aleutian tsunamis to Kaloko-Honokōhau NHP seems minimal primarily due to the shadowing effect of the islands to the northwest.

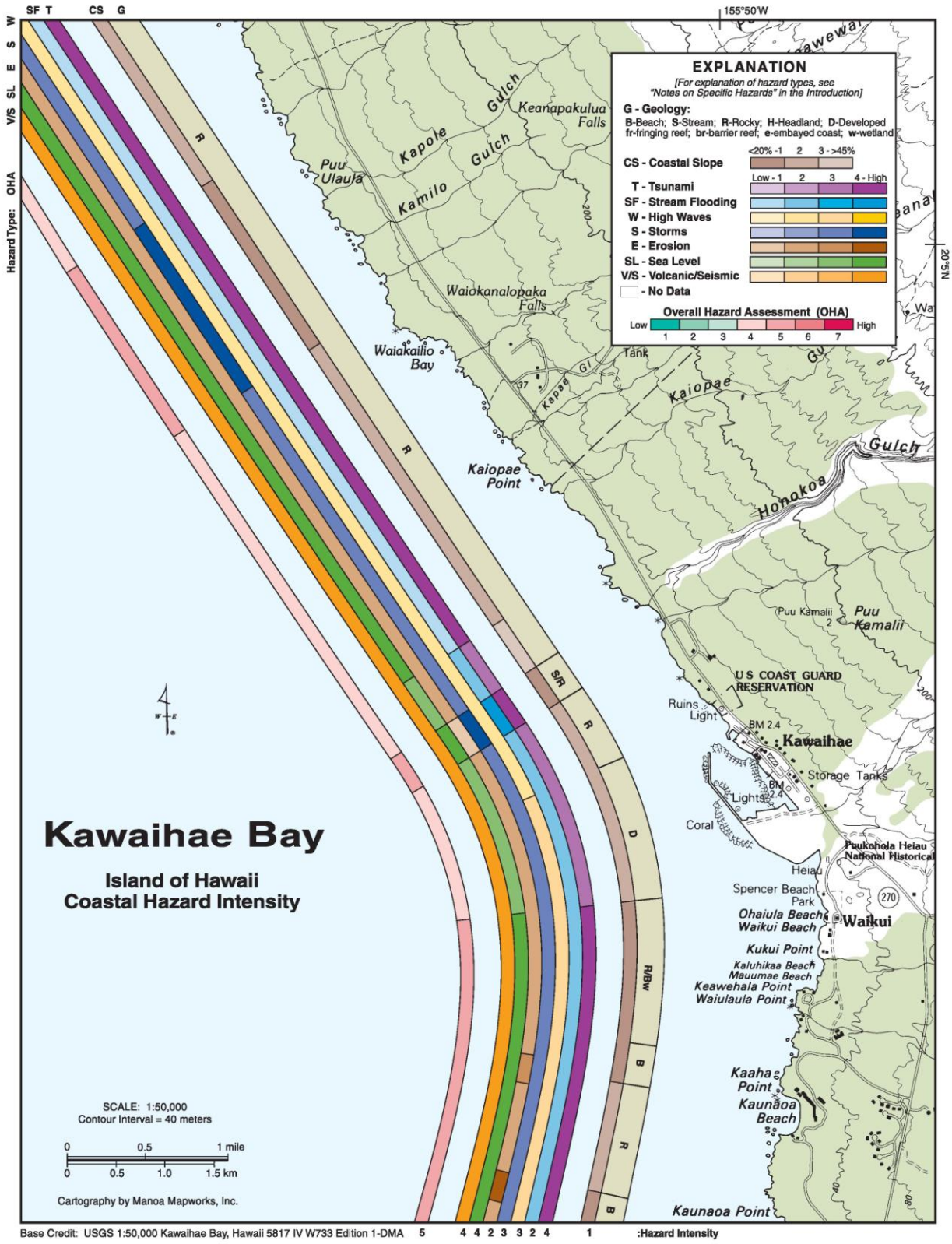

Figure 28. Coastal hazards for Kawaihae Bay, Hawai‘i (from Fletcher et al. 2002).. Pu‘ukoholā Heiau NHS is part of Kawaihae. The map shows 7 natural hazards, including tsunami hazards (http://pubs.usgs.gov/imap/i2761/).

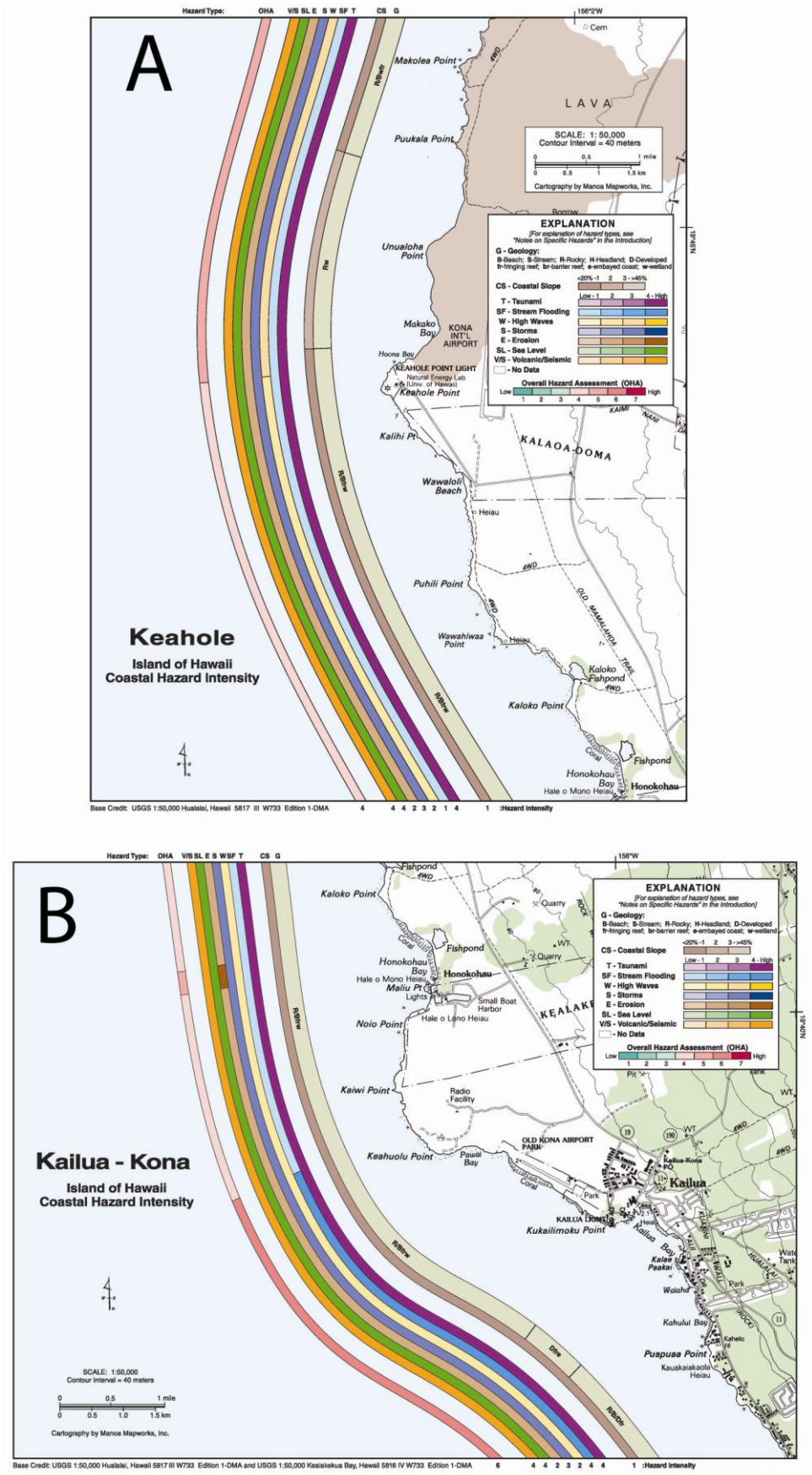

Figure 29. Coastal hazards for Keahole (A) and Kailua-Kona (B), Hawai'i (from Fletcher et al. 2002).. Kaloko-Honokōhau NHP is part of Keahole and Kailua-Kona. The map shows 7 natural hazards, including tsunami hazards (http://pubs.usgs.gov/imap/i2761/).

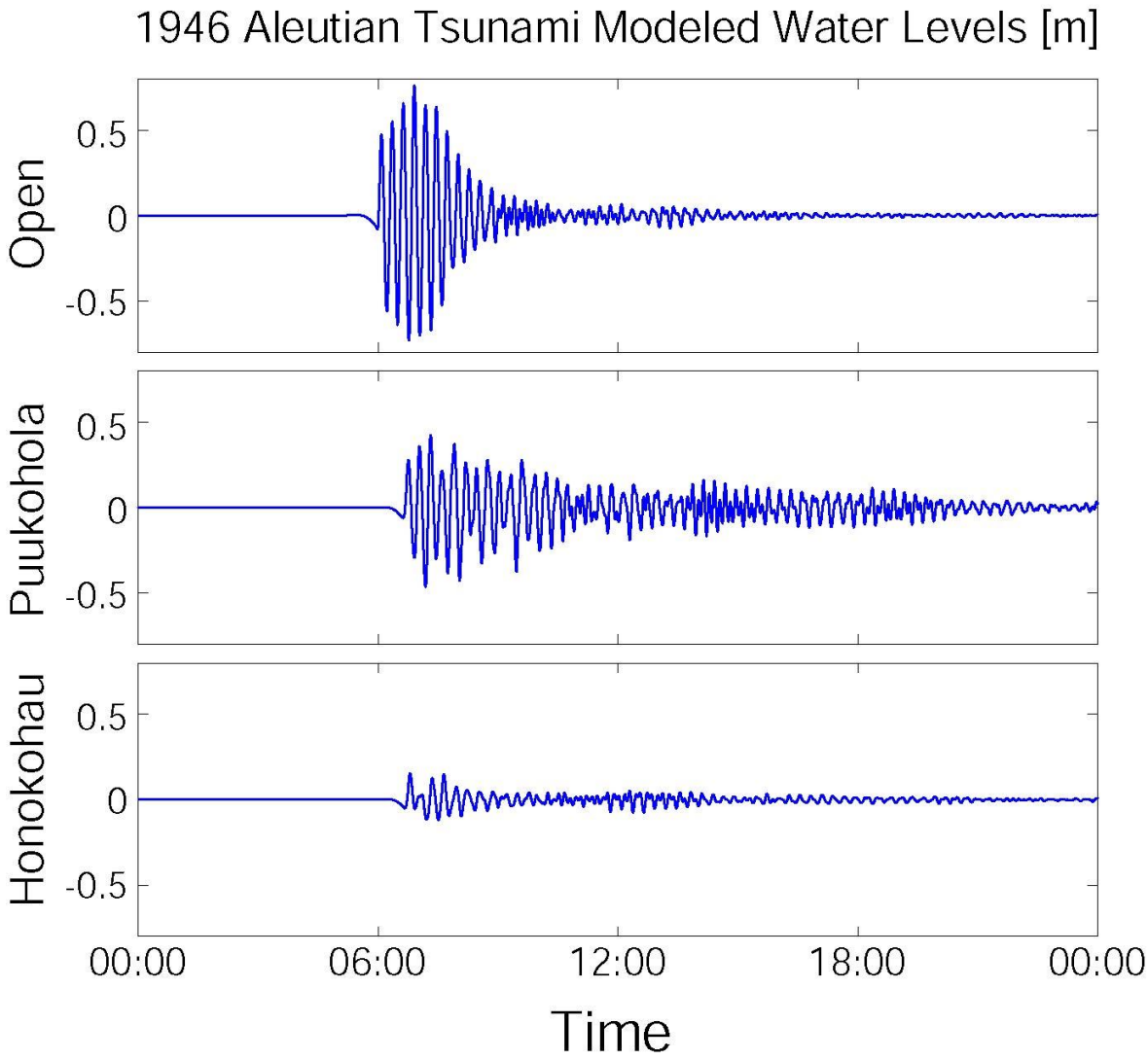

Figure 30. 1946 Alaska Aleutian tsunami scenario modeled water-levels for the Hawaiian Island regional grid at Pu'ukoholā Heiau NHS and Kaloko-Honokōhau NHP using Delft3D.

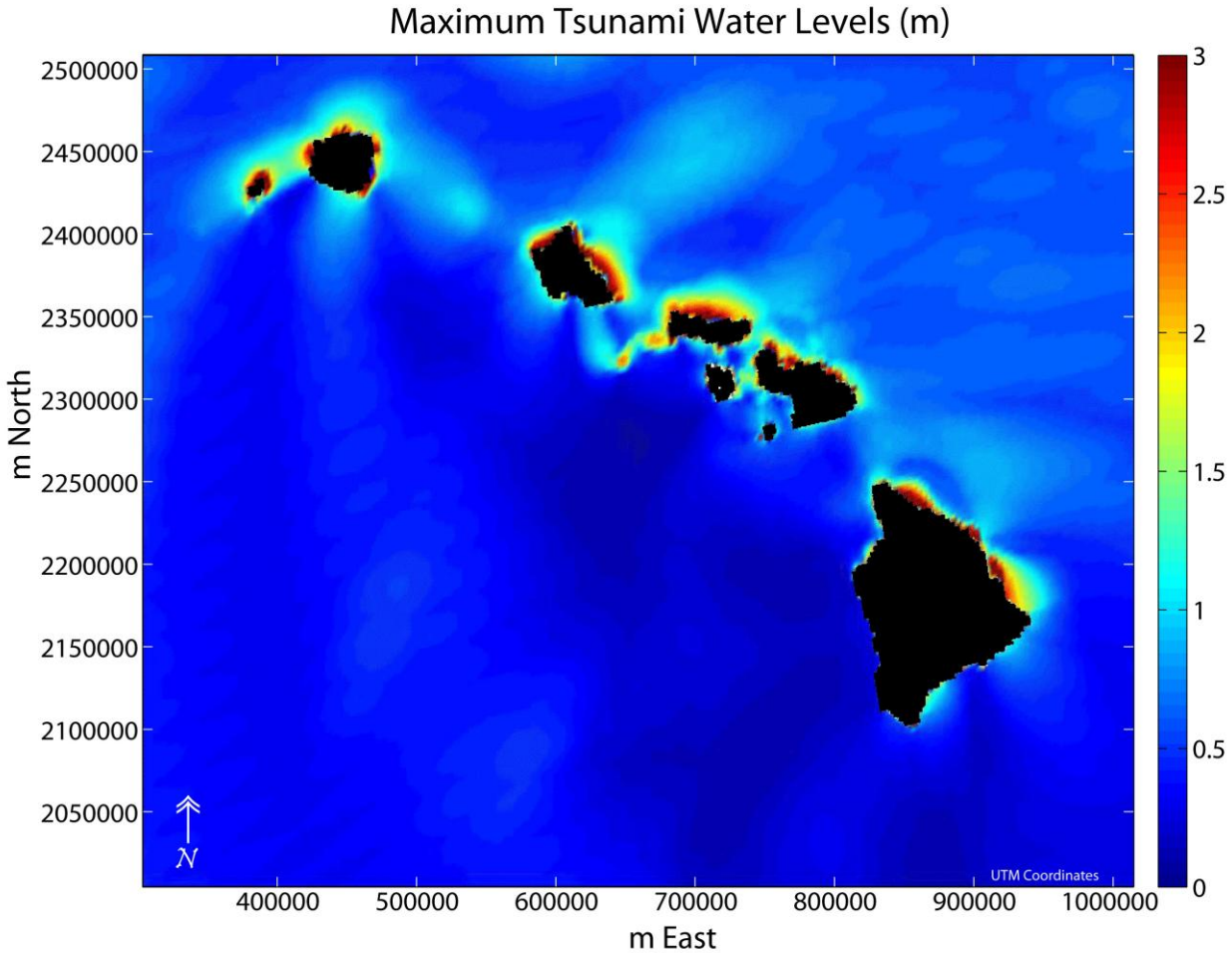

Figure 31. The maximum water levels of the 1946 tsunami model.

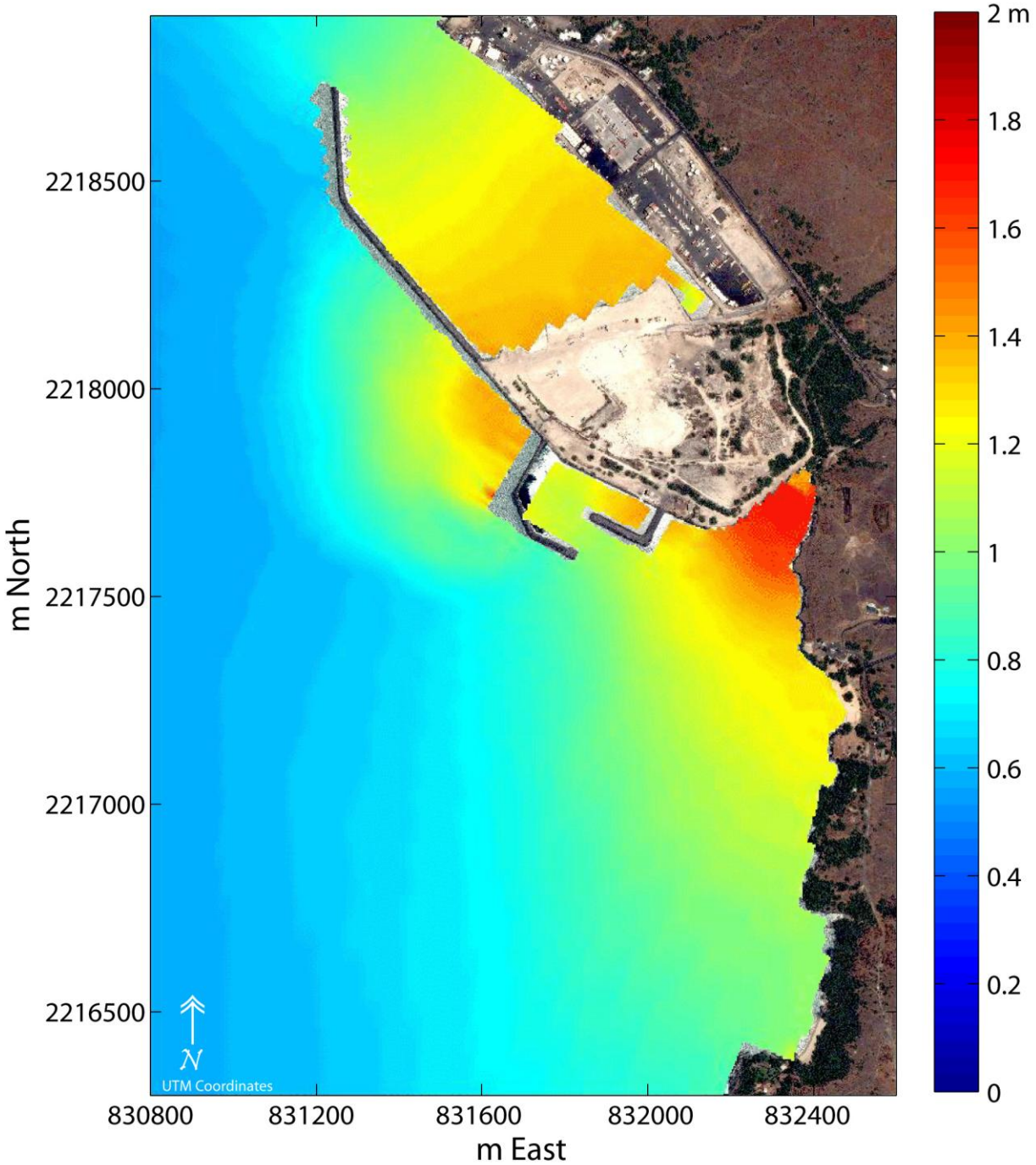

Figure 32. Maximum 1946 tsunami scenario water levels at Pu'ukoholā Heiau NHS modeled by Delft3D.

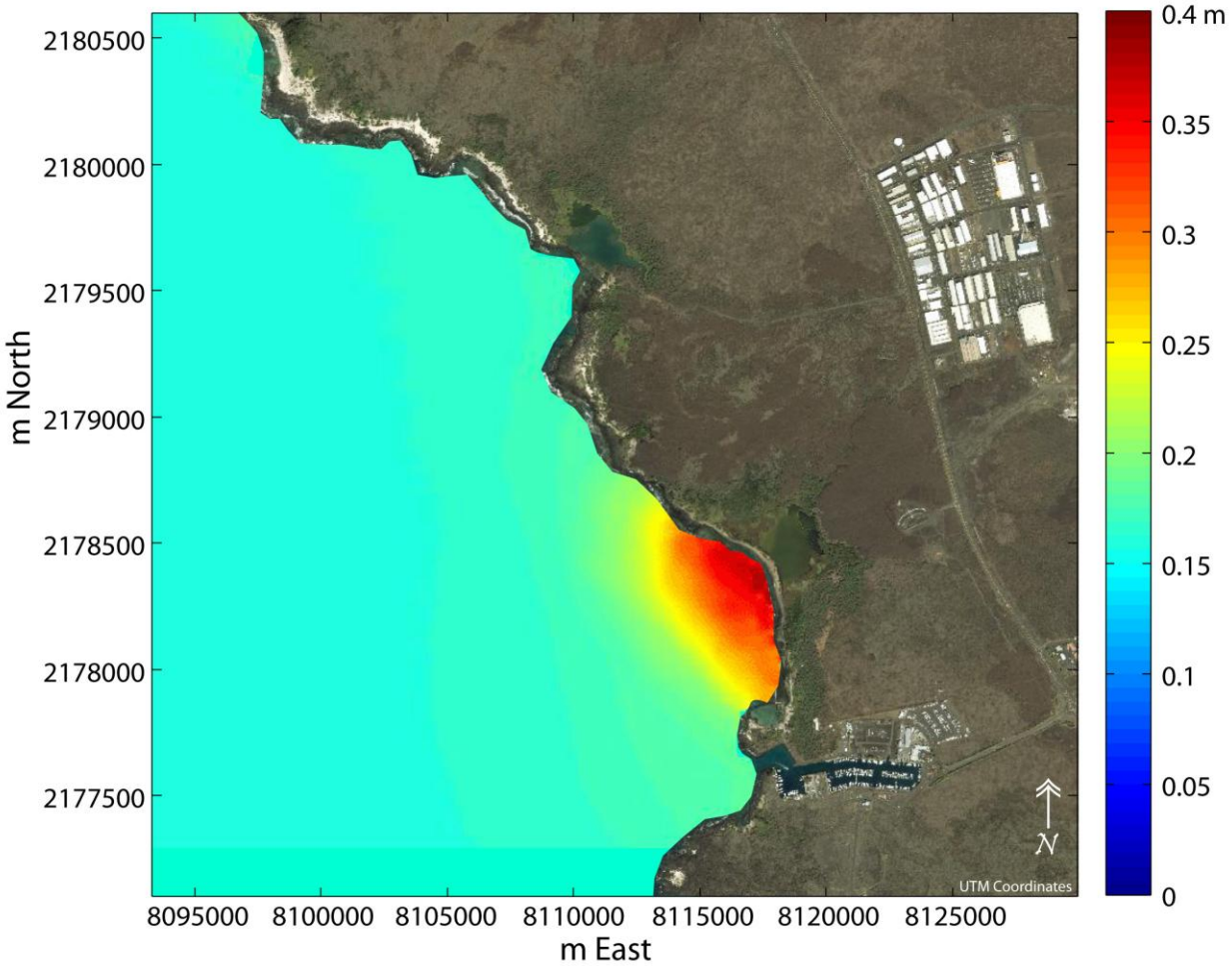

Figure 33. Maximum 1946 tsunami scenario water levels at Kaloko-Honokōhau NHP modeled by Delft3D.

Figure 34. 1946 tsunami scenario maximum inundation contours at Pu‘ukoholā Heiau NHS.

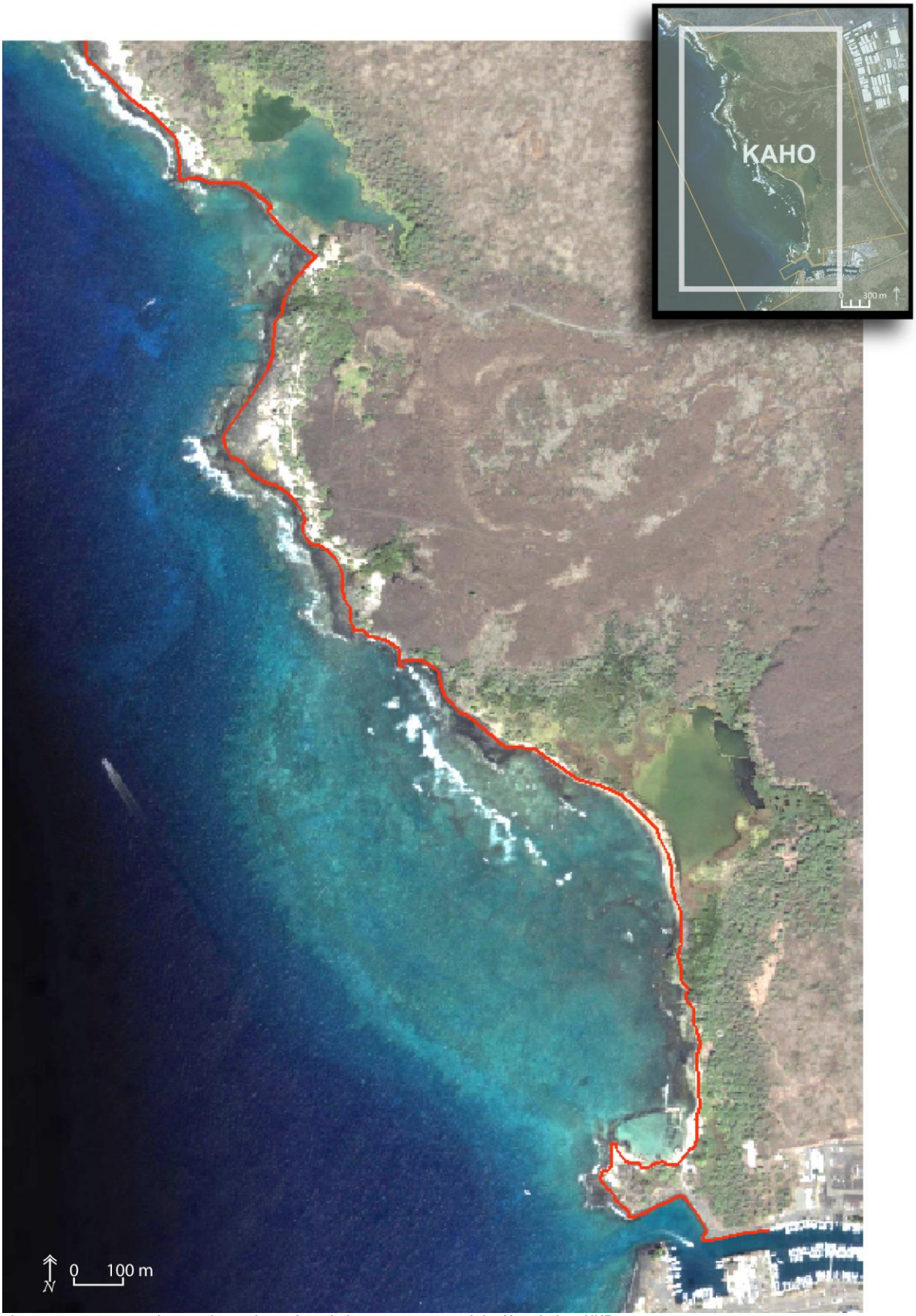

Figure 35. 1946 tsunami scenario maximum inundation contours at Kaloko-Honokōhau NHP.

Shoreline Morphology

This section describes the method and results of the digital elevation models at Pu‘ukoholā Heiau NHS and Kaloko-Honokōhau NHP.

Integrated Coastal Digital Elevation Model (C-DEM)

One objective of this study was to examine the vulnerability of the coastal area to overtopping, inundation and sea level change. An important component to these investigations is accurate detail of the topography at the coastline at various scales. C-DEMs were produced for Pu‘ukoholā Heiau NHS and Kaloko-Honokōhau NHP areas at three different grid sizes (1, 5, and 25 m) to examine wave setup and inundation scenarios. The 5-m grid size C-DEM was also used in the imagery orthorectification process.

Data Sources

Light Detection and Ranging (LiDAR) data were collected for the Federal Emergency Management Agency (FEMA) and the Army Corps of Engineers (ACE) by the Joint Airborne LiDAR Bathymetry Technical Center of Expertise (JALBTCX). FEMA terrain data extends landward from the water line to include the 15-m elevation contour at the time of collection. ACE SHOALS (Scanning Hydrographic Operational Airborne LiDAR System) data extends from just below the calm water surface to approximately 40 m (~130 ft) water depth or survey boundary offshore, whichever is reached first. Ten-meter USGS DEM data from spot elevations were used to fill areas that lie landward of the data bounds of these two data sources.

FEMA LiDAR data were received as two processed separate data products; bare earth returns and extracted features. The bare earth returns were used as the primary terrain dataset. Bare earth returns are a subset of the acquired LiDAR data, features in the landscape such as buildings, vegetation and structures are removed to leave ‘bare earth’. The extracted features from this process are retained in the ‘extracted features’ dataset. We identified structures of interest for this study and replaced them into the final terrain LiDAR dataset. The data are vertically referenced to the Local Tidal Datum (LTD) which is usually a local iteration of the North American Vertical Datum of 1988 (NAVD88). SHOALS LiDAR was used as the submarine coverage for this study for the purpose of image orthorectification and wave inundation modeling. Data received were vertically referenced to local mean lower low water (MLLW) tidal elevation. USGS 10-m data were received as raster DEM files and converted to points using ArcMap toolbox function raster to point for each cell yielding a point file with 10 m horizontal spacing. The vertical reference of the USGS data is inferred to be MHW after Taylor et al. (2007). Coverage of elevation databases for each site is indicated in Figure 36.

Methods – vertical datum migration

NAVD88 is specific to the continental US and does not exist for Hawai‘i. Survey data associated with the FEMA LiDAR indicates the vertical datum, which the data is referenced to, is an iteration of the LTD – based on the last (1975) leveling network – updated to the present 1983-01 tidal epoch (MSL) – based on the 3 Kawaihae tidal benchmarks (+0.16 m), and accounting for sea level rise between the epochs (-0.031 m). This superseding survey places FEMA LiDAR in a modernized MSL datum approximately 0.13 m above the Kawaihae Harbor MSL elevation. SHOALS data were received in the MLLW tidal datum based on a survey that regionally references the data to the closest tidal station.

The USGS 10-m DEM was used at Pu‘ukoholā Heiau NHS where some landward historical photo data required approximate elevations during the orthorectification process. No USGS DEM data were used at Kaloko-Honokōhau NHP since FEMA terrain LiDAR data exist for the entire region of interest.

All data were processed in ArcMap and vertical adjustments were made using the data field calculator for each dataset. Data gaps were not filled. SHOALS data were filtered to reject any elevation points above 0 and where there appears to be FEMA points on bare earth. This results in well characterized near-shore features. FEMA data appears to have been collected near a lower tide stage with inter-tidal features. Cultural features such as fishpond walls and selected ground returns that were mis-classified as vegetation (algae covered rock in most cases), were re-introduced into the DEM dataset. All masks for the terrain LiDAR data were manually digitized based on a 2-m resolution hillshade characterization of an interpolation of the point data to highlight the shore-water interface present in the data. The mask was used to define the shoreline boundary for both the terrain (seaward extend) and bathymetric (landward extent) data. Datasets were then spatially edited to remove overlap between the different elevation sources. The data merging process used ArcToolbox – Merge and a common elevation field between the databases. The result was an irregular point cloud including both on and off-shore elevation values. A natural neighbor interpolation within Arc 3D Analyst was chosen to create a raster DEM.

Results

FEMA LiDAR data were migrated from the modernized MSL to the local MLLW on the Kawaihae tide gauge by subtracting 0.415 m from the point elevation. This study found differences in the standard deviations of the overlapping bare earth coverage areas after this migration of 0.1 m at Pu‘ukoholā Heiau NHS and 0.22 m at Kaloko-Honokōhau NHP using all points within 0.5-m radius of the SHOALS data points. These values fall within the vertical accuracy associated with each data source and the control survey, which located the data within the vertical datum.

The results of merging of the databases created point clouds of more than 4.9 million points for Kaloko-

Honokōhau NHP and more than 7.4 million for Pu‘ukoholā Heiau NHS. The results of the interpolation of the merged datasets were two 32-bit depth DEM grids for each area at 1 and 5-m horizontal resolution. The C-DEM was used in the orthorectification process and an XYZ format version of each grid was generated for modeling. Characterizations of the two generated 5 m C-DEMs are shown in Figure 37.

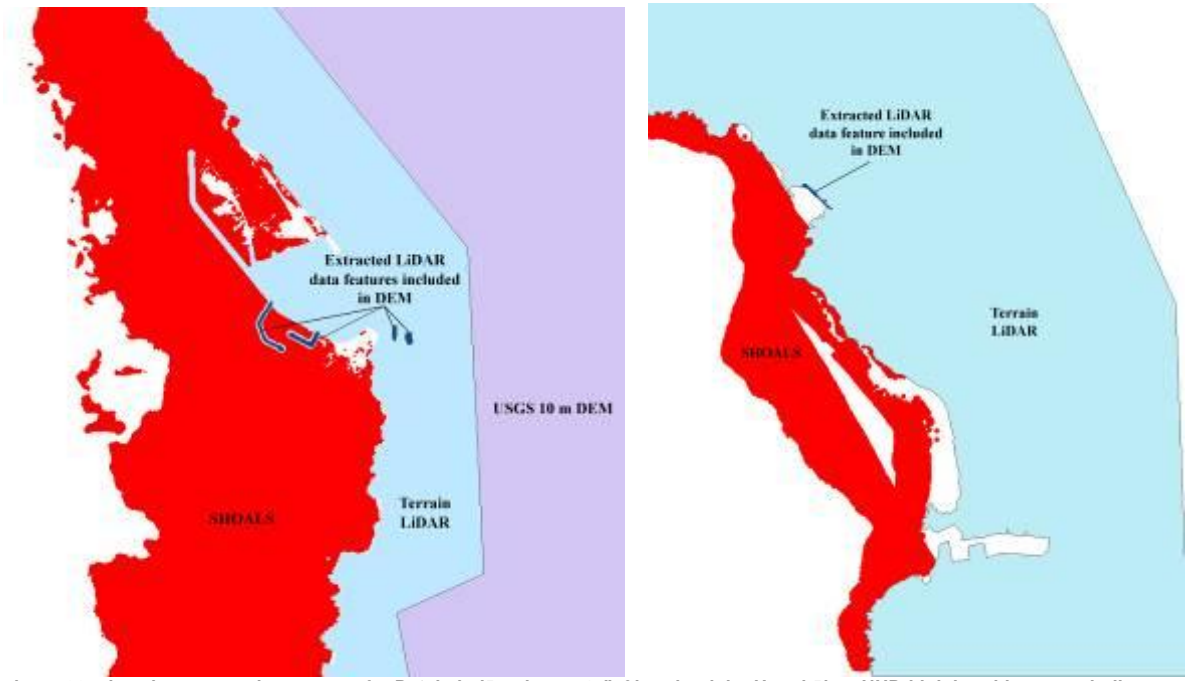

Figure 36. Elevation source data extents for Pu'ukoholā Heiau NHS (left) and Kaloko-Honokōhau NHP (right). White space indicates No Data while the dark blue features were added into the final DEM from the extracted features product of the FEMA LiDAR datasets.

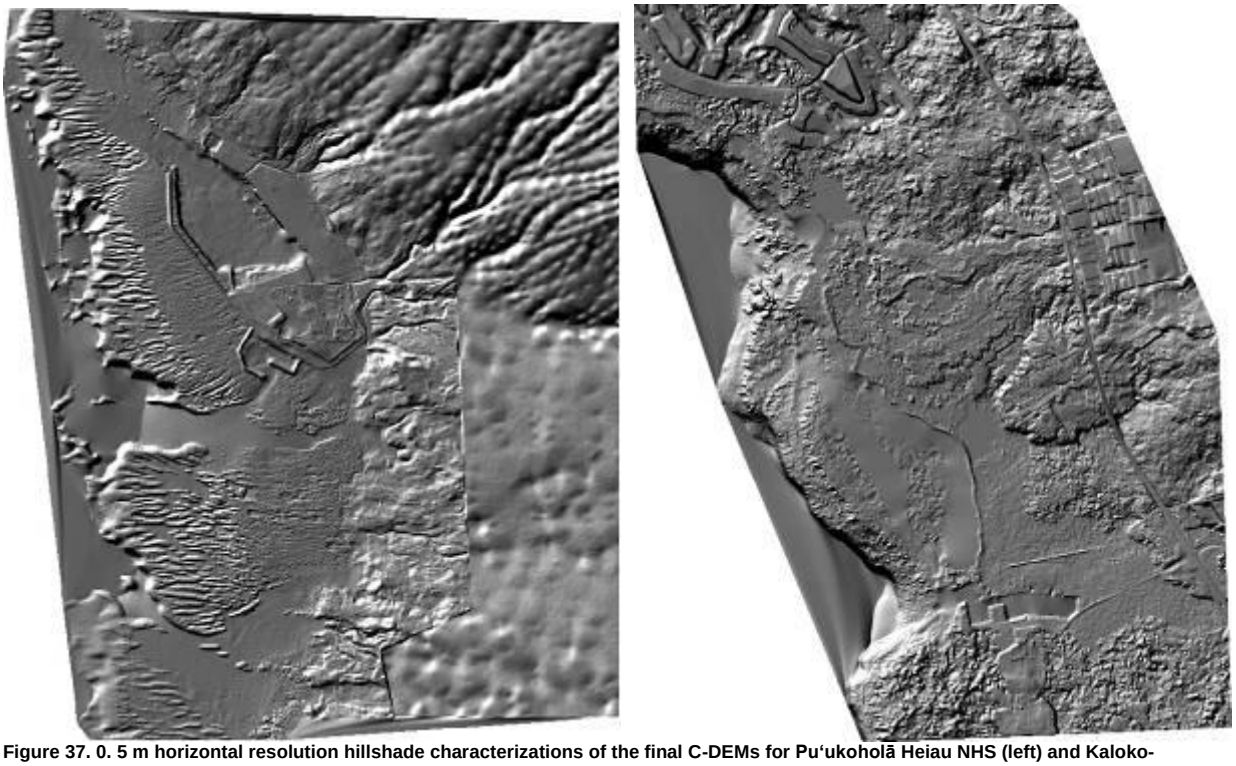

Figure 37. 0. 5 m horizontal resolution hillshade characterizations of the final C-DEMs for Pu'ukoholā Heiau NHS (left) and Kaloko-Honokōhau NHP (right). These DEMS are composites of SHOALS LiDAR (bathymetric), FEMA terrain LiDAR, and USGS 10 m DEM data.

Coastal Erosion Hazard

This section describes the method and results for the historical shoreline change at Pu'ukoholā Heiau NHS and Kaloko-Honokōhau NHP.

Shoreline change evaluations are based on comparing historical shorelines derived from processed vertical aerial photography. Historical shorelines generally represent the period of the last 70 years. Long-term rates of change are calculated using most shorelines (1940's to most recent shoreline) using the standard single-transect (ST) method as well as an alternative method incorporating principal component analysis (EX). Short-term rates of change are calculated using most shorelines (1940's to most recent shoreline) using an advanced form of EX called EXT. The historical rates of change presented in this report represent past conditions and therefore are not intended for predicting future shoreline positions or rates of change.

Compilation of historical shorelines

Coastal scientists in universities and government agencies have been quantifying rates of shoreline movement and studying coastal change for decades. The most commonly used sources of historical shoreline data have traditionally been NOAA Topographic Sheets (T-sheets, see Shalowitz, 1964) and vertical aerial photographs. Ideally, extraction of past shoreline positions from these data sources involves geo-referencing and removing distortions from maps and aerial photographs, followed by digitizing the shoreline position. Depending on coastal location, data source, and investigator, different proxies for shoreline position are used to represent the position of the shoreline at the time the map or photo was produced. Time series of shoreline positions document coastal change and are interpreted to improve our understanding of shoreline stability. Common shoreline proxies include the high water line (for discussion of the high water line (HWL) see Shalowitz, 1964), a wet-dry line, the first line of vegetation, the toe or crest of the abutting dune, a low water line such as the toe of the beach, a cliff base or top, and a tidal datum or elevation – typically the location where the plane of mean high water (MHW) intersects the beach face.

Delineation of aerial photo based shoreline

In Hawai'i, the high reflectivity of Hawaiian white carbonate beaches reduces the visibility of the HWL on contact prints of historical aerial photography (Fletcher et al. 2003). Norcross et al. (2002) and Eversole (2002) found that the low water mark (LWM), or toe of the beach, played a significant role as a pivot point for along-shore transportation processes at their study sites of Kailua, Oahu and Kaanapali, Maui respectively. High water clarity and the absence of significant flotsam in Hawaiian waters allow the delineation of the LWM on historical 0.5 m orthorectified aerial photomosaics as a color (Black and White or Color) tone change at the base of the foreshore, most easily identified during a wave runup on the beach.

Uncertainties and errors

Several sources of error impact the accuracy of historical shoreline positions and final shoreline change rates. We define two types of uncertainty: positional uncertainty and measurement uncertainty. We quantify 7 different sources of error in identifying shoreline positions on aerial photographs and T-sheets (3 positional and 4 measurement errors). The 7 different sources of errors are summed in quadrature (the square root of the sum of the squares) to get a total positional uncertainty (U_t). Table 8 contains values of each error for Kaloko-Honokōhau NHP and Pu'ukoholā Heiau NHS.

Positional uncertainty is related to all features and phenomena that reduce the precision and accuracy of defining a representative shoreline position in a given year. These uncertainties mostly center on the nature of the shoreline position at the time an aerial photo is collected. Influences on position include the stage of tide, the incidence of storms, and the seasonal state of the beach.

Seasonal error (E_s) is quantified by using summer and winter beach profiles (or shoreline positions from aerial photographs). Many beaches have seasonal cycles where they accrete in summer and erode in winter (or vice versa). Because the availability of high resolution aerial photographs is limited for the two national parks, the selection of aerial photographs cannot be based on seasonal time frames. To account for the shifts in shoreline position due to seasons, the seasonal error is the standard deviation of a randomly generated uniform distribution with minimum and maximum values equal to the mean plus two times the standard deviation of the difference in the seasonal shoreline positions.

Tidal fluctuation error (E_{td}) is only calculated for aerial photographs. The aerial photographs were obtained without regard to tidal cycles, which can result in inaccuracies on the digitized shoreline. The horizontal movement of the LWM during a spring tidal cycle was estimated based on the morphology of the different beaches within each study area. Because the tides are cyclical fluctuating between low and high, there is an equal chance of taking a photograph of the shoreline at different stages of the tides. Therefore, the tidal error is the standard deviation of a randomly generated uniform distribution with minimum and maximum values equal to two times the horizontal movement of the LWM.

Digitizing error (E_d) is the error associated with digitizing the shoreline. Only one analyst digitizes the shorelines for all photographs and T-sheets to minimize different interpretations from multiple users. The error is the standard deviation of the differences between repeat digitization measurements. The error is calculated for photos/T-sheets at different resolutions.

Pixel error (E_p) is the pixel size of the image. The pixel size in orthorectified images is 0.5 m, which means anything less than 0.5 m cannot be resolved.

Rectification error (E_r) is calculated from the orthorectification process. Aerial photographs are corrected, or rectified, to reduce displacements caused by lens distortions, earth curvature, refraction, cameral tilt, and terrain relief using remote sensing software. The Root Mean Square (RMS) values calculated by the software are measures of the misfit between points on a photo and established ground control points (GCP). The rectification error is the RMS value.

T-sheet plotting error (E_{ts}) is only calculated for T-sheets. The error is based on Shalowitz (1964) thorough analysis of topographic surveys. There are three major errors involved in the accuracy of T-sheet surveys: (1) measuring distances has an accuracy of 1 m, (2) planetable position has an accuracy of 3 m, and (3) delineation of the actual high water line has an accuracy of 4 m. The three errors are summed in quadrature to get the plotting error.

These errors are random and uncorrelated and may be represented by a single measure calculated by summing in quadrature (the square root of the sum of the squares). The total positional uncertainty (U_t) is:

$$U_t = \pm\sqrt{E_s^2 + E_{td}^2 + E_c^2 + E_d^2 + E_p^2 + E_r^2 + E_{ts}^2}$$

For aerial photographs, E_c and E_{ts} are omitted. For T-sheets, E_r and E_{td} are omitted.

These uncertainty values can be propagated into the shoreline change result using the analysis methods discussed below. The resulting uncertainty of the rate will incorporate the uncertainty of each shoreline and the uncertainty of the model.

TABLE 8. Range of errors for Kaloko-Honokōhau NHP and Pu'ukoholā Heiau NHS.

Magnitude Ranges (m)		
Source	***KAHO***	***PUHE***
Es, Seasonal Error	± 2.9	± 1.7
Etd, Tidal Error	± 5	± 5
Ec, T-sheet Conversion Error	N/A	N/A
Ed, Digitizing Error	± 0.8 – 1.7	± 0.8
Ep, Pixel Error	± 0.5	± 0.5
Er, Rectification Error	± 0.9 – 5	± 0.4 – 2.6
Ets, T-sheet Plotting Error	N/A	N/A

Analysis methods

Single-Transect (ST) method

For the single-transect method (ST) a rate is calculated at each transect spaced every 20 m alongshore. A rate is calculated at each transect location regardless of the effects of shoreline positions at adjacent transects. Several different statistical methods can be used to calculate the rate at each transect (e.g., End-Point Rate (EPR), Ordinary Least Squares (OLS), and Weighted Least Squares (WLS)). The change-rate approach used for the ST analysis of Kaloko-Honokōhau NHP and Pu'ukoholā Heiau NHS is WLS.

One assumption of ST is that shoreline behavior at one transect is independent of shoreline behavior at an adjacent transect. However, rarely does a single transect behave independently from neighboring transects, as sediment transport usually affects shorelines in the cross-shore and alongshore directions. One way to determine whether transects along a beach are independent or not is to determine the spatial correlation distance. If the correlation distance is greater than the transect spacing, then the assumption for ST fails and ST is over-fitting the data (Frazer et al. in press).

Rate uncertainty is high with ST since the rate is calculated using between four and ten shoreline positions at one transect. With less information (about adjacent shoreline position), the uncertainty will be greater. Hence many rates with ST will not be significant.

Eigenbeaches (EX and EXT): Alternatives to ST method

Eigenbeaches is an alternative method that incorporates all data within a beach system to calculate a rate at each transect. For a comprehensive description of Eigenbeaches, see Frazer et al. (in press). Eigenbeaches uses a linear sum of basis functions on a finite scale to determine shoreline change. Basis functions are building blocks that are used in a function. For Eigenbeaches, the principal components of the shoreline data (or eigenvectors) are the basis functions, and are used to model the rate in the alongshore direction (spatially along the transects).

This method reduces the number of parameters needed to describe shoreline change on a beach. If there are 30 transects on a beach, ST calculates a rate at each transect, making the number of rate terms equal to 30 to describe shoreline change. The number of parameters in Eigenbeaches is limited to the number of shorelines present at a specific beach. If there are 30 transects, but 10 shorelines, the maximum number of basis functions that describes the rate term is equal to 10. The reduction in terms and the increase in data points in Eigenbeaches reduce the uncertainty values of the shoreline change rate (Frazer et al. in press).

There are two types of Eigenbeaches: (1) EX – rates are modeled in the alongshore direction (X) using basis functions, but the rates are constant through time (Figure 38); (2) EXT – rates are modeled in the alongshore direction (X) using basis functions, and the rates change with time (T) using a quadratic fit (i.e., acceleration) (Figure 39). Both EX and EXT use the same basis functions. Because the basis functions are the principal components of the shoreline data, using the same data set to calculate the rates and their uncertainties is inappropriate, hence shoreline data is divided into two data sets. The first data set is used to generate the basis functions, which are then used to model the second data set. We use an information criterion (IC) to

determine the number of basis functions needed to model the data. An IC is a test statistic that determines the best model from a group of models that are not necessarily nested (Sugiura 1978, Hurvich and Tsai 1989).

Before running EX or EXT, we use ST to determine the spatial correlation distance. Transects are usually closely spaced and shoreline measurements from these transects can be correlated in the alongshore direction. To calculate the correlation distance, ST is first run to determine the data residuals. A decaying exponential function is fit to the autocorrelation of the data residuals . The best-fit exponential decay is the correlated data error with equation: $\exp\left(-\left|x_i - x_j\right| / L\right)$, where x_i and x_j are transect locations, and *L* is the estimated correlation distance. In computing ST, we use WLS to calculate the rate at each transect. WLS takes into account the uncertainty at each time position (covariance matrix) and propagates it into the model. The resulting rate and rate-uncertainty incorporate the uncertainty of the model and the uncertainty in the time positions. For EX and EXT, we combine the correlated data errors with the uncertainty in the time position in the covariance matrix. Because this matrix is more complicated, we use Generalized Least Squares (GLS) to calculate the rate terms (WLS is a simplified form of GLS).

Eigenbeaches has similar limitations to ST despite improvements in calculating uncertainty and not assuming transects are independent. Both methods are susceptible to outliers, whether the outlier is statistical or based on *a priori* knowledge (i.e., storms). Both methods use least squares, which assumes Gaussian errors. Robust methods such as Least Absolute Deviation (LAD) and Least Median of Squares (LMS) can be applied to both methods to overcome limitations. LMS finds statistical outliers and removes them from the data. LAD does not discard data, rather it puts less emphasis than least squares on outlier points.

Reporting ST, EX and EXT results

ST and EX results are used for long-term predictions because it is more reliable than EXT (Genz et al. in press; Romine et al., accepted). Genz et al. (in press) found that EX did better than EXT in cross-validating the most recent shoreline. Romine et al. (accepted) found that EXT rates were strongly influenced by more recent shoreline data and was a better indicator of change that was occurring at a more recent, short-term time scale. Therefore, we use EX for long-term predictions and EXT for short-term changes. Rates reported with EXT are the rates at the most recent time position.

Similar to ST, EX and EXT do not smooth rates in the alongshore direction. EX and EXT use eigenvectors of the shoreline data to model rates in the alongshore direction. Any discontinuities present in the alongshore direction will be embedded in the eigenvectors. Hence, the resulting EX and EXT rates are not smoothed. If other basis functions were used (e.g., Legendre polynomials or trigonometric functions), the rates would be smoothed in the alongshore direction. A disadvantage of smoothing within the analysis is that if there is a discontinuity (e.g., hardened shoreline affects one segment of the beach causing a significant rate shift), the basis function methods that smooth would be susceptible to ringing and the resulting rates would not reflect the alongshore variation. However, many coastal managers prefer smoothed rates in the alongshore direction for policy purposes.

A smoothing technique can be applied to ST, EX and EXT rates after the analyses are complete. The rates are smoothed using a center-weighted five-point moving average (Rooney et al. 2003). The weighting scheme is 1, 3, 5, 3, 1 for each set of transects. We present the ST and smoothed EX rates in the results representing long term historic trends in shoreline position while EXT is presented to indicate recent shoreline trends.

Rectification of vertical aerial photography

Historical and modern aerial photographic coverage of Pu‘ukoholā Heiau NHS and Kaloko-Honokōhau NHP areas was achieved using two methods (Table 9). Historical imagery of Kaloko-Honokōhau NHP was received via DVD from the National Park Service (NPS). The received imagery was georeferenced but lacked camera calibration and geometric information for each scene. Data were visually inspected using modern (2006) satellite imagery and the 2002 imagery from NPS. Inspection focused on the comparison of hard shoreline and geologic features such as headlands and reef along the coast. Significant offset (excess of 5 m) was found for several images. Those images were ‘refined’ using ESRI ArcMap georeferencing tool to locate ground control points on the stable features visible in both the historical images and modern satellite imagery. The images were processed using a 3rd Order Polynomial solution and checked for shoreline feature matching. Final images are included in **Appendix C**.

Vertical aerial imagery of Pu‘ukoholā Heiau NHS was acquired from local vendors and received as digital image scans on DVD. Following the orthorectification methods used by Fletcher et al. (2003) in their shoreline mapping on Maui, integrated coastal digital elevation models and a modern (2006) satellite image were used in the processing. Resulting map-correct images and mosaics were inspected using the satellite reference image and comparing the locations of stable features visible in both the reference and processed images. Final images are included in **Appendix C.**

TABLE 9. Imagery acquired for Pu‘ukoholā Heiau NHS and Kaloko-Honokōhau NHP areas. Delineated into two groups: Reference Imagery and Processed Imagery.

AREA	REFERENCE IMAGERY	PROCESSED IMAGERY
PUHE	2006 Quickbird Satellite	1949, 1950, 1966, 1970, 1975-June, 1975-Nov, 1977, 1981, 1987, 1989, 1990, 1998, 2006
KAHO	2006 Quickbird Satellite	1950, 1954, 1965, 1968, 1970, 1980, 1987, 1988, 1992, 2000, 2002

ST, EX and EXT results at Kaloko-Honokōhau NHP and Pu‘ukoholā Heiau NHS

The low water mark (LWM) is used as the shoreline change reference feature (SCRF) for this study. Transects are spaced every 20 m alongshore. Results are presented on poster maps, as individual ‘transect plots’, and in table form (see Appendix D). There were no consistent trends found at a scale that includes both study areas, rather Kaloko-Honokōhau NHP and Pu‘ukoholā Heiau NHS are unique in morphology, shoreline history, and responses to periodic events. The EX method is used to project an erosion hazard line at CI 95% and is used in the area descriptions.

Kaloko-Honokōhau NHP

The Kaloko-Honokōhau NHP study area extends from Noio Point (just south of Honokōhau Harbor) to just north of Kaloko Fishpond. The coastline is composed of carbonate sand beach in the south (Honokōhau Beach), low basalt headlands at Kaloko Point and basalt fronted supratidal carbonate beach in the north. Two sections of shoreline were selected for analysis: (1) Maliu Point to just north of ‘Aimakapā Fishpond, including Honokōhau Beach (transects 0 – 63; Figure 40) in the south; (2) the supratidal beach just north of Kaloko Fishpond (transects 66 – 87; Figure 41).

The thin carbonate beach between Maliu Point and north of ‘Aimakapā Fishpond is experiencing long term erosion (EX) at an average rate of -0.8 ± 0.1 ft/yr. Recent shoreline data indicate a slight slowing of this trend at an average recent change rate (EXT) of -0.4 ± 0.1 ft/yr. At the southern end of Honokōhau Beach is ‘Ai‘ōpio Fishtrap. Aerial photography from 1950 to present show sand migrating north along the beach and out to ‘Aimakapā Fishpond area exposing several cultural sites to minor wave action. This portion of shoreline has experienced long term erosion (EX) at an average rate of -0.7 ± 0.1 ft/yr. The average EXT change rate at this section of shoreline in 2006 is -0.4 ± 0.4 ft/yr.

The ‘Aimakapā Fishpond is marked on the seaward side by Honokōhau Beach. This ~550 ft section of the beach (transects 33 – 41) has been moderately stable over the period of study with an average long term shoreline change rate (EX) of -0.3 ± 0.1 ft/yr. Recent data suggests it continues to be stable with an average rate (EXT) of 0.5 ± 0.2 ft/yr.

The northern segment of Kaloko-Honokōhau NHP (transects 66 – 87) is active during storm and large swell events. It extends northward from Kaloko Fishpond. This section of coast is relatively stable with long (EX) and short term (EXT) average rates of change within the range of uncertainty (EX = -0.1 ± 0.1 ft/yr and EXT = -0.1 ± 0.3 ft/yr).

Pu‘ukoholā Heiau NHS

The Pu‘ukoholā Heiau NHS study area is comprised of two separate carbonate sand beaches. Pelekane Beach (Figure 42) prior to construction of Kawaihae Harbor in the 1950’s is noted as a thin black sand beach that stretched along the shoreline the length of the present day harbor. Today’s Pelekane Beach was created with carbonate spoil from reef dredging during harbor construction. 1970 data were removed from analysis due the apparent result of an episodic event severely altering the beach. This is possibly due to the 1968 tsunami. Analysis of Pelekane Beach for this study begins with 1966 data, the first aerial coverage identified after the creation of the harbor and beach creation. Since 1966, Pelekane beach has been accreting at a long (EX) and short term (EXT) average rate of 1.4 ± 0.7 ft/yr.

South along the low rocky shoreline, lies Spencer State Beach Park at Ohaiula Beach (Figure 43). Although Spencer State Beach Park is not within park boundaries, it was included in the study in order to document changes in areas abutting the park that might have future effects on the park. This small pocket beach of carbonate sand has experienced long (EX) and short term (EXT) erosion with an average rate of -0.8 ± 0.5 ft/yr.

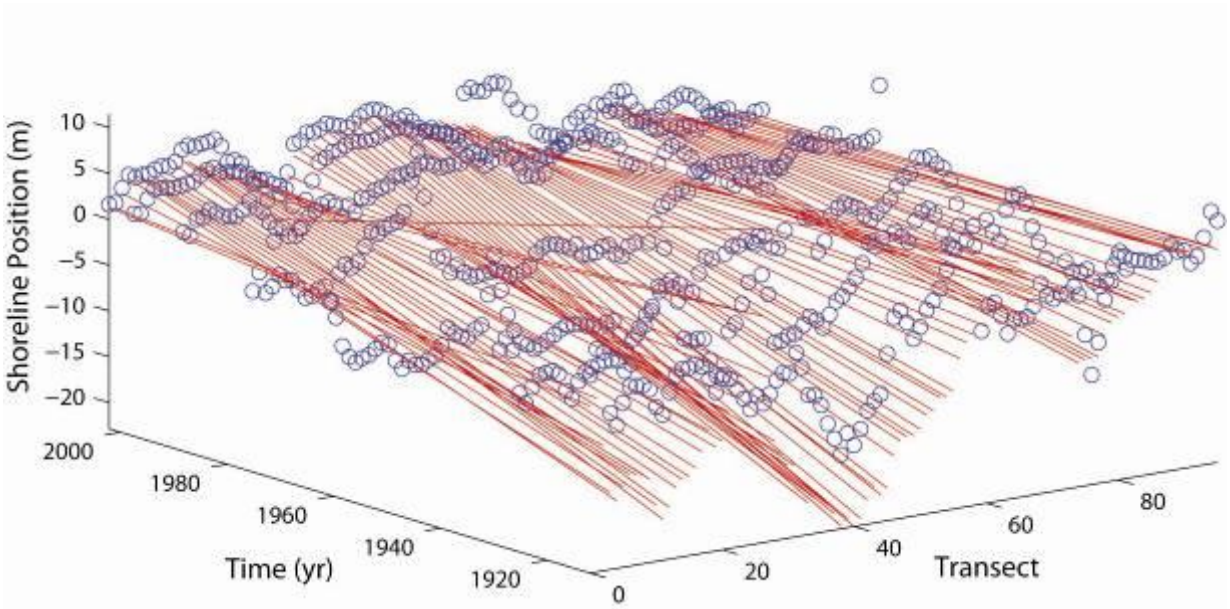

Figure 38. EX fit at each transect. The rates are modeled spatially along the transect location, but are constant through time.

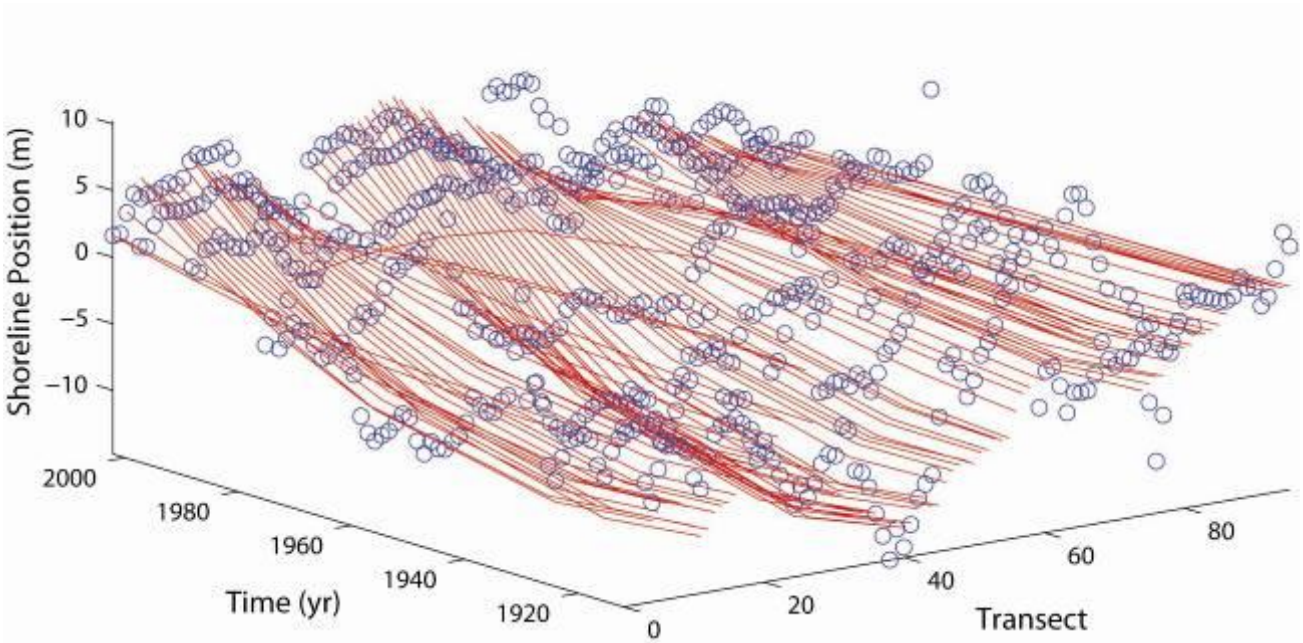

Figure 39. EXT fit at each transect. The rates are modeled spatially along the transect location, and are modeled with a quadratic fit though time.

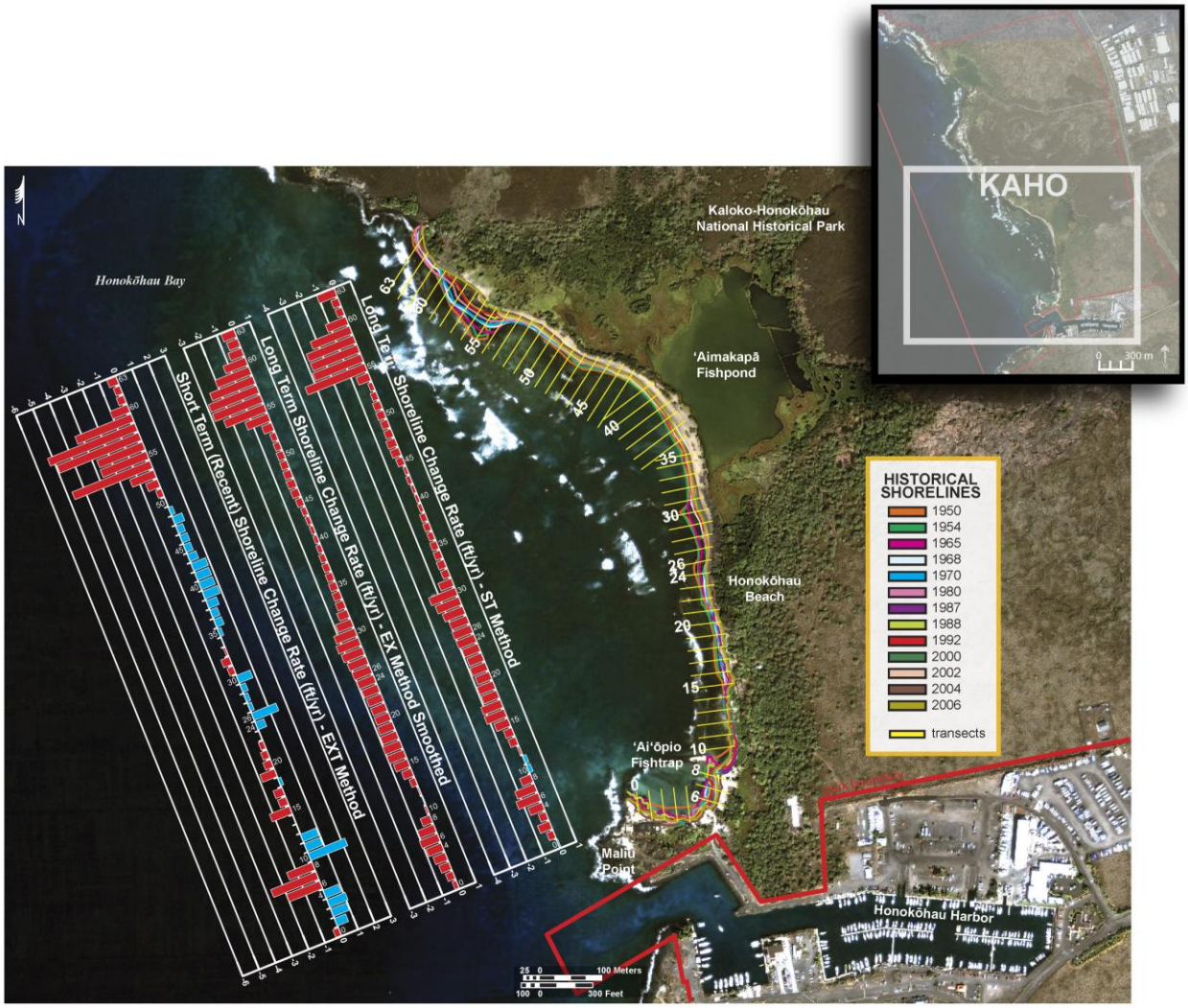

Figure 40. Maliu Point to north of 'Aimakapā Fishpond shoreline positions, transects and results. Shoreline change rates are displayed in graph form offshore. Each bar corresponds to a transect location (yellow shore-normal lines) on the shoreline. Negative rates (erosion) are indicated in red. Positive rates (accretion) are indicated in blue.

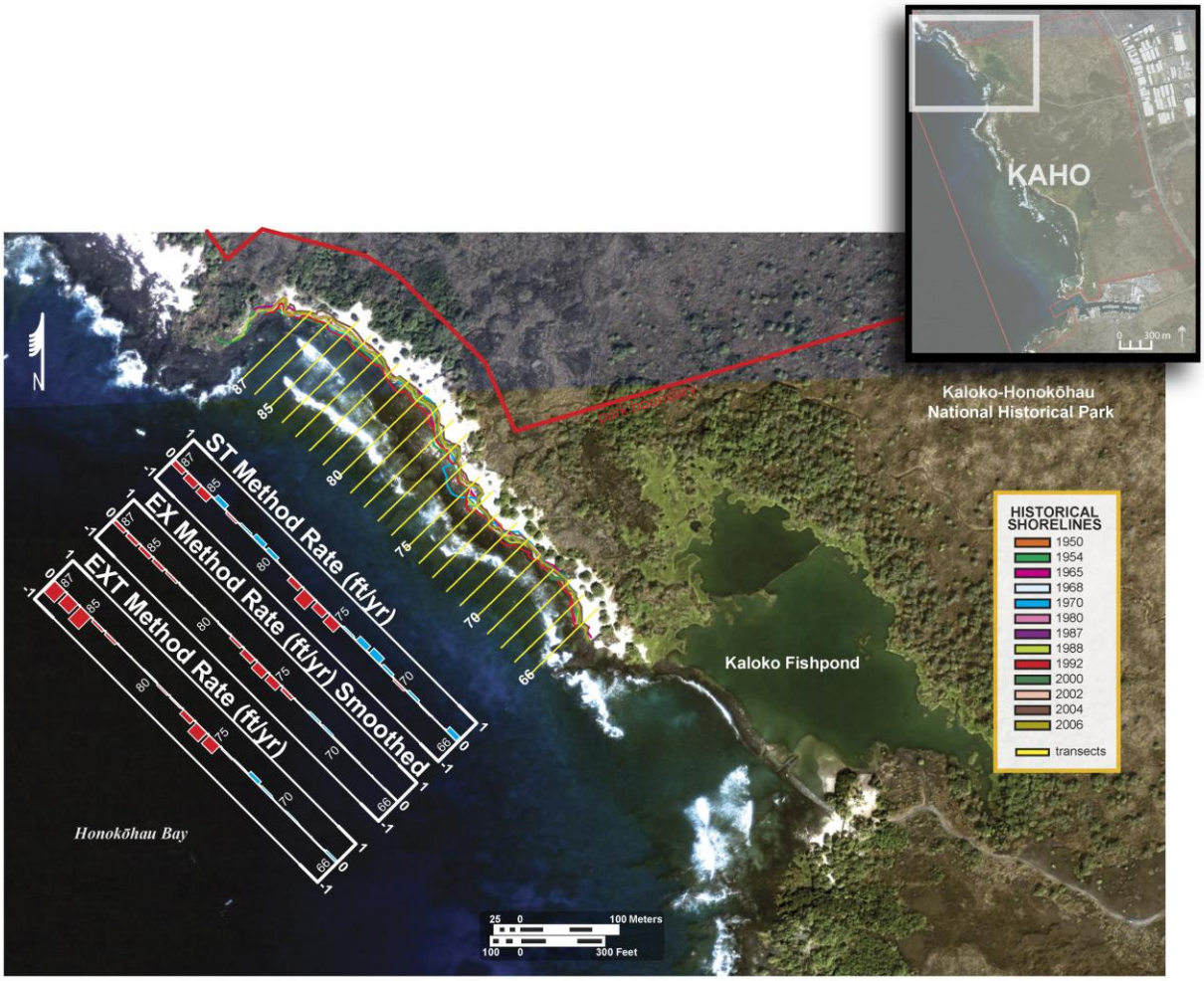

Figure 41. North of Kaloko Fishpond shoreline positions, transects and results. Shoreline change rates are displayed in graph form offshore. Each bar corresponds to a transect location (yellow shore-normal lines) on the shoreline. Negative rates (erosion) are indicated in red. Positive rates (accretion) are indicated in blue.

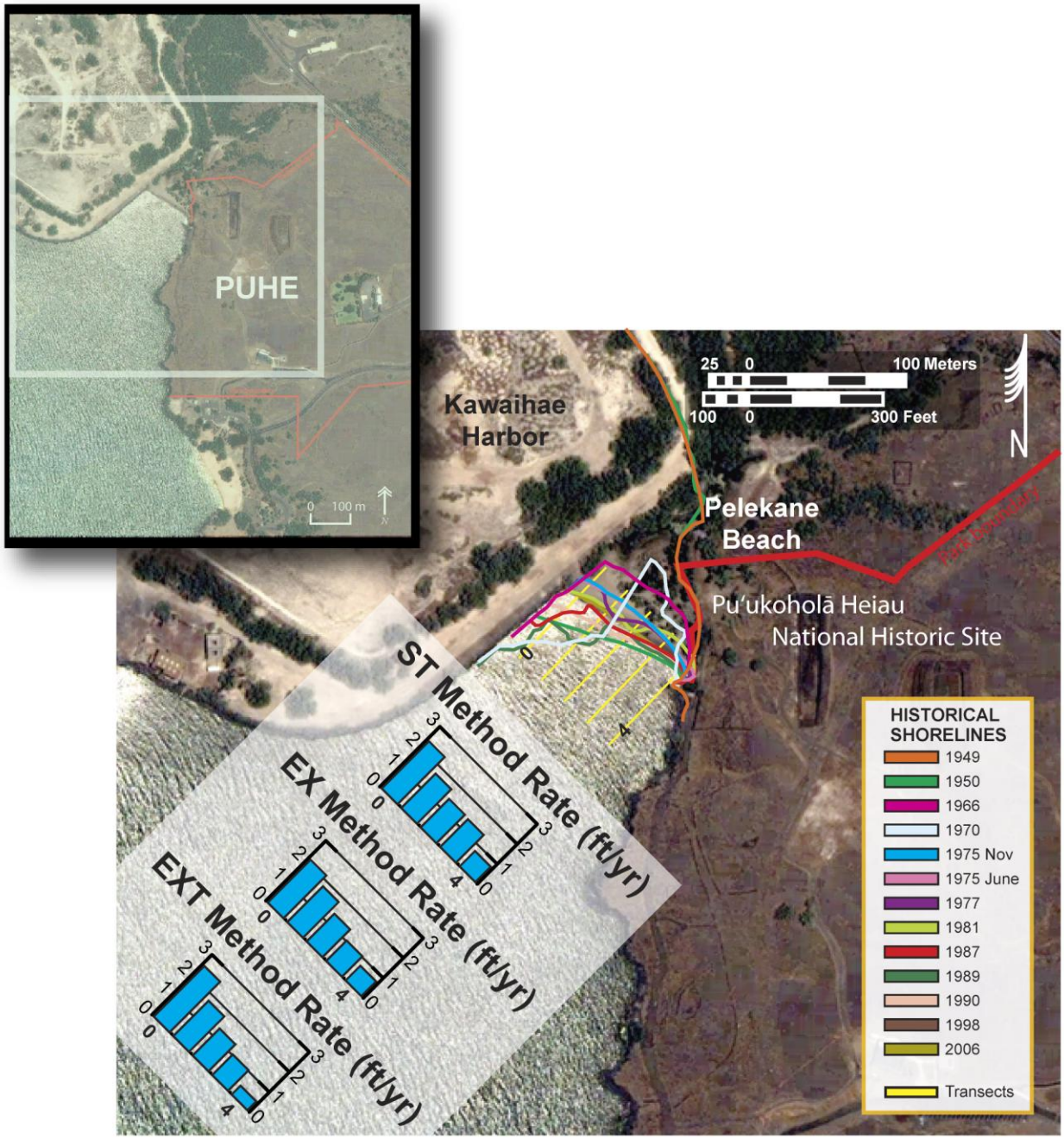

Figure 42. Pelekane Beach shoreline positions, transects and results. Shoreline change rates are displayed in graphs offshore. Each bar corresponds to a transect location (yellow shore-normal lines) on the shoreline. Negative rates (erosion) are indicated in red. Positive rates (accretion) are indicated in blue.

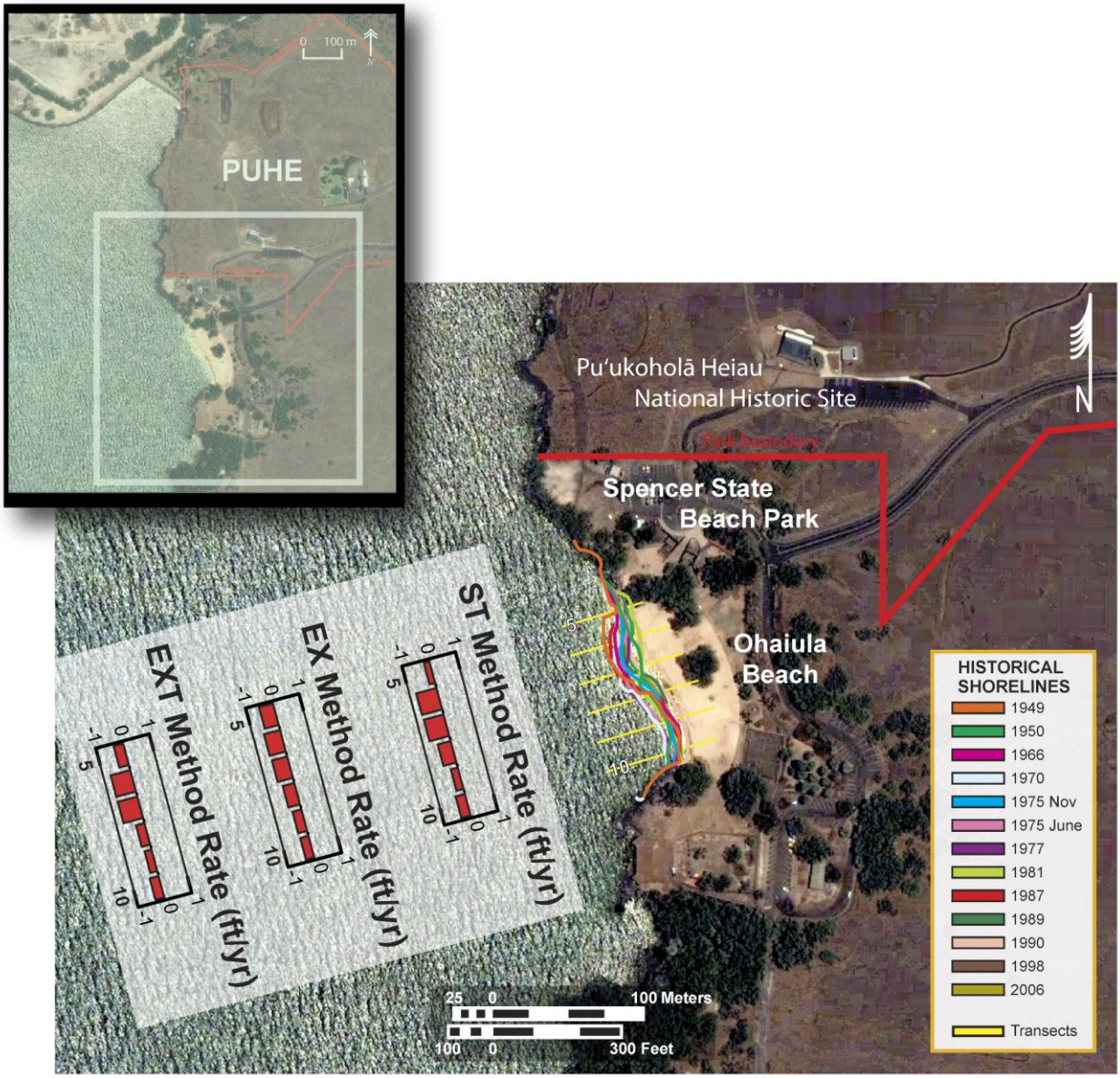

Figure 43. Ohaiula Beach shoreline positions, transects and results. Shoreline change rates are displayed in graphs offshore. Each bar corresponds to a transect location (yellow shore-normal lines) on the shoreline. Negative rates (erosion) are indicated in red. Positive rates (accretion) are indicated in blue.

Impacts and Recommendations

The following section briefly describes the impacts at Pu‘ukoholā Heiau NHS and Kaloko-Honokōhau NHP. This section describes conditions that may require attention from resource managers.

It is estimated that sea-level on the Big Island of Hawai‘i will be approximately 0.15-0.41 m above present by 2050, and 0.32-1.55 m by 2100 (Table 2). This will create a number of coastal impacts to Pu‘ukoholā Heiau NHS and Kaloko-Honokōhau NHP ranging from passive flooding of low-lying areas, to increased coastal overtopping and erosion. These impacts will threaten the existence of low-lying coastal landmarks, historic sites, and coastal habitat.

Kaloko-Honokōhau NHP

Coastal overtopping at Kaloko Seawall will increase significantly under projected sea-level rise. The number of large swell events which fully overtop the seawall will increase by a factor of 3-4 by 2050 and by a factor of greater than 10 by 2100. This overtopping will continue to cause significant undermining of the seawall. The seawall is currently being rehabilitated and maintained after decades of disrepair. The northern portion of the wall is currently undergoing rehabilitation, the southern portion was completed in 2004. If maintenance of the seawall does not actively continue into the future, the wall will begin to fall into disrepair as overtopping increases.

Coastal erosion will continue along the beach fronting ‘Aimakapā Fishpond. The beach is approximately 11-22 ft wide and the average erosion rate is between 0.2-0.5 ft per year. If these rates continue the beach will erode to the point where the likelihood of a breach of the fishpond is possible by 2050. If the beach experiences erosional events to the point where a breach is possible, then mitigation measures should be considered. One measure is salinity testing to determine the amount of mixing occurring between seawater and the groundwater-fed fishpond. Also, monitoring high tides and large swell events can be done (e.g., using photography). This monitoring can help determine if active measures (e.g., sandbagging) need to be taken to prevent a breach.

Sea-level rise will passively flood the wetlands of the middle portion of Kaloko-Honokōhau NHP between Kaloko Seawall and the beach fronting ‘Aimakapā Fishpond. Impacts from this flooding include hampering park access along coastal trails and habitat changes, especially to vegetation that is not salt-tolerant. Because sea-level rise is a subtle process, flooding will increase gradually. Long-term monitoring of wave damage should be conducted in this section. Monitoring can include beach profiles for sections where beaches exist or photographs of wave action on the coast before, during, and after the maximum annual high tide and should include land that will be inundated in 2050 (**Figure 14**). The Heiau on the southern portion at ‘Ai‘ōpio Fishtrap will be impinged by sea-level rise, although it is *not* likely to experience failure based on 2050 projected sea-level rise.

Sea-level rise will submerge the ‘Ai‘ōpio Fishtrap during low tide by 2050, and constantly submerge the fish trap by 2100. Long-term monitoring of the fishtrap during high tide and large swell events is recommended. If the fishtrap is in danger of submersion, we recommend working with local cultural agencies to determine whether to prevent or allow submersion of the cultural site.

Potential tsunami hazards based on the 1946 tsunami appear to be minimal. Measured runup from the 1946 tsunami is higher than the modeled runup and should be taken into account during decision-making processes. Tsunamis originating from other directions were not analyzed for this report, but could be a potential topic for future work.

Pu‘ukoholā Heiau NHS

Projected sea levels will passively flood Pelekane Beach on the northern portion of Pu‘ukoholā Heiau NHS. This will result in increased erosion and loss of trees backing the beach. By 2100 the entire beach will likely be submerged at high tide. The archeological sites behind Pelekane Beach will also be flooded under large swell by 2100. We recommend monitoring this section of beach. Beach profiling (either biannually or annually) can be used to document any changes in the beach which could threaten archeological sites. Differential GPS can be used to monitor these archeological sites. Also, long-term monitoring of wave action due to high tide and large swell events will document any impacts and changes that occur due to sea level. If archeological sites show deterioration due to wave action, we recommend consulting with local cultural agencies to discuss appropriate action for these sites.

Sea-level rise will passively flood sections of the Ala Kahakai NHT by 2100. However, impacts other than the loss of Pelekane Beach appear minimal. The main Heiau of Pu‘ukoholā Heiau NHS (Pu‘ukoholā Heiau and Mailekini Heiau) will not be threatened by coastal hazards in the foreseeable future. We recommend continuous monitoring of the coastal trail.

Potential tsunami hazards based on the 1946 tsunami appear to be minimal. Measured runup from the 1946 tsunami is higher than the modeled runup and should be taken into account during decision-making processes. Tsunamis originating from other directions were not analyzed for this report, but could be a potential topic for future work.

Conclusion

This section briefly summarizes the results for Pu‘ukoholā Heiau NHS and Kaloko-Honokōhau NHP.

This report completes an assessment of coastal vulnerability to wave overtopping, sea-level rise, and flooding for two national park units in the Pacific Islands Network. Products included with this report include maps of coastal inundation and historical shoreline change, and digital elevation models of shoreline morphology. The identification of vulnerable sections in the two parks will allow NPS managers to monitor and possibly move cultural structures that might be threatened by coastal hazards.

Pu‘ukoholā Heiau NHS and Kaloko-Honokōhau NHP currently experience impacts from coastal hazards including large swell, tsunamis, and coastal erosion. The impacts include damage to coastal landmarks, archeological sites, and coastal habitats with local flora and fauna. These impacts will be greatly increased under future sea level conditions. The clearest indication of the effects of sea level is the increase of seasonal wave damage. To protect the historic sites near the coast, continuous monitoring of wave action should be done, specifically monitoring before, during, and after annual high tide events. Frequency of monitoring should increase as seasonal wave damage increases. Areas that will be threatened by sea-level rise include Pelakane Beach and Ala Kahakai NHT in Pu‘ukoholā Heiau NHS. Kaloko Seawall, the beach fronting ‘Aimakapā Fishpond, and ‘Ai‘ōpio Fishtrap in Kaloko-Honokōhau NHP are at greatest risk of deterioration due to coastal impacts. Tsunami hazards appear to be minimal for both parks.

Acknowledgements

This section acknowledges the people and institutions that funded the research used in this report on Pu‘ukoholā Heiau NHS and Kaloko-Honokōhau NHP.

We would like to thank the Office of Naval Research for the use of Delft3D, the Hawai‘i Sea Grant College, the Hawai‘i Department of Land and Natural Resources, the U.S. Geological Survey, National Park Service, Rebecca Beavers (for getting the funding), Rich Boston, and last but not least the other members of the Coastal Geology Group at the University of Hawai‘i. Funding was provided by the National Park Service (Task Agreement No.: J8320070030)

References

This section lists references cited in this report.

Allan, J., and Komar, P., 2000. Are ocean wave heights increasing in the eastern North Pacific? Eos 81: 561–567.

Armstrong, R.W., 1983. Atlas of Hawai‘i. Honolulu: University of Hawai‘i Press, p. 54.

Aucan, J., 2006. Directional Wave Climatology for the Hawaiian Islands from Buoy Data and the Influence of ENSO on Extreme Wave Events from Model Hindcast. 9th International Workshop on Wave Hindcasting and Forecasting. JCOMM Technical Report No. 34 / WMO-TD. No. 1368.

Beckley, B. D., Lemoine, F. G., Luthcke, S. B., Ray, R. D., and Zelensky, N. P., 2007. A reassessment of global and regional mean sea level trends from TOPEX and Jason-1 altimetry based on revised reference frame and orbits, Geophysical Research Letters., 34(14), L14608.

Booij, N., Holthuijsen, L.H., and Ris, R.C., 1999. A third-generation wave model for coastal regions 1. Model description and validation. Journal of Geophysical Research, Vol. 104 No. C4, pp. 7649-7666.

Caldwell, P., 1992. Surfing the El Niño. Mariners Weather Log 36: 60–64.

Caldwell, P., 2005. Validity of North Shore, Oahu, Hawaiian Islands Surf Observations, Journal of Coastal Research, 21, 1127-1138.

Caldwell, P., Vitousek, S., Aucan, J., 2008. Frequency and Duration of Coinciding High Surf and Tides along the North Shore of Oahu, Hawai‘i 1981-2007. Journal of Coastal Research.

Church, J. A., and White, N. J., (2006), A 20th century acceleration in global sea-level rise, Geophys. Res. Lett., 33, L01602.

Cochran, S.A., Gibbs, A.E., Logan, J.B., 2006. Geologic resource evaluation of Pu‘ukoholā Heiau National Historic Site, Hawai‘i: Part II: Benthic Habitat Mapping. U.S. Geological Survey Scientific Investigations Report 2006-5254.

Day, S.J., Watts,P., Grilli, S., Kirby, J.T., 2005. Mechanical models of the 1975 Kalapana Hawai‘i earthquake and tsunami. Marine Geology, 215, 59-92.

Dollar, S. J. and Tribble, G.W., 1993. Recurrent storm disturbance and recovery: a long-term study of coral communities in Hawai‘i. Coral Reefs, 12, 223–233.

Dudley, W.C. and Lee, M., 1998. Tsunami! 2nd Ed: Honolulu, University of Hawai‘i Press, p. 132

Eversole, D., 2002. Large-scale beach change: Kaanapali, Hawai‘i. Honolulu: University of Hawai‘i, Manoa, M.S., p. 63.

Firing, Y. L. and Merrifield, M. A., 2004. Extreme sea level events at Hawai‘i: Influence of mesoscale eddies. Geophysical Research Letters, 31, L24306.

Flament, P., Keenan, S., Lumpkin, R., Sawyer, M., Stroup, E.D., 1996. The Ocean Atlas of Hawai‘i. Department of Oceanography, School of Ocean and Earth Science and Technology, University of Hawai‘i (poster).

Fletcher, C.H., Richmond, B.M., Grossman, E.E., Gibbs, A.E., 2002. Atlas of natural hazards in the Hawaiian coastal zone. U.S. Geological Survey Geologic Investigations Series I-2716, p. 186.

Fletcher, C.H., Rooney, J.J.B., Barbee, M., Lim, S.C., and Richmond, B.M., 2003. Mapping shoreline change using digital orthophotogrammetry on Maui, Hawai‘i. Journal of Coastal Research, v. Special Issue 38, p. 106-124.

Frazer, L.N., Genz, A.S., and Fletcher, C.H., 2009. Toward parsimony in shoreline change prediction (I): Basis function methods. Journal of Coastal Research, 25(2), 366-379.

Genz, A.S., Frazer, L.N., Fletcher, C.H., 2009. Toward parsimony in shoreline change prediction (II): Applying basis function methods to real and synthetic data. Journal of Coastal Research, 25(2), 380-392.

Giambelluca, T.W., Nullet, D., Schroeder, T.A., 1986. Rainfall atlas of Hawai‘i. Honolulu: Water Resources Research Center, University of Hawai‘i (Report No. R76).

Giambelluca, T.W. and Schroeder, T.A., 1998. Climate. In: Juvik, S.P., and Juvik, J.O. (eds.), Atlas of Hawai‘i. Honolulu: University of Hawai‘i Press, pp. 49-59.

Gibbs, A.E., Cochran, S.A., Logan, J.B., Grossman, E.E., 2006. Benthic habitats and offshore geological resources of Kaloko-Honokōhau National Historical Park, Hawai‘i. U.S. Geological Survey Scientific Investigations Report 2006-5256.

Goddard, L. and Graham, N.E., 1997. El Niño in the 1990s. Journal of Geophysical Research, 102(C5), 10423-10436.

Goff, J., Dudley, W.C., deMaintenon, M.J., Cain, G., Coney, J.P., 2006. The largest local tsunami in 20th century Hawai‘i. Marine Geology, 226, 65-79.

Graham, N.E. and Diaz, H.F., 2001. Evidence for intensification of north pacific winter cyclones since 1948. Bulletin of the American Meteorological Society.

Green, C.K., 1946. Seismic Sea Wave of April 1, 1946 as Recorded on Tide Gauges. Transactions of the American Geophysical Union, 27, pp 460-502.

Hapke, C.J., Gmirkin, R., Richmond, B.M., 2005. Coastal change rates and patterns: Kaloko-Honokōhau NHP, Kona Coast, Hawai'i. U.S. Geological Survey Open-file report 2005-1069. http://pubs.usgs.gov/of/2005/1069.

Harney, J.N., Grossman, E.E., Richmond, B.M., and Fletcher, C.H., 2000. Age and composition of carbonate shoreface sediments, Kailua Bay, Oahu, Hawai'i. Coral Reefs, 19, 141-154.

Harney, J.N. and Fletcher, C.H., 2003. A budget of carbonate framework and sediment production, Kailua Bay, Oahu, Hawai'i. Journal of Sedimentary Research, 73(6), 856-868.

Hurvich, C.M. and Tsai, C.-L., 1989. Regression and time series model selection in small samples. Biometrica, 76, 297-307.

Inman, D. L., and Jenkins, S. A., 1997. Changing wave climate and littoral drift along the California coast. Pages 314–327 in O. T. Magoon, ed. Proceedings of the California and the World Ocean Conference '97 Conference. American Society of Civil Engineers, San Diego.

IPCC, 2007. Climate Change 2007: The Physical Science Basis. Contribution of Working Group I to the Fourth Assessment Report of the Intergovernmental Panel on Climate Change [Solomon, S., D. Qin, M. Manning, Z. Chen, M. Marquis, K.B. Averyt, M.Tignor and H.L. Miller (eds.)]. Cambridge University Press, Cambridge, United Kingdom and New York, NY, USA.

Kaminsky, G.M., Ruggiero, P., Gelfenbaum, G., 1998. Monitoring coastal change in southwest Washington and northwest Oregon during the 1997/98 El Nino. Shore & Beach. 66(3), 42-51.

Lander, J.F., and Lockridge, P.A., 1989. United States tsunamis: (including United States possessions): 1690-1988. U.S. Dept. of Commerce, National Oceanic and Atmospheric Administration, National Environmental Satellite, Data, and Information Service, National Geophysical Data Center, Boulder, CO, USA.

Mader C.L., 2004. Numerical Modeling of Water Waves. second edition. CRC press. New York.

Mantua, N.J., Hare, S.R., Zhang, Y., Wallace, J.M., and Francis, R.C., 1997. A Pacific interdecadal climate oscillation with impacts on salmon production. Bulletin of the American Meteorological Society, 78, 1069-1079.

McMurty, G.M., Fryer, G.J., Tappin, D.R., Wilkinson, I.P., Williams, M., Fietzke, J., Garbe-Schoenberg, D., Watts, P., 2004. Megatsunami deposits on Kohala volcano, Hawai'i, from flank collapse of Mauna Loa. Geology, 32(9), 741-744.

Moberly, R. and Chamberlain, T. 1964. Hawaiian Beach Systems. Hawai'i Institute of Geophysics Report 64-2, University of Hawai'i.

Norcross, Z.M., Fletcher, C.H, and Merrifield, M., 2002. Annual and interannual changes on a reef-fringed pocket beach: Kailua Bay, Hawai'i. Marine Geology, 3203, p. 1-28.

Presto, M.K., Storlazzi, C.D., Logan, J.B. and Grossman, E.E., 2007. Submarine ground water discharge and fate along the coast of Kaloko-Honokōhau National Historical Park, Hawai'i, Part I: Time-series measurements of currents, waves and water properties: November, 2005 – July, 2006. U.S. Geological Survey Open-File Report 2007-1310, 47 p. http://pubs.usgs.gov/of/2007/1310.

Rahmstorf, S., 2007. A Semi-Empirical Approach to Projecting Future Sea-Level Rise. Science, 315, p. 368-370.

Richmond, B.M., Gibbs, A.E., Cochran, S.A., 2008. Geologic resource evaluation of Kaloko-Honokōhau National Historical Park, Hawai'i; Geology and coastal landforms. U.S. Geological Survey Open-File Report 2008-1191. http://pubs.usgs.gov/of/2008/1191.

Ris, R.C., Holthuijsen, L.H., Booij, N., 1999. A third-generation wave model for coastal regions 2. Verification. Journal of Geophysical Research, 104(C4), pp. 7667-7681.

Romine, B.M., Fletcher, C.H., Frazer, L.N., Genz, A.S., Barbee, M.M., and Lim, S.C, in press. Historical shoreline trends and management implications: Southeast Oahu, Hawai'i. Journal of Coastal Research.

Rooney, J.J.B., Fletcher, C.H., Barbee, M.M., Eversole, D., Lim, S.C., Richmond, B.M., and Gibbs, A., 2003. Dynamics of sandy shorelines in Maui, Hawai'i: Consequences and causes. Coastal Sediments '03 Proceedings. Clearwater Beach, Florida.

Rooney, J. Fletcher, C.H., Grossman, E., Engels, M. and Field, M., 2004. El Niño Influence on Holocene Reef Accretion in Hawai'i, Pacific Science,58, p. 305–324.

Rooney, J. and Fletcher, C.H., 2005. Shoreline Change and Pacific Climatic Oscillations in Kihei, Maui, Hawai'i. Journal of Coastal Research, 21(3), 535-547.

Ruggiero, P., Kaminsky, G.M., Komar, P.D., and McDougal, W.G. 1997. Extreme waves and coastal erosion in the Pacific Northwest, Ocean Wave Measurements and Analysis, Proceedings of the 3rd International Symposium on Ocean Wave Measurement and Analysis. ASCE, Virginia Beach, VA, Nov., 947-961.

Ruggiero, P., Kaminsky, G.M., Gelfenbaum, G., and Voigt, B., 2005. Seasonal to interannual morphodynamics along a high-energy dissipative littoral cell. Journal of Coastal Research, 21(3), 553-578.

Seymour, R.J. 1998. Effect of El Niños on west coast wave climate. Shore & Beach 66: 3–11.

Seymour, R.J., Strange III, R.R., Cayan, D.R., and Nathan, R.A., 1984. Influence of El Niños on California's wave climate. in B. L. Edge, ed. Proceedings of the 19th International Conference on Coastal Engineering. American Society of Civil Engineers, New York. 35, p. 215–230.

Shalowitz, A.L., 1964. Shore and sea boundaries. Washington, D.C., Publication 10-1, U.S. Department of Commerce. 2(2).

Snodgrass, F.E., Groves, G.W., Hasselmann, K.F., Miller, G.R., Munk W.H., and Powers, W.H., 1966. Propagation of Ocean Swell across the Pacific. Philosophical Transactions of the Royal Society of London. Series A, Mathematical and Physical Sciences, 259(1103) (May 5,), pp. 431-497.

Stockdon H.F., Holman R.A., Howd P.A., Sallenger, A.H., 2006. Empirical parameterization of setup, swash, and runup. Coastal Engineering, 53, p. 573-588.

Storlazzi, C.D., and Griggs, G.B., 2000. Influence of El Niño–Southern Oscillation (ENSO) events on the evolution of central California's shoreline. GSA Bulletin. 112, p. 236-249.

Storlazzi, C.D., and Presto, M.K., 2005. Coastal circulation and sediment dynamics along Kaloko-Honokōhau National Historical Park, Hawai'i: Part I: -- Measurements of waves, currents, temperature, salinity and turbidity: April-October 2004. U.S. Geological Survey Open-File Report 2005-1161. http://pubs.usgs.gov/of/2005/1161.

Sugiura, N., 1978. Further analysis of the data by Akaike's Information Criterion and the finite corrections. Communications in Statistics, Theory and Methods, A7, 13-26.

Taylor, L.A., Eakins, B.W., Carignan, K.S., Warnken, R.R., Sazonova, T., Schoolcraft, D.C., 2007. Digital elevation model for Kawaihae, Hawai'i: Procedures, data sources and analysis. Prepared pacific marine environmental laboratory NOAA Center for Tsunami Research by NOAA National Geophysical Data Center (NGDC).

Vitousek, S. and Fletcher, C.H., 2008. Maximum annually recurring wave heights in Hawai'i. Pacific Science.

Vitousek, S., Fletcher, C.H., Barbee, M.M., 2008. A practical approach to mapping extreme wave inundation: consequences of sea-level rise and coastal erosion. ASCE Solutions to Coastal Disasters 2008. pp. 85-96.

Walker, D.A., 1994. Tsunami Facts. SOEST Technical Report 94-03, University of Hawai'i, Honolulu, pp. 91.

Wang, S. L., and Swail, V. R., 2001. Changes of extreme wave heights in Northern Hemisphere oceans and related atmospheric circulation regimes. J. Clim. 14, p. 2204–2221.

Zhang, Y., Wallace, J.M., and Battisti, D.S., 1997. ENSO-like interdecadal variability: 1990-93. Journal of Climate, 10(5), p. 1004-1020.

Appendix A: Model Settings

The following are model settings for the wave and tsunami inundation models

SWAN wave model

Directional resolution: 180 bins (every 2 degrees)
Spectral resolutions: 24 bins (1 sec – 20 sec)
Spectral parameterization: none (parametric wave conditions only)
Default Friction and Breaking parameters
No Triads or Quadruplets (non-linear interactions)

Delft3D tsunami inundation model

2-D depth averaged simulation
Timestep: 6 sec
(salt) water density: 1025 kg/m^3
Forcing: Water-level time series from regional model
Roughness: Chezy coefficient 50 – frequently used parameter for flows rougher than sandy bottoms
No wind or (short) wave forcing
No temperature, salinity or density variation
No sediment transport
Using default solvers for momentum
Using default eddy viscosities:
    eddy viscosity – 1 m^2/s
    eddy diffusivity = 10 m^2/s

Appendix B: Model Results

The following figures are the model results for Puʻukoholā Heiau NHS and Kaloko-Honokōhau NHP.

Bathymetry of Puʻukoholā Heiau NHS

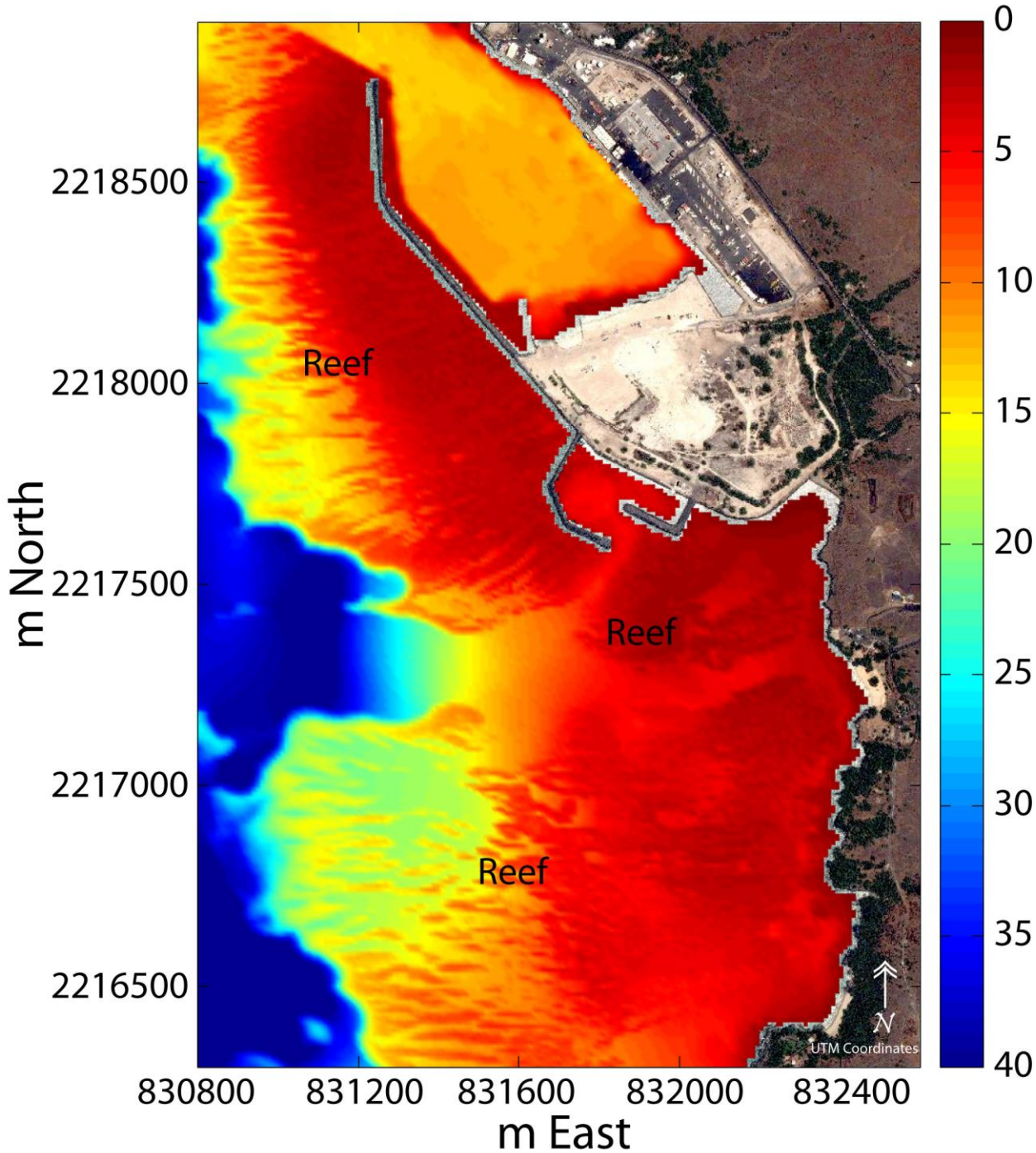

Model results of the nearshore wave height field at Puʻukoholā Heiau NHS.

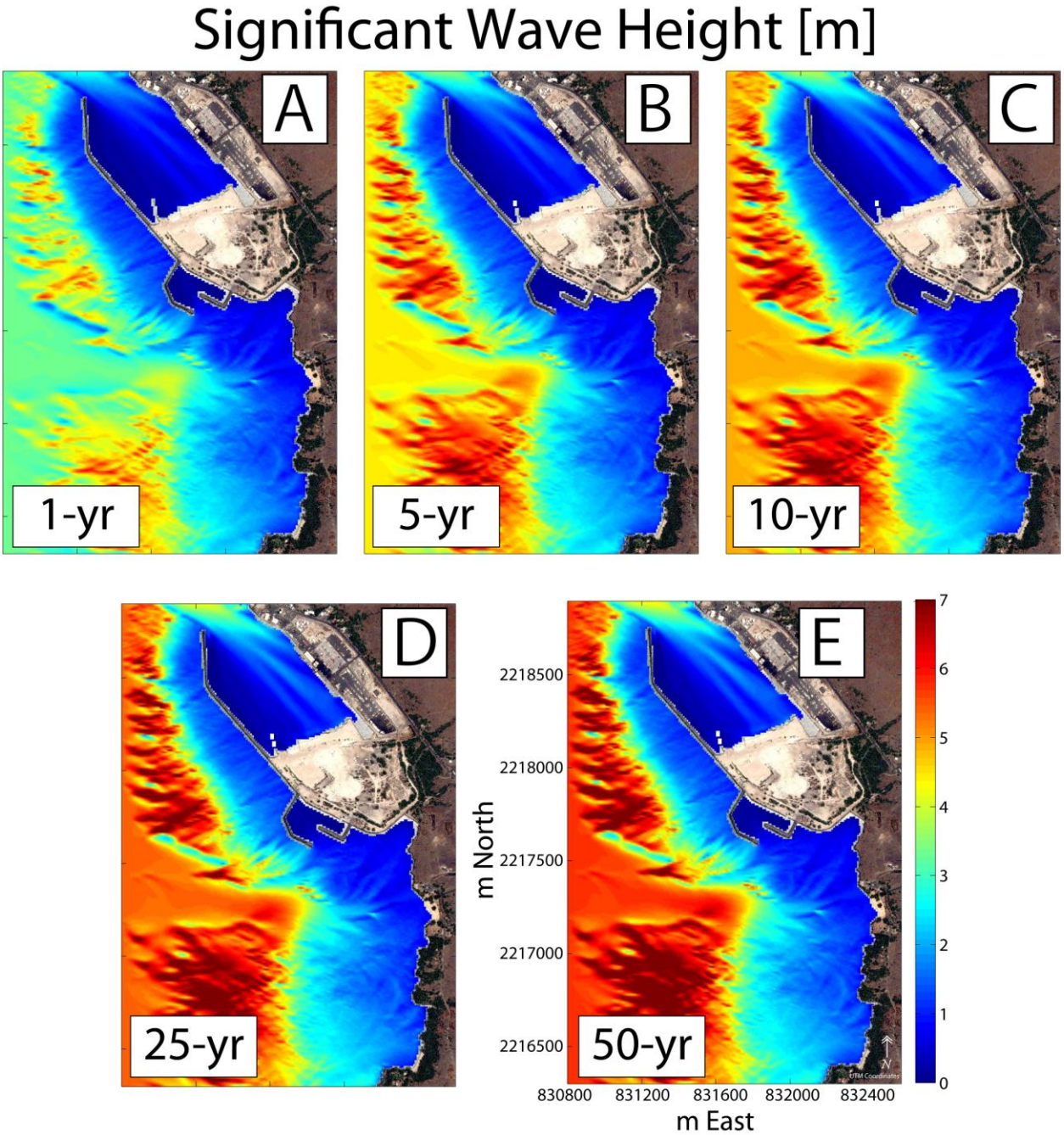

Model results of the nearshore wave length field at Puʻukoholā Heiau NHS.

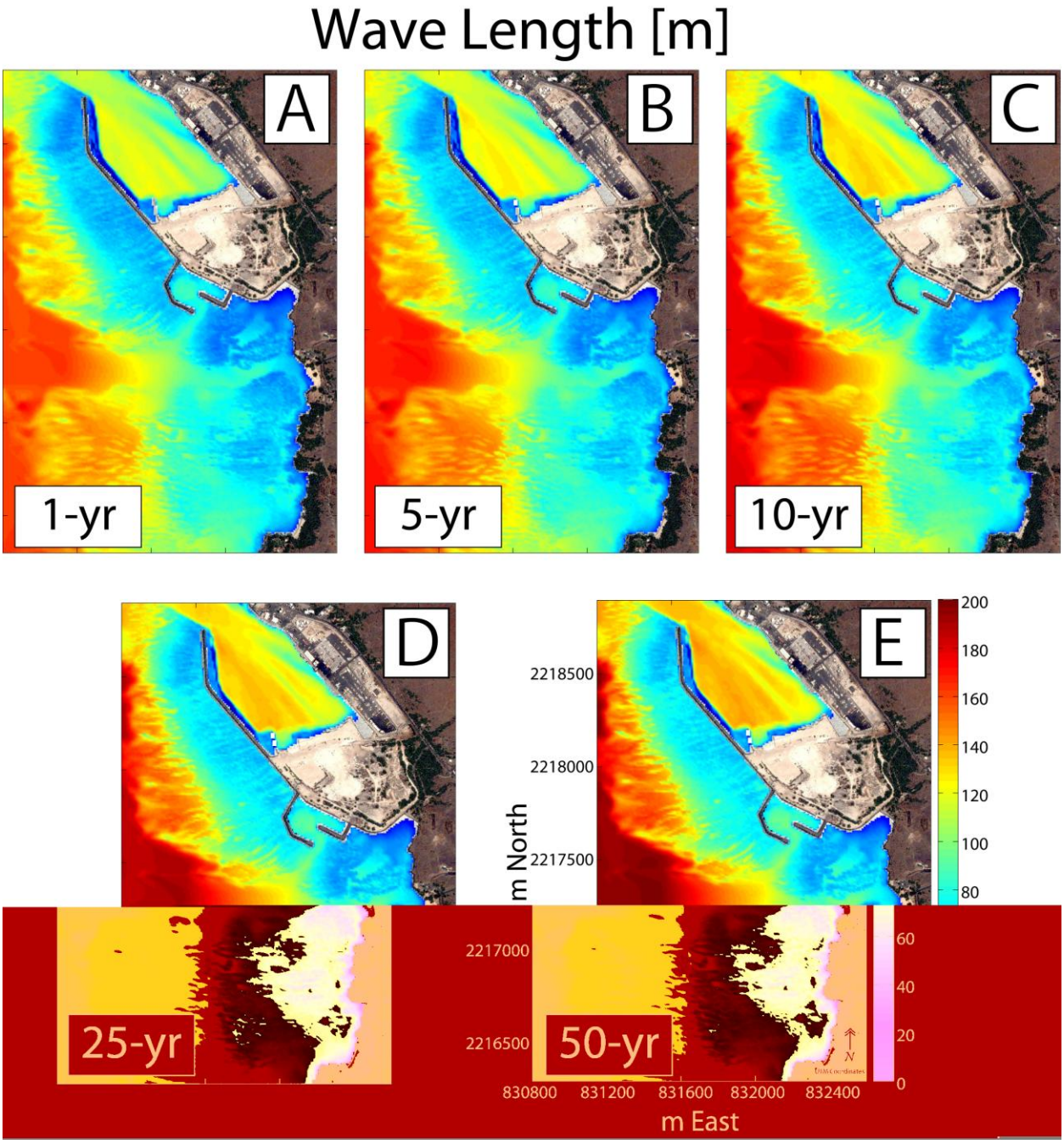

Model results of the nearshore wave setup field at Pu‘ukoholā Heiau NHS.

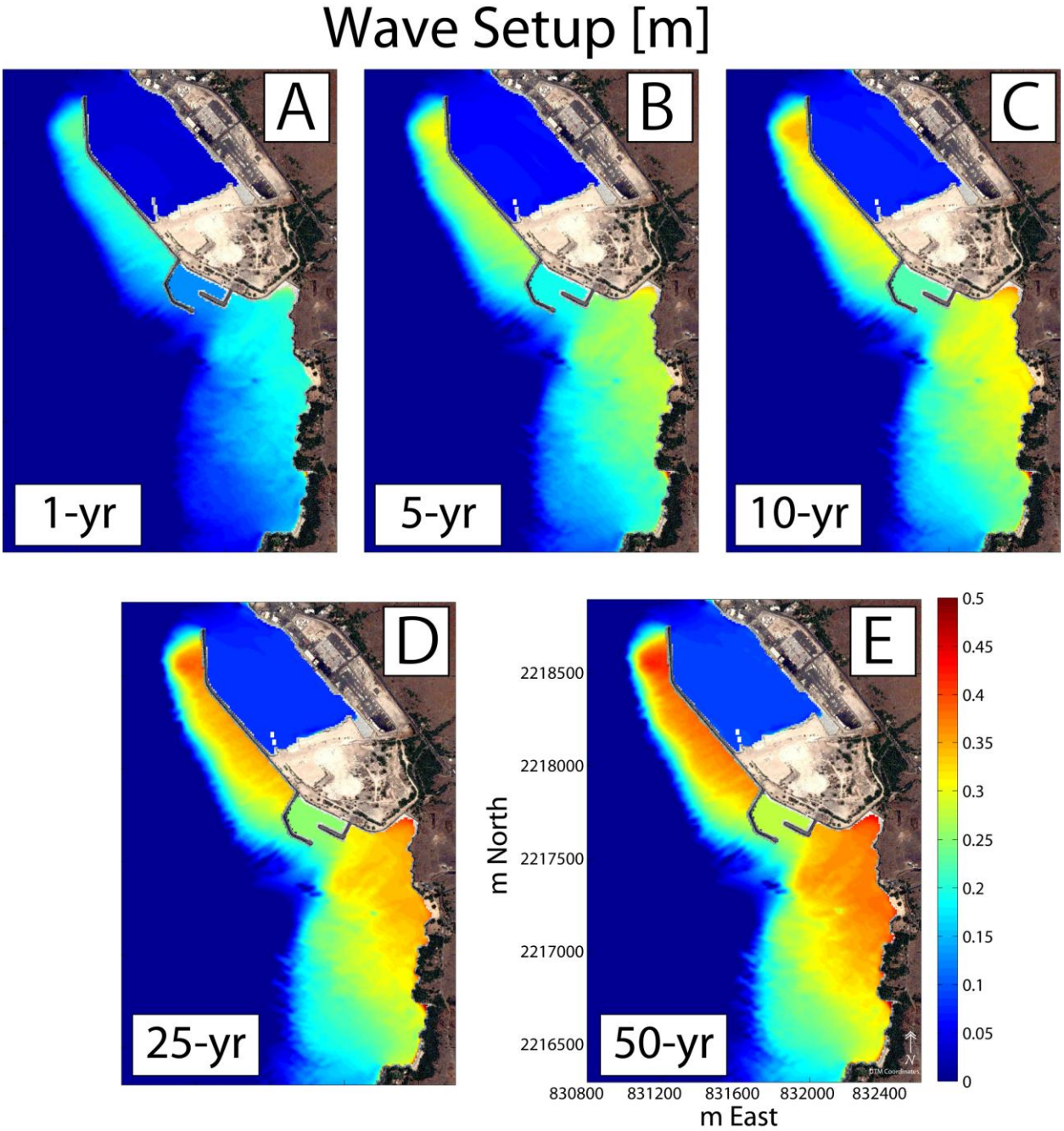

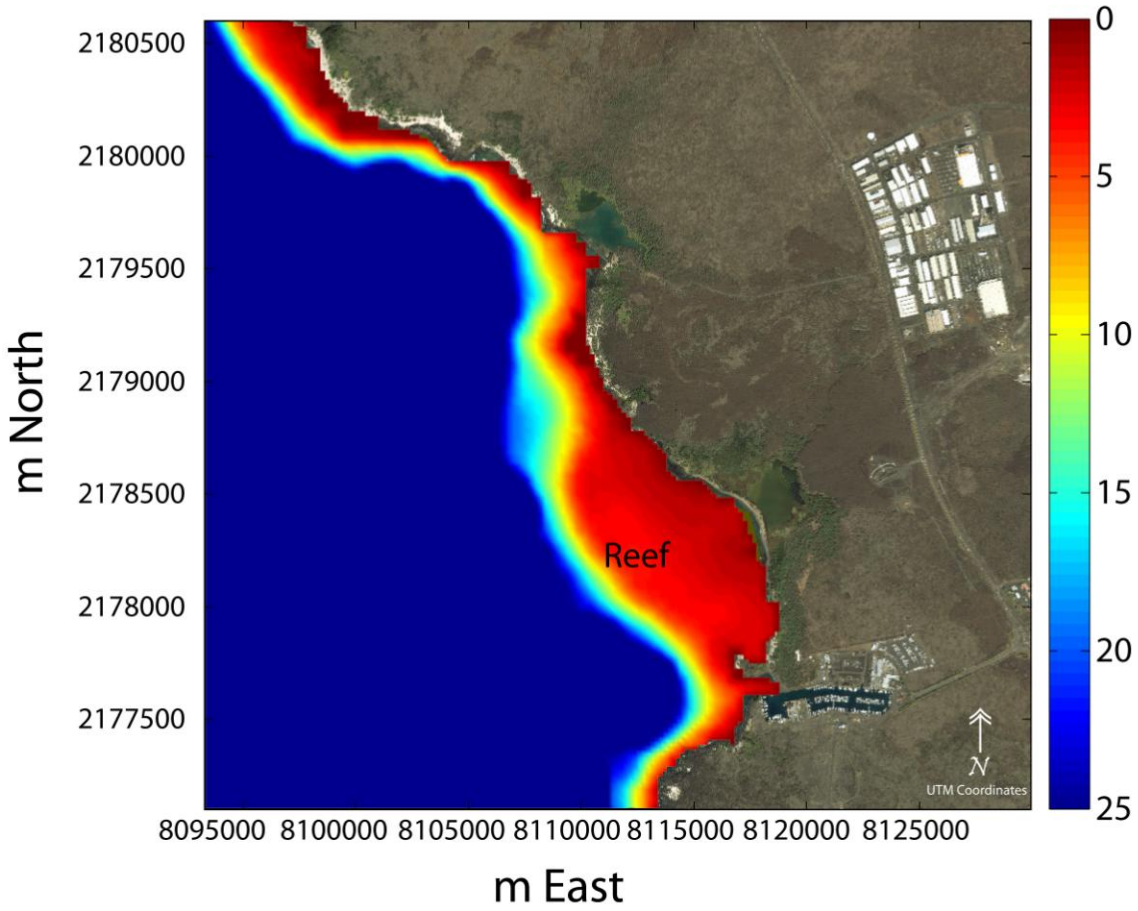
2180500
2180000
2179500
2179000
2178500
2178000
2177500
m North
8095000 8100000 8105000 8110000 8115000 8120000 8125000
m East
Reef
N
UTM Coordinates
0
5
10
15
20
25

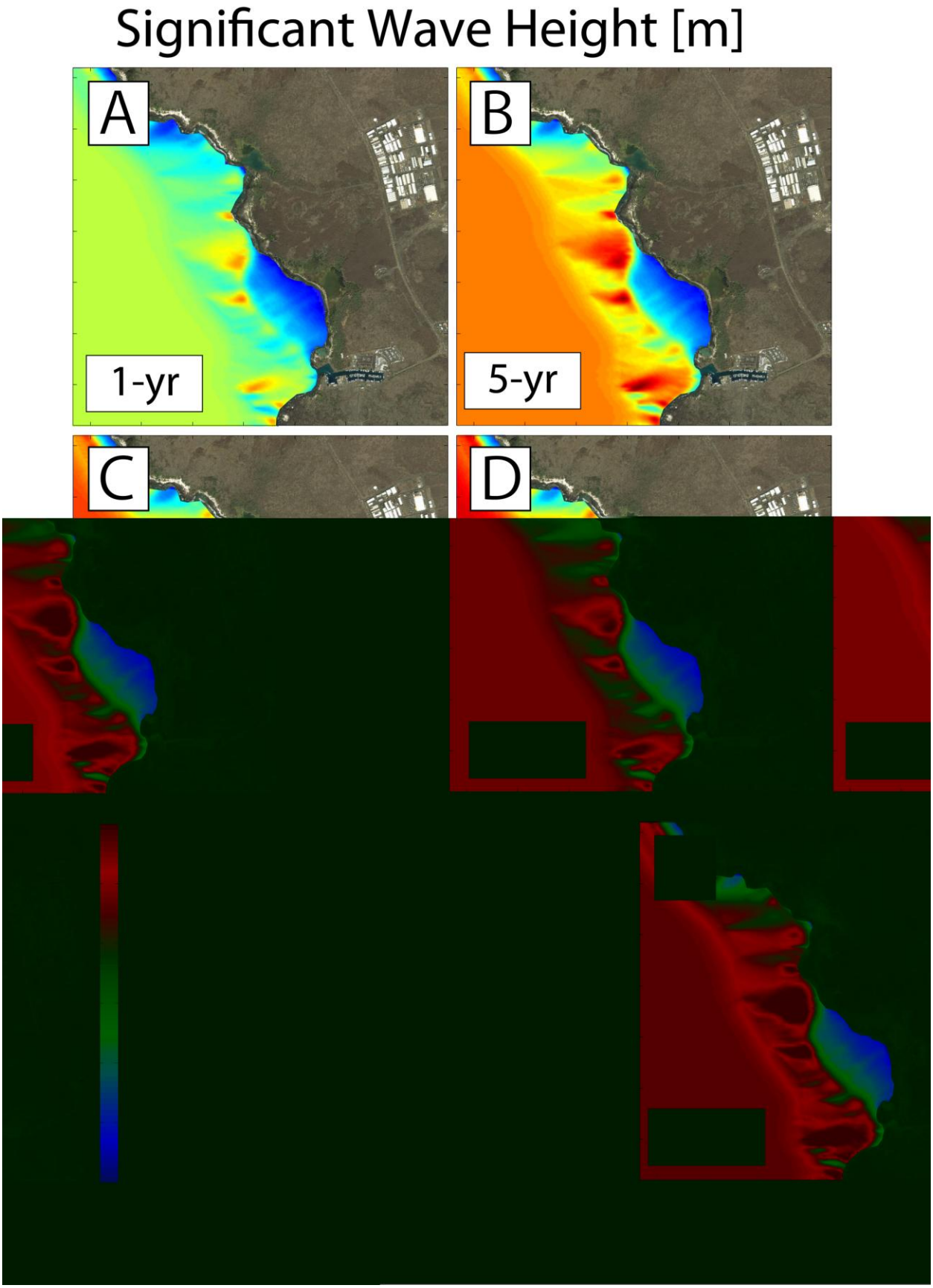
Significant Wave Height [m]
A
1-yr
B
5-yr
C
D

Model results of the nearshore wave length field at Kaloko-Honokōhau NHP

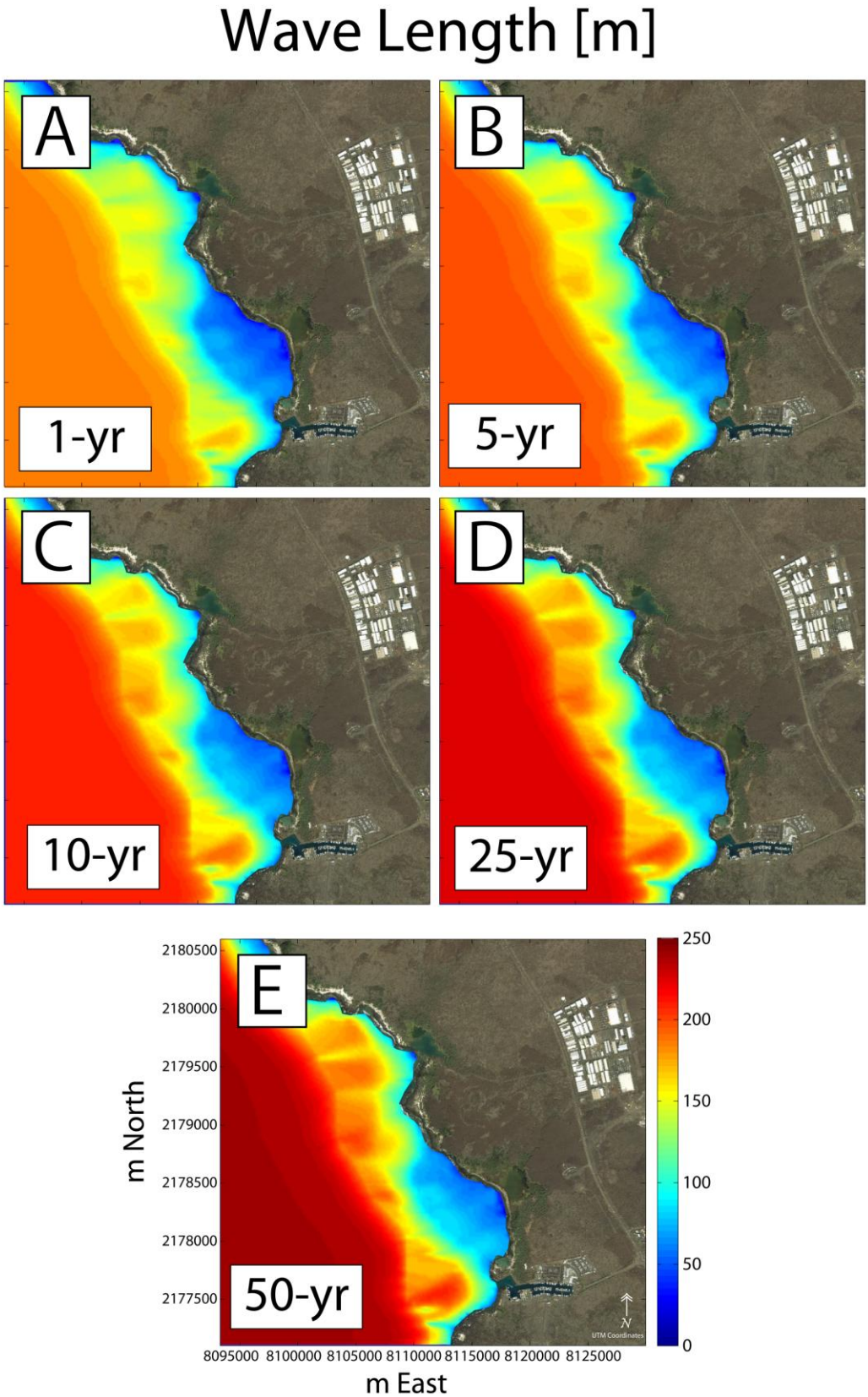

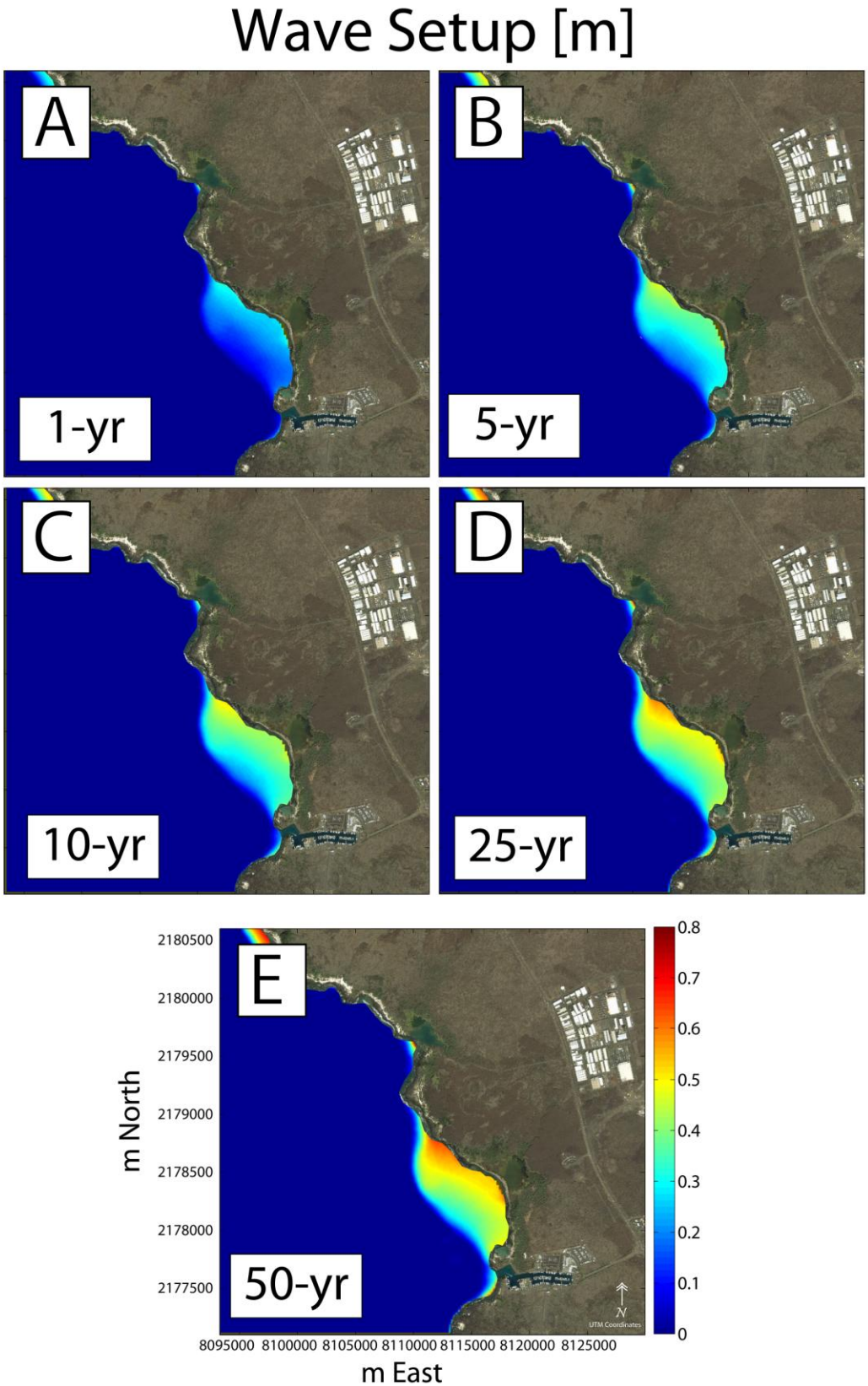
Wave Setup [m]
A
1-yr
B
5-yr
C
10-yr
D
25-yr
E
50-yr
2180500
2180000
2179500
2179000
2178500
2178000
2177500
m North
8095000 8100000 8105000 8110000 8115000 8120000 8125000
m East
0.8
0.7
0.6
0.5
0.4
0.3
0.2
0.1
0
N
UTM Coordinates

Appendix C: Historical Imagery

The following figures are historical imagery for Pu‘ukoholā Heiau NHS and Kaloko-Honokōhau NHP.

Historical Imagery – Kaloko-Honokōhau NHP 1:12000

1950

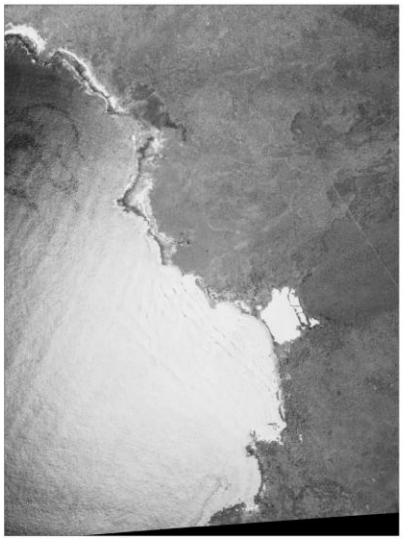

1954

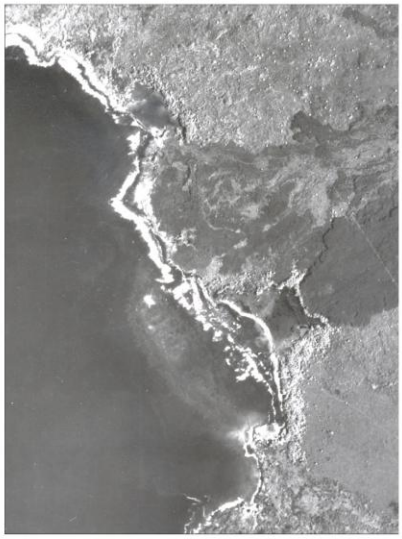

1965

1968

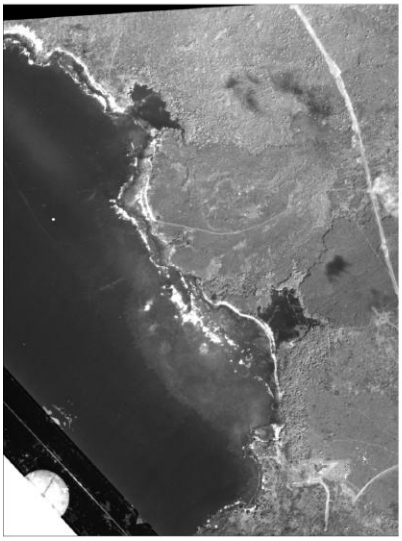

1970

1980

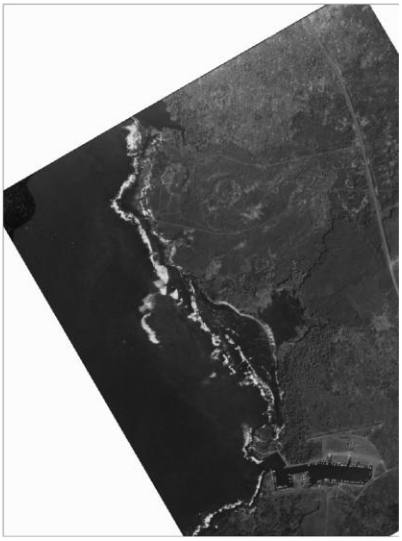

1987

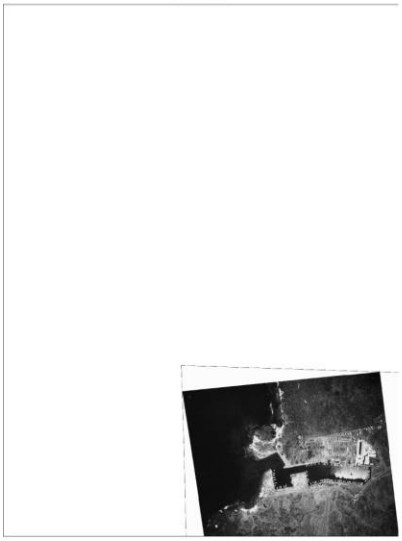

1988

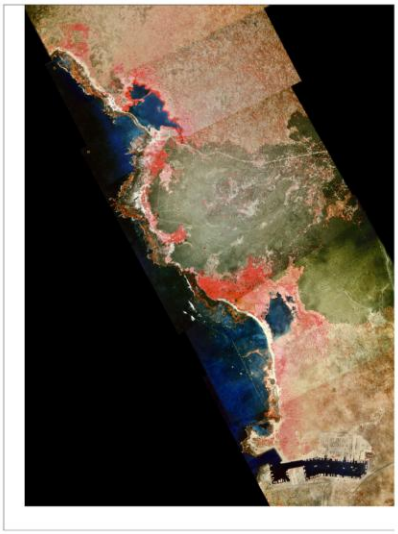

1992

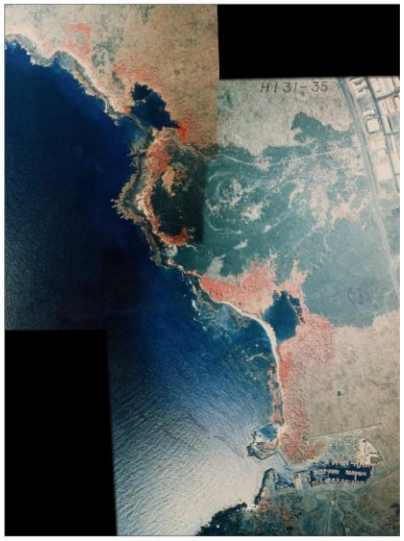

2000

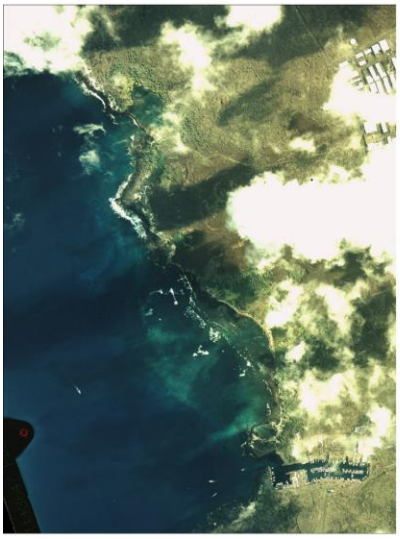

2002

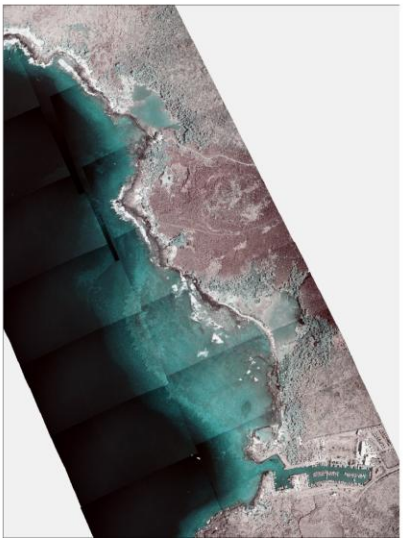

2004

2006 Satellite Reference

1949

1950

1966

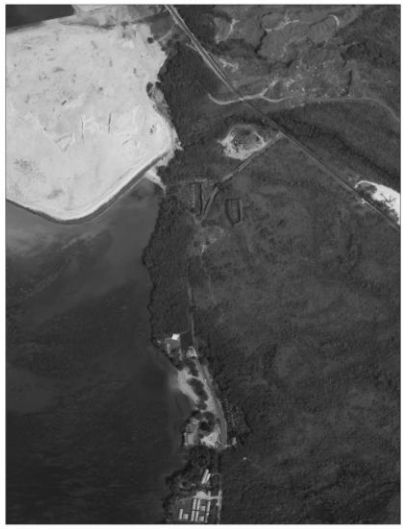

1970

June 1975

November 1975

1977

1981

1987

1989

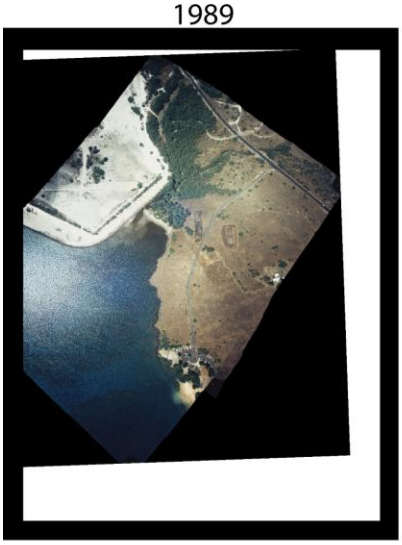

1990

1998

2006

2006 satellite reference

Appendix D: Shoreline Change Results

The following figures depict the shoreline change rate at each transect for Pu'ukoholā Heiau NHS and Kaloko-Honokōhau NHP.

Shoreline change rates (transect plots) of Kaloko-Honokōhau NHP

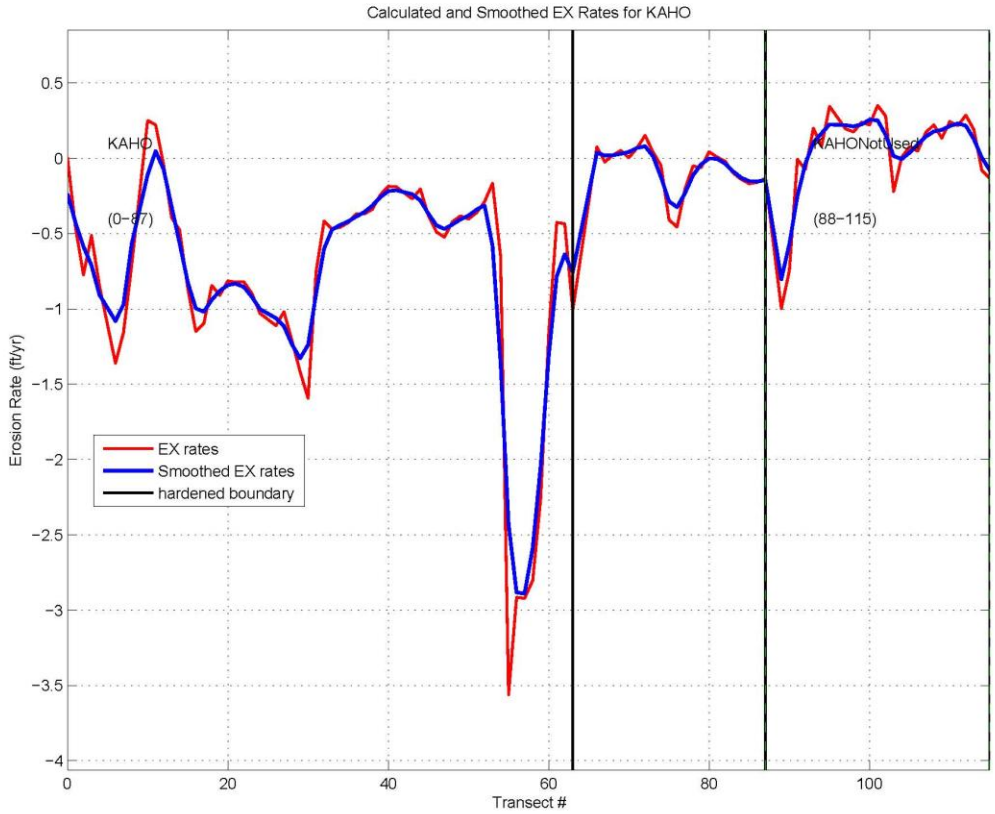

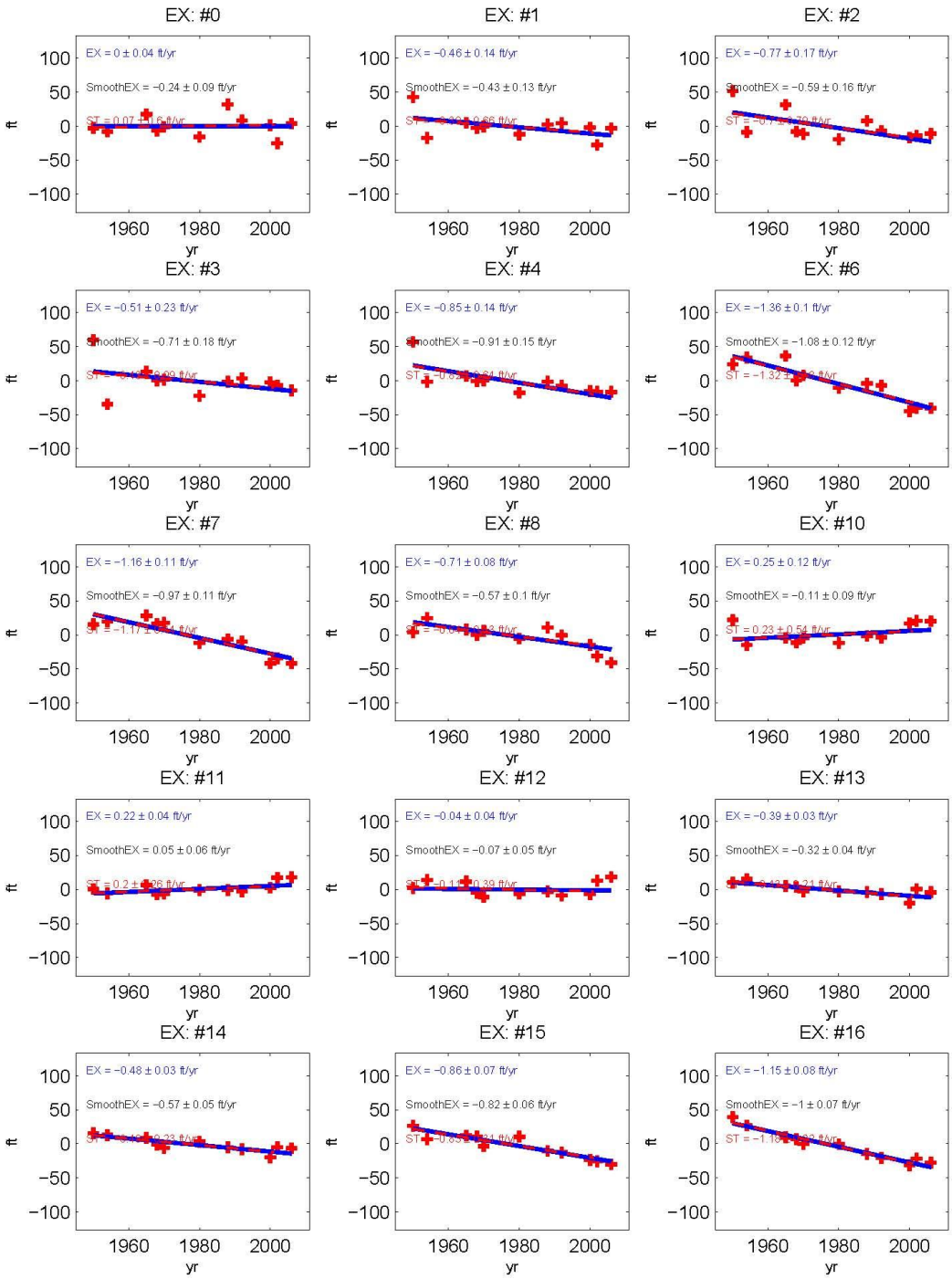
EX: #0
EX = 0 ± 0.04 ft/yr
SmoothEX = −0.24 ± 0.09 ft/yr
EX: #1
EX = −0.46 ± 0.14 ft/yr
SmoothEX = −0.43 ± 0.13 ft/yr
EX: #2
EX = −0.77 ± 0.17 ft/yr
SmoothEX = −0.59 ± 0.16 ft/yr
EX: #3
EX = −0.51 ± 0.23 ft/yr
SmoothEX = −0.71 ± 0.18 ft/yr
EX: #4
EX = −0.85 ± 0.14 ft/yr
SmoothEX = −0.91 ± 0.15 ft/yr
EX: #6
EX = −1.36 ± 0.1 ft/yr
SmoothEX = −1.08 ± 0.12 ft/yr
EX: #7
EX = −1.16 ± 0.11 ft/yr
SmoothEX = −0.97 ± 0.11 ft/yr
EX: #8
EX = −0.71 ± 0.08 ft/yr
SmoothEX = −0.57 ± 0.1 ft/yr
EX: #10
EX = 0.25 ± 0.12 ft/yr
SmoothEX = −0.11 ± 0.09 ft/yr
EX: #11
EX = 0.22 ± 0.04 ft/yr
SmoothEX = 0.05 ± 0.06 ft/yr
EX: #12
EX = −0.04 ± 0.04 ft/yr
SmoothEX = −0.07 ± 0.05 ft/yr
EX: #13
EX = −0.39 ± 0.03 ft/yr
SmoothEX = −0.32 ± 0.04 ft/yr
EX: #14
EX = −0.48 ± 0.03 ft/yr
SmoothEX = −0.57 ± 0.05 ft/yr
EX: #15
EX = −0.86 ± 0.07 ft/yr
SmoothEX = −0.82 ± 0.06 ft/yr
EX: #16
EX = −1.15 ± 0.08 ft/yr
SmoothEX = −1 ± 0.07 ft/yr
ft
yr
100
50
0
−50
−100
1960
1980
2000

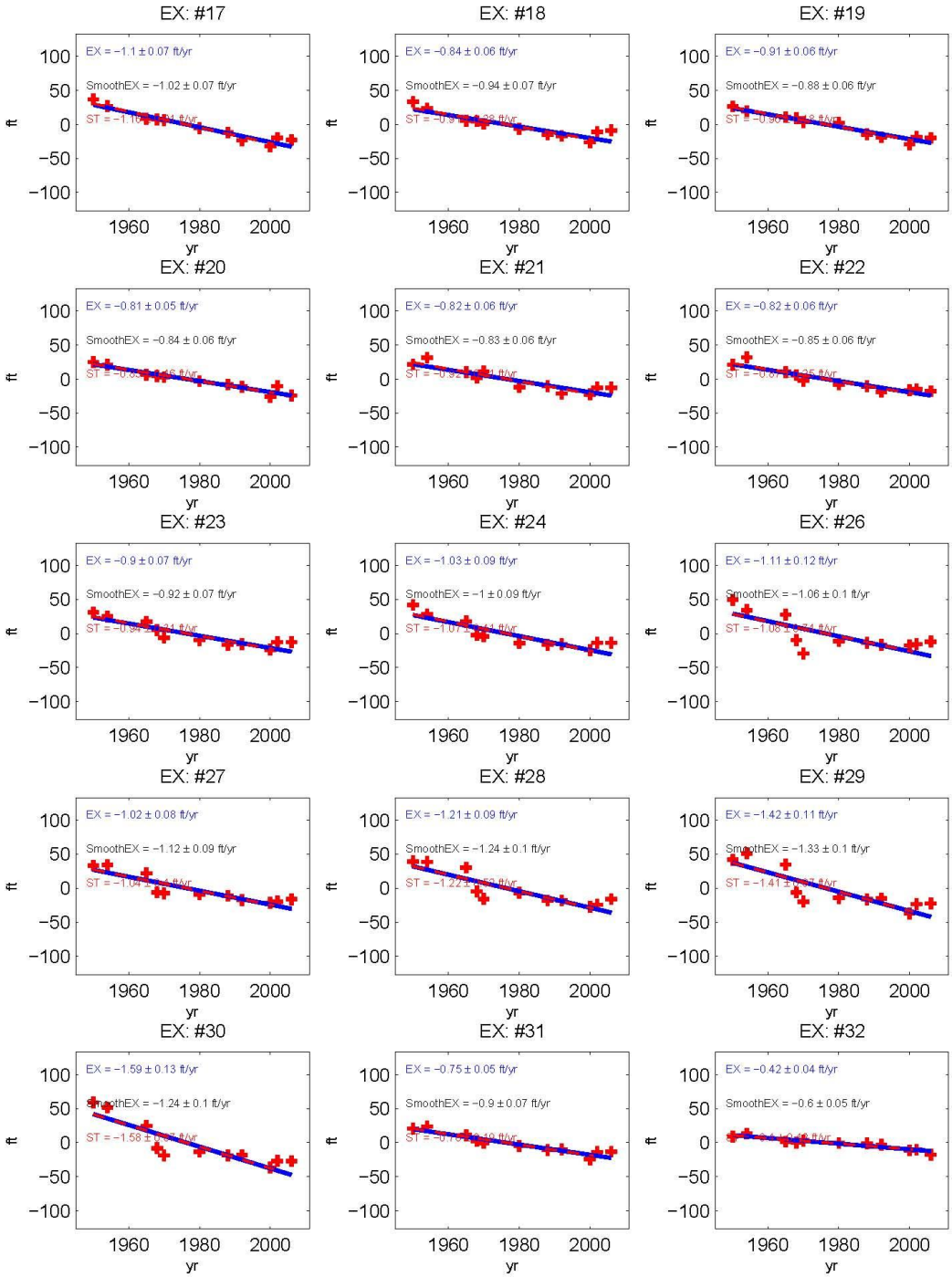
EX: #17
EX = −1.1 ± 0.07 ft/yr
SmoothEX = −1.02 ± 0.07 ft/yr
EX: #18
EX = −0.84 ± 0.06 ft/yr
SmoothEX = −0.94 ± 0.07 ft/yr
EX: #19
EX = −0.91 ± 0.06 ft/yr
SmoothEX = −0.88 ± 0.06 ft/yr
EX: #20
EX = −0.81 ± 0.05 ft/yr
SmoothEX = −0.84 ± 0.06 ft/yr
EX: #21
EX = −0.82 ± 0.06 ft/yr
SmoothEX = −0.83 ± 0.06 ft/yr
EX: #22
EX = −0.82 ± 0.06 ft/yr
SmoothEX = −0.85 ± 0.06 ft/yr
EX: #23
EX = −0.9 ± 0.07 ft/yr
SmoothEX = −0.92 ± 0.07 ft/yr
EX: #24
EX = −1.03 ± 0.09 ft/yr
SmoothEX = −1 ± 0.09 ft/yr
EX: #26
EX = −1.11 ± 0.12 ft/yr
SmoothEX = −1.06 ± 0.1 ft/yr
EX: #27
EX = −1.02 ± 0.08 ft/yr
SmoothEX = −1.12 ± 0.09 ft/yr
EX: #28
EX = −1.21 ± 0.09 ft/yr
SmoothEX = −1.24 ± 0.1 ft/yr
EX: #29
EX = −1.42 ± 0.11 ft/yr
SmoothEX = −1.33 ± 0.1 ft/yr
EX: #30
EX = −1.59 ± 0.13 ft/yr
SmoothEX = −1.24 ± 0.1 ft/yr
EX: #31
EX = −0.75 ± 0.05 ft/yr
SmoothEX = −0.9 ± 0.07 ft/yr
EX: #32
EX = −0.42 ± 0.04 ft/yr
SmoothEX = −0.6 ± 0.05 ft/yr
ft
yr
100
50
0
−50
−100
1960
1980
2000

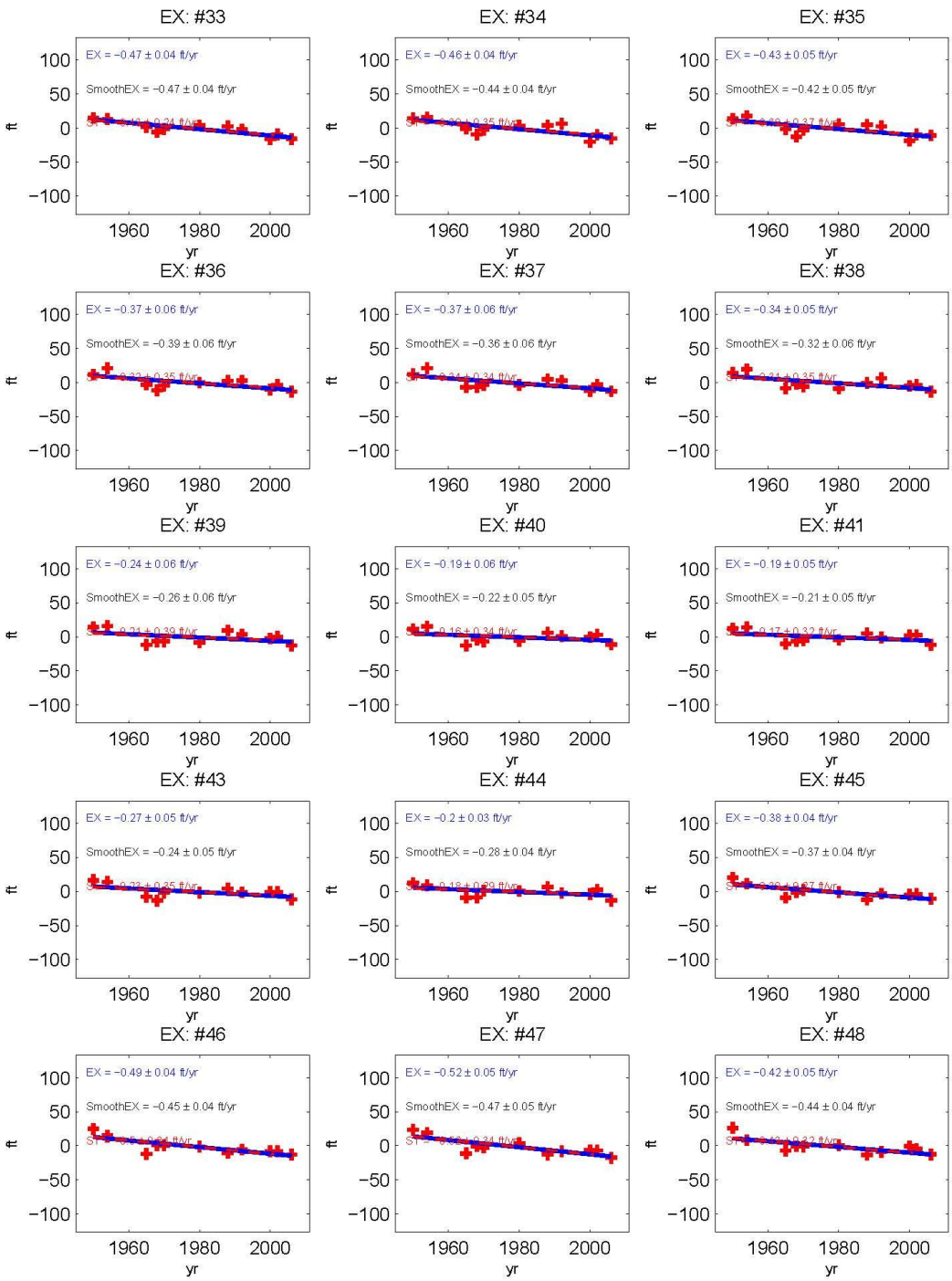
EX: #33
EX = −0.47 ± 0.04 ft/yr
SmoothEX = −0.47 ± 0.04 ft/yr
EX: #34
EX = −0.46 ± 0.04 ft/yr
SmoothEX = −0.44 ± 0.04 ft/yr
EX: #35
EX = −0.43 ± 0.05 ft/yr
SmoothEX = −0.42 ± 0.05 ft/yr
EX: #36
EX = −0.37 ± 0.06 ft/yr
SmoothEX = −0.39 ± 0.06 ft/yr
EX: #37
EX = −0.37 ± 0.06 ft/yr
SmoothEX = −0.36 ± 0.06 ft/yr
EX: #38
EX = −0.34 ± 0.05 ft/yr
SmoothEX = −0.32 ± 0.06 ft/yr
EX: #39
EX = −0.24 ± 0.06 ft/yr
SmoothEX = −0.26 ± 0.06 ft/yr
EX: #40
EX = −0.19 ± 0.06 ft/yr
SmoothEX = −0.22 ± 0.05 ft/yr
EX: #41
EX = −0.19 ± 0.05 ft/yr
SmoothEX = −0.21 ± 0.05 ft/yr
EX: #43
EX = −0.27 ± 0.05 ft/yr
SmoothEX = −0.24 ± 0.05 ft/yr
EX: #44
EX = −0.2 ± 0.03 ft/yr
SmoothEX = −0.28 ± 0.04 ft/yr
EX: #45
EX = −0.38 ± 0.04 ft/yr
SmoothEX = −0.37 ± 0.04 ft/yr
EX: #46
EX = −0.49 ± 0.04 ft/yr
SmoothEX = −0.45 ± 0.04 ft/yr
EX: #47
EX = −0.52 ± 0.05 ft/yr
SmoothEX = −0.47 ± 0.05 ft/yr
EX: #48
EX = −0.42 ± 0.05 ft/yr
SmoothEX = −0.44 ± 0.04 ft/yr
ft
yr
100
50
0
−50
−100
1960
1980
2000

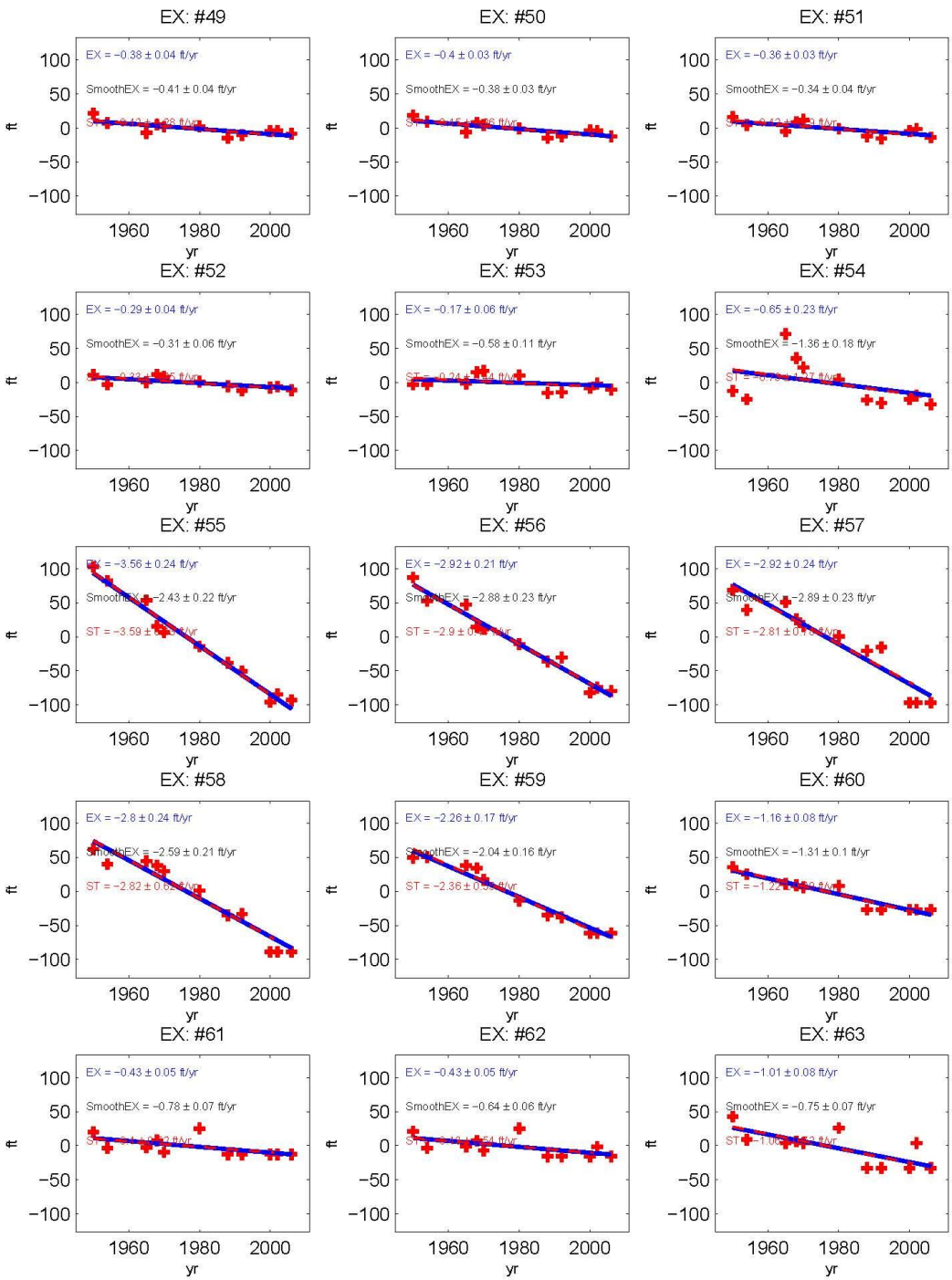
EX: #49
EX = −0.38 ± 0.04 ft/yr
SmoothEX = −0.41 ± 0.04 ft/yr
EX: #50
EX = −0.4 ± 0.03 ft/yr
SmoothEX = −0.38 ± 0.03 ft/yr
EX: #51
EX = −0.36 ± 0.03 ft/yr
SmoothEX = −0.34 ± 0.04 ft/yr
EX: #52
EX = −0.29 ± 0.04 ft/yr
SmoothEX = −0.31 ± 0.06 ft/yr
EX: #53
EX = −0.17 ± 0.06 ft/yr
SmoothEX = −0.58 ± 0.11 ft/yr
EX: #54
EX = −0.65 ± 0.23 ft/yr
SmoothEX = −1.36 ± 0.18 ft/yr
EX: #55
EX = −3.56 ± 0.24 ft/yr
SmoothEX = −2.43 ± 0.22 ft/yr
ST = −3.59 ± 0.
EX: #56
EX = −2.92 ± 0.21 ft/yr
SmoothEX = −2.88 ± 0.23 ft/yr
EX: #57
EX = −2.92 ± 0.24 ft/yr
SmoothEX = −2.89 ± 0.23 ft/yr
EX: #58
EX = −2.8 ± 0.24 ft/yr
SmoothEX = −2.59 ± 0.21 ft/yr
EX: #59
EX = −2.26 ± 0.17 ft/yr
SmoothEX = −2.04 ± 0.16 ft/yr
EX: #60
EX = −1.16 ± 0.08 ft/yr
SmoothEX = −1.31 ± 0.1 ft/yr
EX: #61
EX = −0.43 ± 0.05 ft/yr
SmoothEX = −0.78 ± 0.07 ft/yr
EX: #62
EX = −0.43 ± 0.05 ft/yr
SmoothEX = −0.64 ± 0.06 ft/yr
EX: #63
EX = −1.01 ± 0.08 ft/yr
SmoothEX = −0.75 ± 0.07 ft/yr
ft
yr
100
50
0
−50
−100
1960
1980
2000

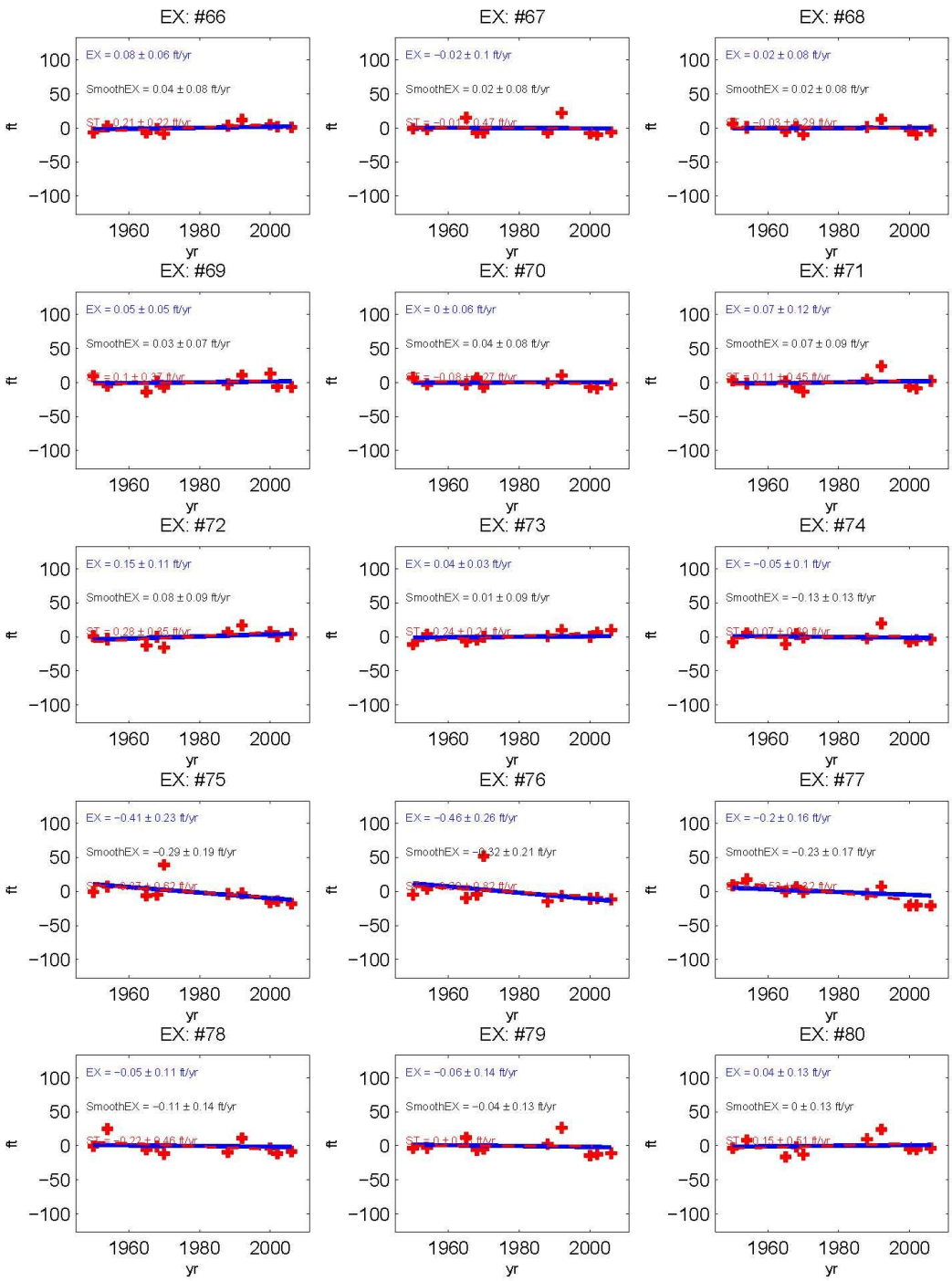
EX: #66
EX = 0.08 ± 0.06 ft/yr
SmoothEX = 0.04 ± 0.08 ft/yr
EX: #67
EX = −0.02 ± 0.1 ft/yr
SmoothEX = 0.02 ± 0.08 ft/yr
EX: #68
EX = 0.02 ± 0.08 ft/yr
SmoothEX = 0.02 ± 0.08 ft/yr
EX: #69
EX = 0.05 ± 0.05 ft/yr
SmoothEX = 0.03 ± 0.07 ft/yr
EX: #70
EX = 0 ± 0.06 ft/yr
SmoothEX = 0.04 ± 0.08 ft/yr
EX: #71
EX = 0.07 ± 0.12 ft/yr
SmoothEX = 0.07 ± 0.09 ft/yr
EX: #72
EX = 0.15 ± 0.11 ft/yr
SmoothEX = 0.08 ± 0.09 ft/yr
EX: #73
EX = 0.04 ± 0.03 ft/yr
SmoothEX = 0.01 ± 0.09 ft/yr
EX: #74
EX = −0.05 ± 0.1 ft/yr
SmoothEX = −0.13 ± 0.13 ft/yr
EX: #75
EX = −0.41 ± 0.23 ft/yr
SmoothEX = −0.29 ± 0.19 ft/yr
EX: #76
EX = −0.46 ± 0.26 ft/yr
SmoothEX = −0.32 ± 0.21 ft/yr
EX: #77
EX = −0.2 ± 0.16 ft/yr
SmoothEX = −0.23 ± 0.17 ft/yr
EX: #78
EX = −0.05 ± 0.11 ft/yr
SmoothEX = −0.11 ± 0.14 ft/yr
EX: #79
EX = −0.06 ± 0.14 ft/yr
SmoothEX = −0.04 ± 0.13 ft/yr
EX: #80
EX = 0.04 ± 0.13 ft/yr
SmoothEX = 0 ± 0.13 ft/yr
ft
yr
100
50
0
−50
−100
1960
1980
2000

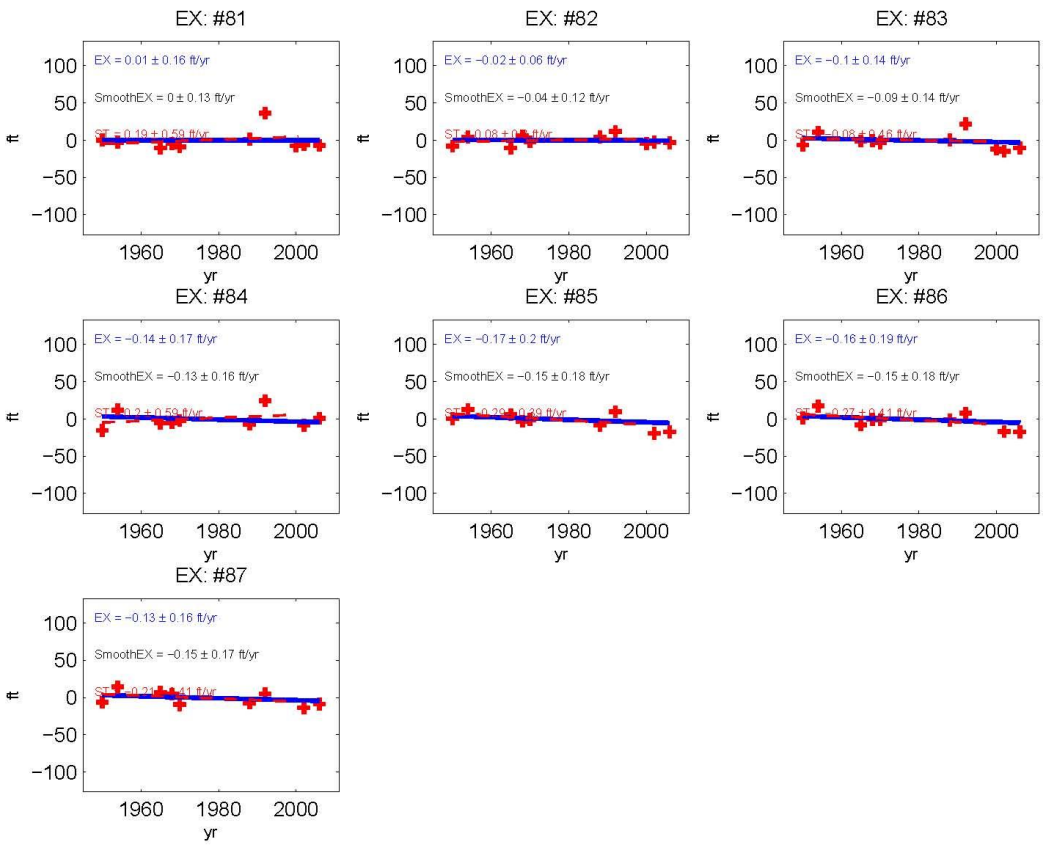
EX: #81
EX = 0.01 ± 0.16 ft/yr
SmoothEX = 0 ± 0.13 ft/yr
EX: #82
EX = −0.02 ± 0.06 ft/yr
SmoothEX = −0.04 ± 0.12 ft/yr
EX: #83
EX = −0.1 ± 0.14 ft/yr
SmoothEX = −0.09 ± 0.14 ft/yr
EX: #84
EX = −0.14 ± 0.17 ft/yr
SmoothEX = −0.13 ± 0.16 ft/yr
EX: #85
EX = −0.17 ± 0.2 ft/yr
SmoothEX = −0.15 ± 0.18 ft/yr
EX: #86
EX = −0.16 ± 0.19 ft/yr
SmoothEX = −0.15 ± 0.18 ft/yr
EX: #87
EX = −0.13 ± 0.16 ft/yr
SmoothEX = −0.15 ± 0.17 ft/yr
ft
yr
100
50
0
−50
−100
1960
1980
2000

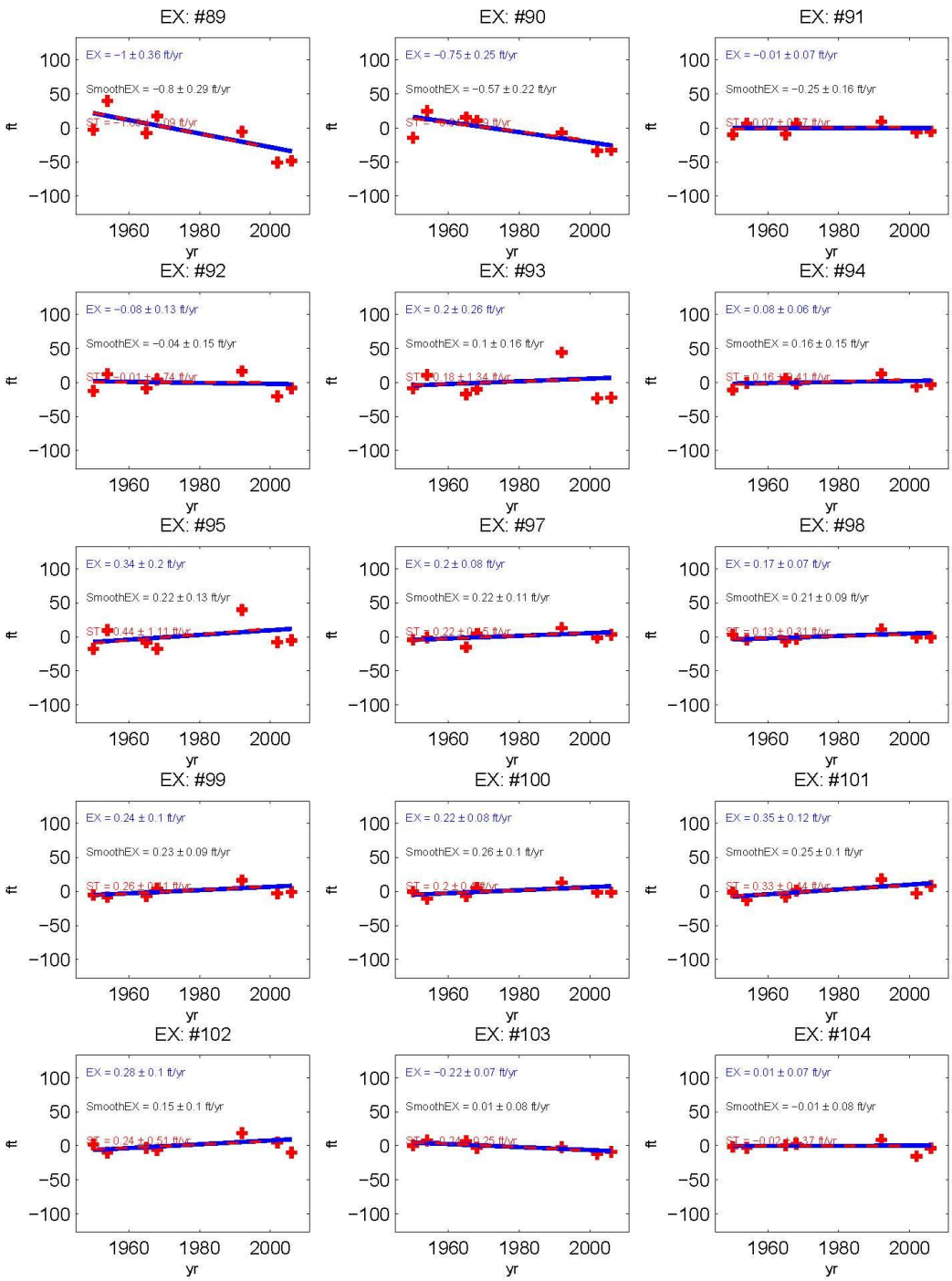
EX: #89
EX = −1 ± 0.36 ft/yr
SmoothEX = −0.8 ± 0.29 ft/yr
EX: #90
EX = −0.75 ± 0.25 ft/yr
SmoothEX = −0.57 ± 0.22 ft/yr
EX: #91
EX = −0.01 ± 0.07 ft/yr
SmoothEX = −0.25 ± 0.16 ft/yr
EX: #92
EX = −0.08 ± 0.13 ft/yr
SmoothEX = −0.04 ± 0.15 ft/yr
EX: #93
EX = 0.2 ± 0.26 ft/yr
SmoothEX = 0.1 ± 0.16 ft/yr
EX: #94
EX = 0.08 ± 0.06 ft/yr
SmoothEX = 0.16 ± 0.15 ft/yr
EX: #95
EX = 0.34 ± 0.2 ft/yr
SmoothEX = 0.22 ± 0.13 ft/yr
EX: #97
EX = 0.2 ± 0.08 ft/yr
SmoothEX = 0.22 ± 0.11 ft/yr
EX: #98
EX = 0.17 ± 0.07 ft/yr
SmoothEX = 0.21 ± 0.09 ft/yr
EX: #99
EX = 0.24 ± 0.1 ft/yr
SmoothEX = 0.23 ± 0.09 ft/yr
EX: #100
EX = 0.22 ± 0.08 ft/yr
SmoothEX = 0.26 ± 0.1 ft/yr
EX: #101
EX = 0.35 ± 0.12 ft/yr
SmoothEX = 0.25 ± 0.1 ft/yr
EX: #102
EX = 0.28 ± 0.1 ft/yr
SmoothEX = 0.15 ± 0.1 ft/yr
EX: #103
EX = −0.22 ± 0.07 ft/yr
SmoothEX = 0.01 ± 0.08 ft/yr
EX: #104
EX = 0.01 ± 0.07 ft/yr
SmoothEX = −0.01 ± 0.08 ft/yr
ft
yr
100
50
0
−50
−100
1960
1980
2000

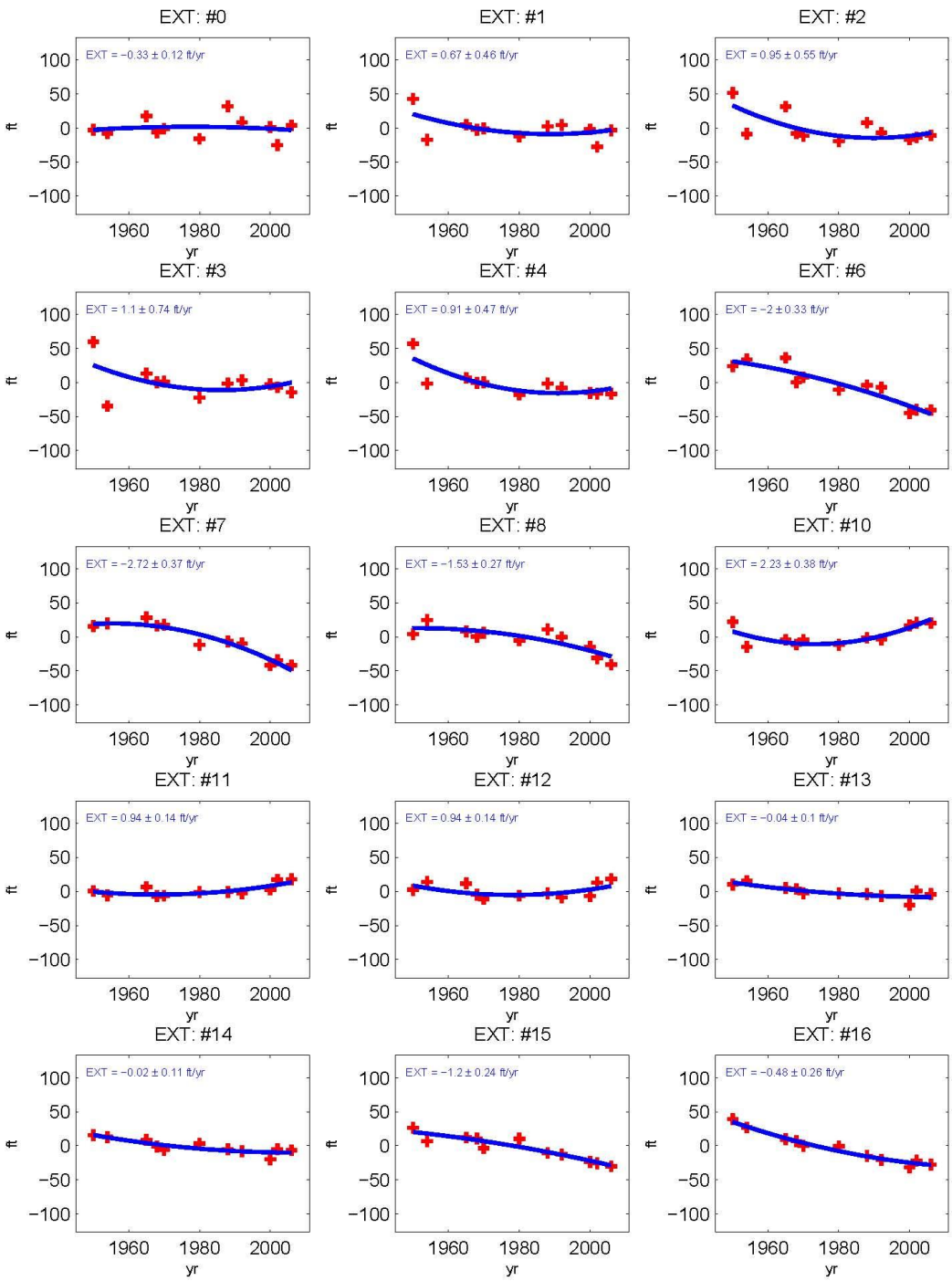
EXT: #0
EXT = −0.33 ± 0.12 ft/yr
EXT: #1
EXT = 0.67 ± 0.46 ft/yr
EXT: #2
EXT = 0.95 ± 0.55 ft/yr
EXT: #3
EXT = 1.1 ± 0.74 ft/yr
EXT: #4
EXT = 0.91 ± 0.47 ft/yr
EXT: #6
EXT = −2 ± 0.33 ft/yr
EXT: #7
EXT = −2.72 ± 0.37 ft/yr
EXT: #8
EXT = −1.53 ± 0.27 ft/yr
EXT: #10
EXT = 2.23 ± 0.38 ft/yr
EXT: #11
EXT = 0.94 ± 0.14 ft/yr
EXT: #12
EXT = 0.94 ± 0.14 ft/yr
EXT: #13
EXT = −0.04 ± 0.1 ft/yr
EXT: #14
EXT = −0.02 ± 0.11 ft/yr
EXT: #15
EXT = −1.2 ± 0.24 ft/yr
EXT: #16
EXT = −0.48 ± 0.26 ft/yr
ft
yr
100
50
0
−50
−100
1960
1980
2000

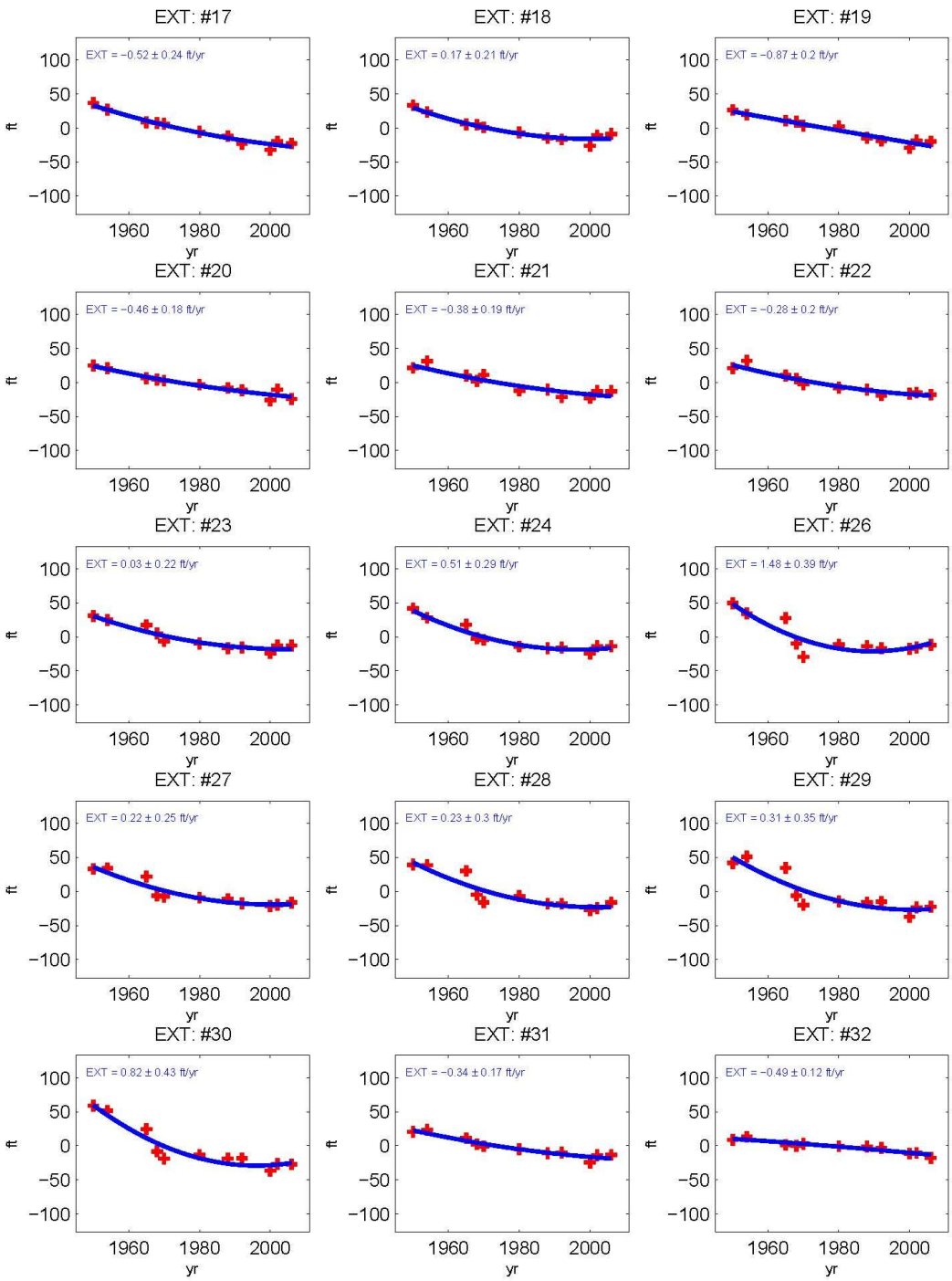
EXT: #17
EXT = −0.52 ± 0.24 ft/yr
EXT: #18
EXT = 0.17 ± 0.21 ft/yr
EXT: #19
EXT = −0.87 ± 0.2 ft/yr
EXT: #20
EXT = −0.46 ± 0.18 ft/yr
EXT: #21
EXT = −0.38 ± 0.19 ft/yr
EXT: #22
EXT = −0.28 ± 0.2 ft/yr
EXT: #23
EXT = 0.03 ± 0.22 ft/yr
EXT: #24
EXT = 0.51 ± 0.29 ft/yr
EXT: #26
EXT = 1.48 ± 0.39 ft/yr
EXT: #27
EXT = 0.22 ± 0.25 ft/yr
EXT: #28
EXT = 0.23 ± 0.3 ft/yr
EXT: #29
EXT = 0.31 ± 0.35 ft/yr
EXT: #30
EXT = 0.82 ± 0.43 ft/yr
EXT: #31
EXT = −0.34 ± 0.17 ft/yr
EXT: #32
EXT = −0.49 ± 0.12 ft/yr
ft
yr
100
50
0
−50
−100
1960
1980
2000

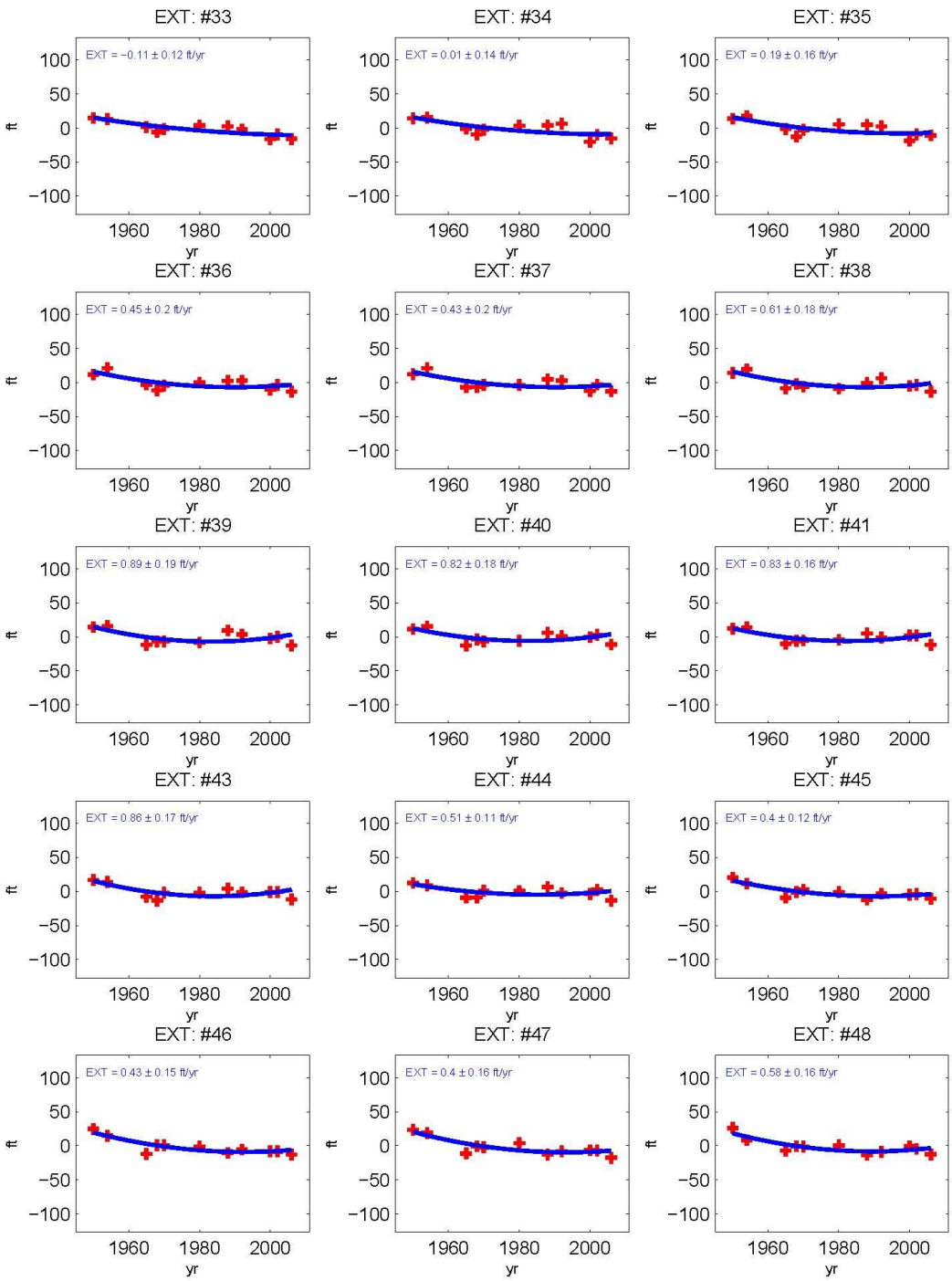
EXT: #33
EXT = −0.11 ± 0.12 ft/yr
EXT: #34
EXT = 0.01 ± 0.14 ft/yr
EXT: #35
EXT = 0.19 ± 0.16 ft/yr
EXT: #36
EXT = 0.45 ± 0.2 ft/yr
EXT: #37
EXT = 0.43 ± 0.2 ft/yr
EXT: #38
EXT = 0.61 ± 0.18 ft/yr
EXT: #39
EXT = 0.89 ± 0.19 ft/yr
EXT: #40
EXT = 0.82 ± 0.18 ft/yr
EXT: #41
EXT = 0.83 ± 0.16 ft/yr
EXT: #43
EXT = 0.86 ± 0.17 ft/yr
EXT: #44
EXT = 0.51 ± 0.11 ft/yr
EXT: #45
EXT = 0.4 ± 0.12 ft/yr
EXT: #46
EXT = 0.43 ± 0.15 ft/yr
EXT: #47
EXT = 0.4 ± 0.16 ft/yr
EXT: #48
EXT = 0.58 ± 0.16 ft/yr
ft
yr
100
50
0
−50
−100
1960
1980
2000

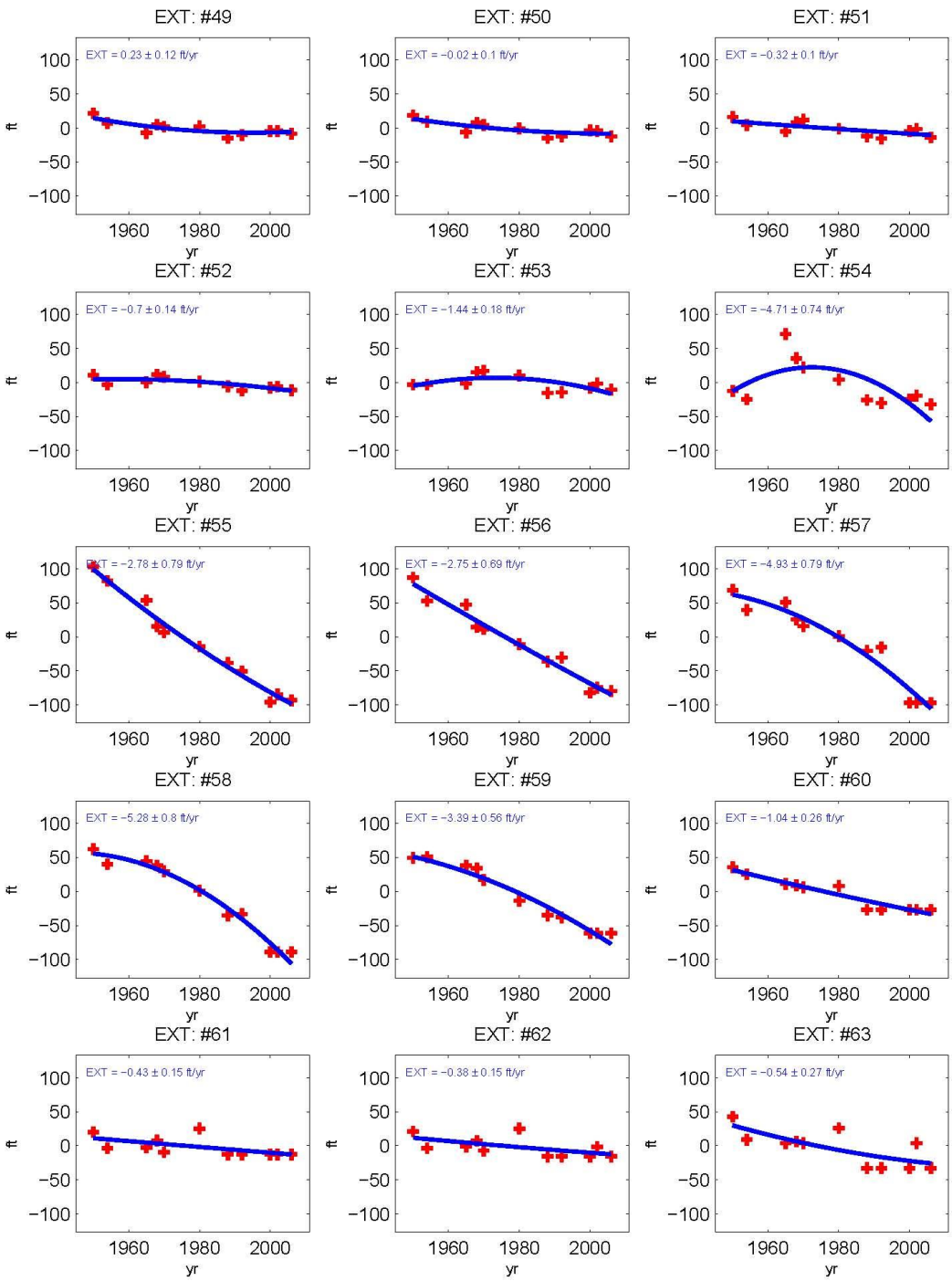
EXT: #49
EXT = 0.23 ± 0.12 ft/yr
EXT: #50
EXT = −0.02 ± 0.1 ft/yr
EXT: #51
EXT = −0.32 ± 0.1 ft/yr
EXT: #52
EXT = −0.7 ± 0.14 ft/yr
EXT: #53
EXT = −1.44 ± 0.18 ft/yr
EXT: #54
EXT = −4.71 ± 0.74 ft/yr
EXT: #55
EXT = −2.78 ± 0.79 ft/yr
EXT: #56
EXT = −2.75 ± 0.69 ft/yr
EXT: #57
EXT = −4.93 ± 0.79 ft/yr
EXT: #58
EXT = −5.28 ± 0.8 ft/yr
EXT: #59
EXT = −3.39 ± 0.56 ft/yr
EXT: #60
EXT = −1.04 ± 0.26 ft/yr
EXT: #61
EXT = −0.43 ± 0.15 ft/yr
EXT: #62
EXT = −0.38 ± 0.15 ft/yr
EXT: #63
EXT = −0.54 ± 0.27 ft/yr
ft
yr
100
50
0
−50
−100
1960
1980
2000

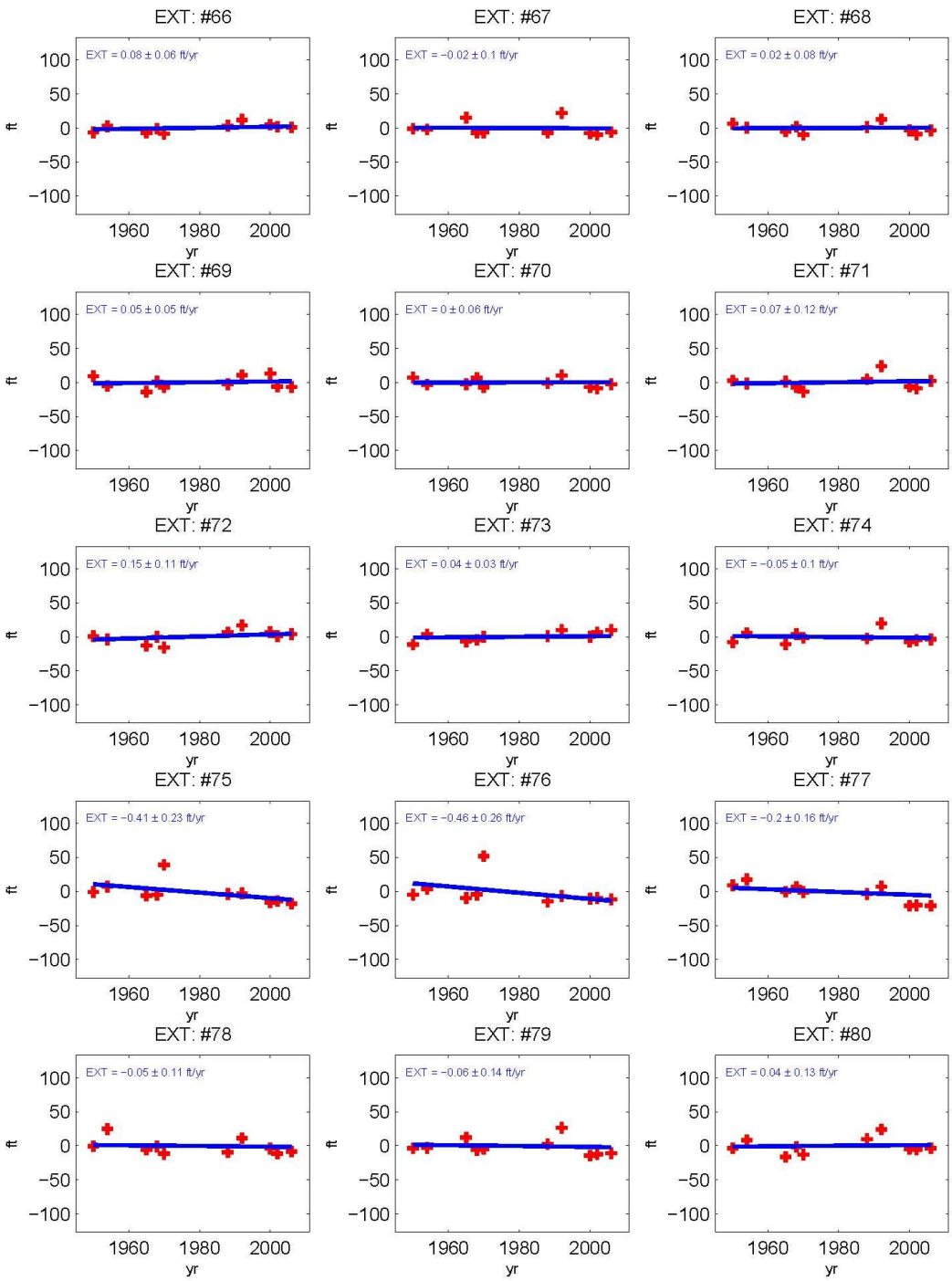
EXT: #66
EXT = 0.08 ± 0.06 ft/yr
EXT: #67
EXT = −0.02 ± 0.1 ft/yr
EXT: #68
EXT = 0.02 ± 0.08 ft/yr
EXT: #69
EXT = 0.05 ± 0.05 ft/yr
EXT: #70
EXT = 0 ± 0.06 ft/yr
EXT: #71
EXT = 0.07 ± 0.12 ft/yr
EXT: #72
EXT = 0.15 ± 0.11 ft/yr
EXT: #73
EXT = 0.04 ± 0.03 ft/yr
EXT: #74
EXT = −0.05 ± 0.1 ft/yr
EXT: #75
EXT = −0.41 ± 0.23 ft/yr
EXT: #76
EXT = −0.46 ± 0.26 ft/yr
EXT: #77
EXT = −0.2 ± 0.16 ft/yr
EXT: #78
EXT = −0.05 ± 0.11 ft/yr
EXT: #79
EXT = −0.06 ± 0.14 ft/yr
EXT: #80
EXT = 0.04 ± 0.13 ft/yr
ft
yr
100
50
0
−50
−100
1960
1980
2000

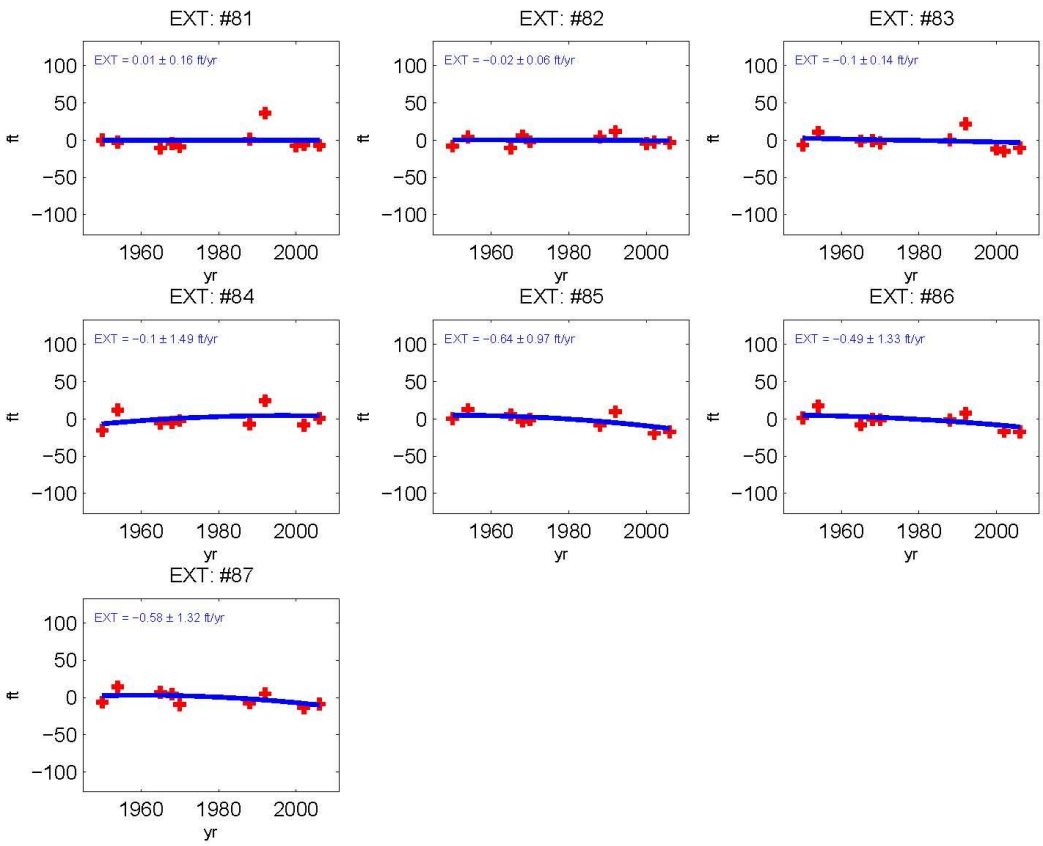
EXT: #81
EXT = 0.01 ± 0.16 ft/yr
EXT: #82
EXT = −0.02 ± 0.06 ft/yr
EXT: #83
EXT = −0.1 ± 0.14 ft/yr
EXT: #84
EXT = −0.1 ± 1.49 ft/yr
EXT: #85
EXT = −0.64 ± 0.97 ft/yr
EXT: #86
EXT = −0.49 ± 1.33 ft/yr
EXT: #87
EXT = −0.58 ± 1.32 ft/yr
ft
yr
100
50
0
−50
−100
1960
1980
2000

Shoreline change rates (transect plots) of Puʻukoholā Heiau NHS

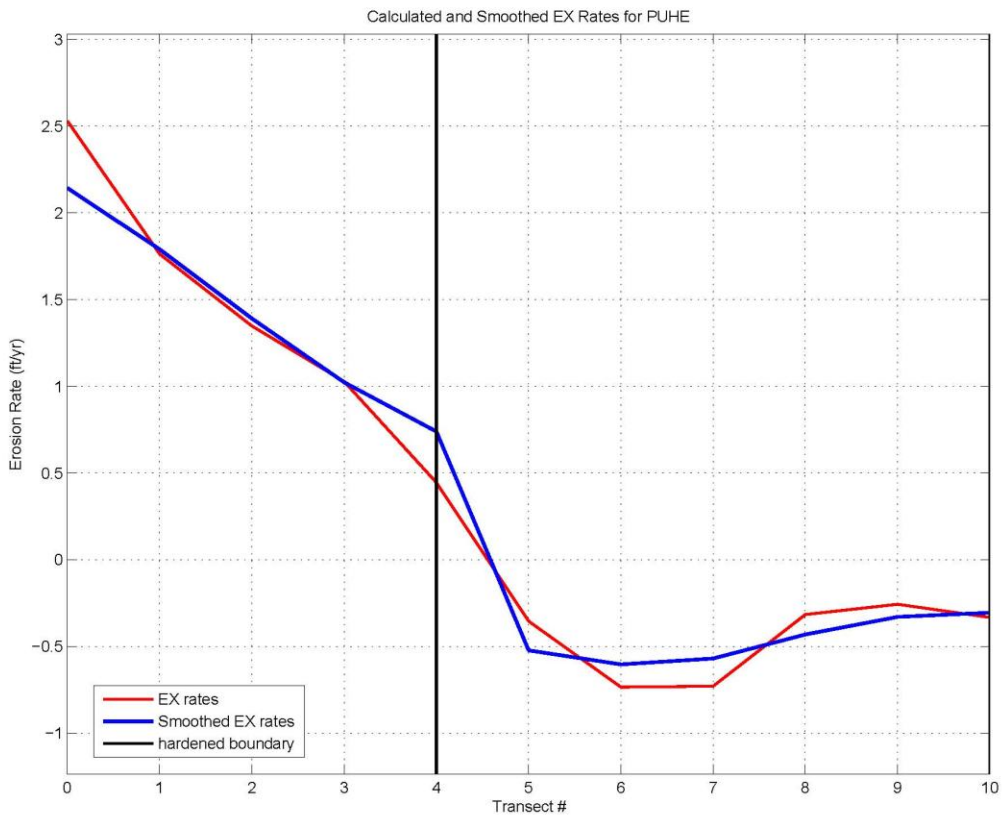

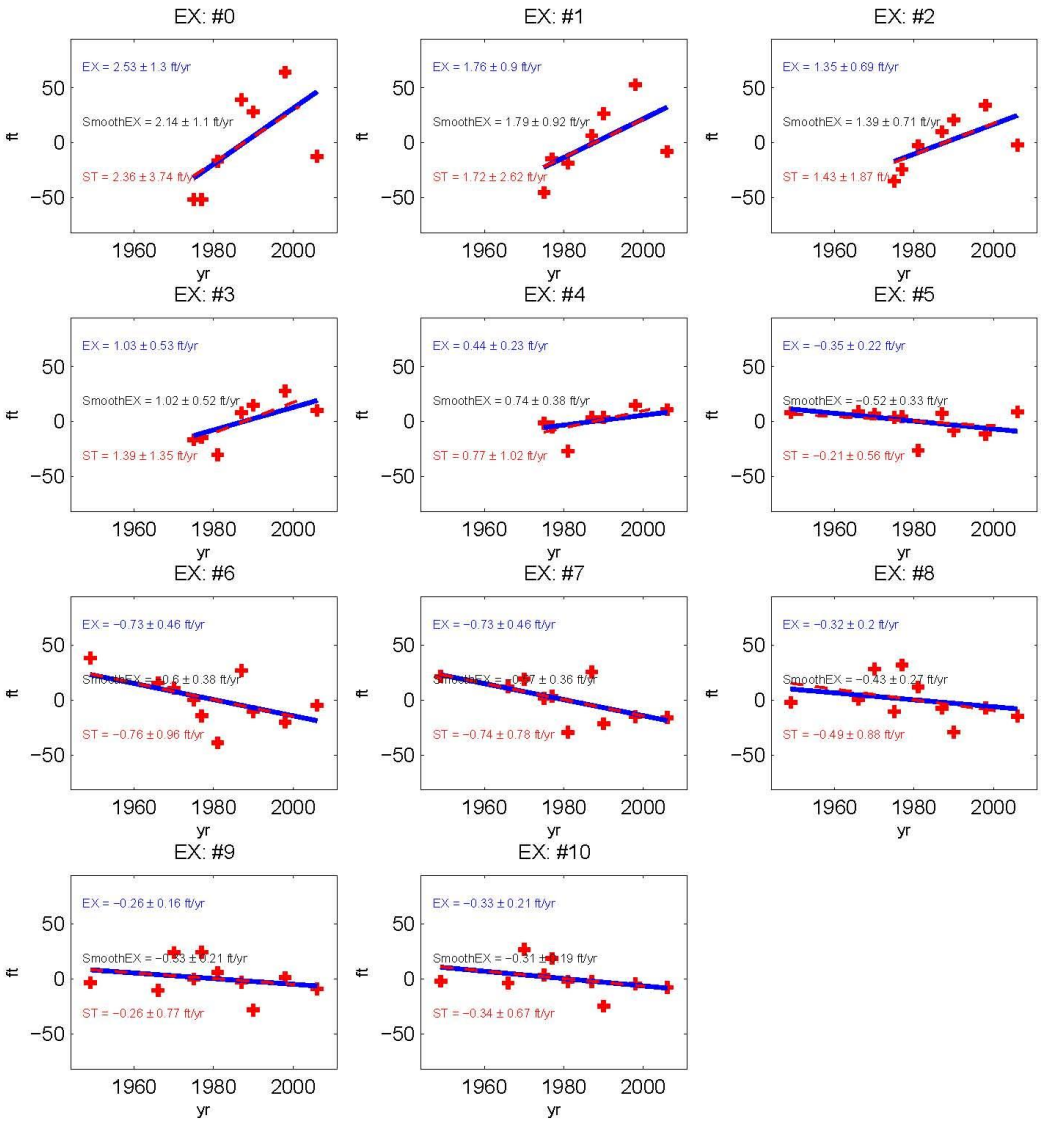
EX: #0
EX = 2.53 ± 1.3 ft/yr
SmoothEX = 2.14 ± 1.1 ft/yr
ST = 2.36 ± 3.74 ft/yr
EX: #1
EX = 1.76 ± 0.9 ft/yr
SmoothEX = 1.79 ± 0.92 ft/yr
ST = 1.72 ± 2.62 ft/yr
EX: #2
EX = 1.35 ± 0.69 ft/yr
SmoothEX = 1.39 ± 0.71 ft/yr
ST = 1.43 ± 1.87 ft/yr
EX: #3
EX = 1.03 ± 0.53 ft/yr
SmoothEX = 1.02 ± 0.52 ft/yr
ST = 1.39 ± 1.35 ft/yr
EX: #4
EX = 0.44 ± 0.23 ft/yr
SmoothEX = 0.74 ± 0.38 ft/yr
ST = 0.77 ± 1.02 ft/yr
EX: #5
EX = −0.35 ± 0.22 ft/yr
SmoothEX = −0.52 ± 0.33 ft/yr
ST = −0.21 ± 0.56 ft/yr
EX: #6
EX = −0.73 ± 0.46 ft/yr
ST = −0.76 ± 0.96 ft/yr
EX: #7
EX = −0.73 ± 0.46 ft/yr
ST = −0.74 ± 0.78 ft/yr
EX: #8
EX = −0.32 ± 0.2 ft/yr
SmoothEX = −0.43 ± 0.27 ft/yr
ST = −0.49 ± 0.88 ft/yr
EX: #9
EX = −0.26 ± 0.16 ft/yr
ST = −0.26 ± 0.77 ft/yr
EX: #10
EX = −0.33 ± 0.21 ft/yr
ST = −0.34 ± 0.67 ft/yr
ft
yr
50
0
−50
1960
1980
2000

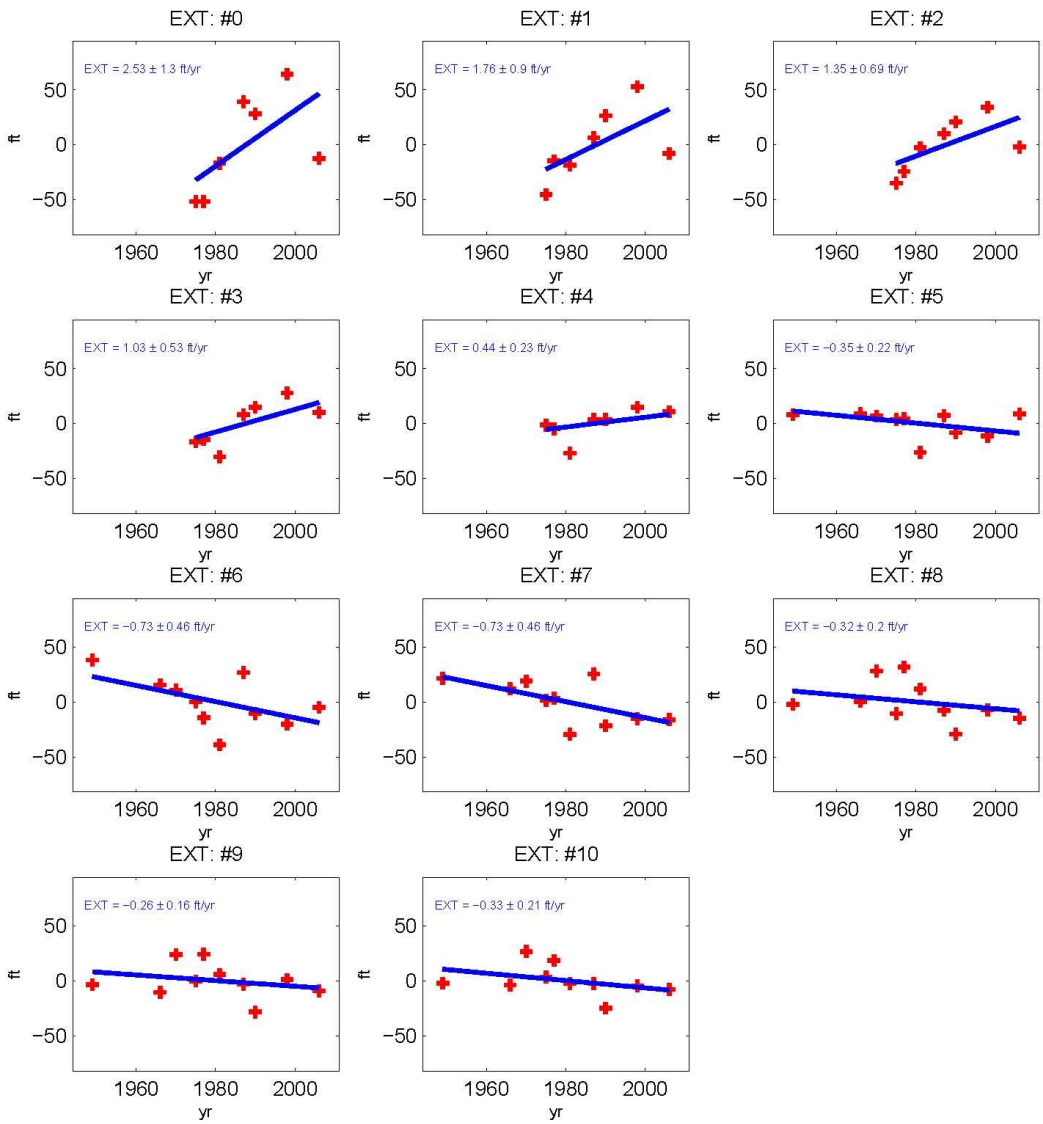
EXT: #0
EXT = 2.53 ± 1.3 ft/yr
EXT: #1
EXT = 1.76 ± 0.9 ft/yr
EXT: #2
EXT = 1.35 ± 0.69 ft/yr
EXT: #3
EXT = 1.03 ± 0.53 ft/yr
EXT: #4
EXT = 0.44 ± 0.23 ft/yr
EXT: #5
EXT = −0.35 ± 0.22 ft/yr
EXT: #6
EXT = −0.73 ± 0.46 ft/yr
EXT: #7
EXT = −0.73 ± 0.46 ft/yr
EXT: #8
EXT = −0.32 ± 0.2 ft/yr
EXT: #9
EXT = −0.26 ± 0.16 ft/yr
EXT: #10
EXT = −0.33 ± 0.21 ft/yr
ft
yr
50
0
−50
1960
1980
2000